Oceania Dairy Outfall Dispersion Modelling

Prepared for:

Babbage

eCoast
eTakutai

MOHIO - AUAHA - TAUTOKO
UNDERSTAND - INNOVATE - SUSTAIN

PO Box 151, Raglan 3225, New Zealand
Ph: +64 7 825 0087 | info@ecoast.co.nz | www.ecoast.co.nz

Oceania Dairy Outfall Dispersion Modelling

Report Status

Version	Date	Status	Approved by
V1	18 July 2019	Final Draft	STM
V2	26 August 2019	Rev. 1	STM

It is the responsibility of the reader to verify the version number of this report.

Authors

Shaw Mead BSc, *MSc (Hons), Ph.D.*

Dougal Greer *BSc, MSc (Hons)*

Rhys McIntosh *BSc, MSc (Hons)*

Jai Davies-Campbell *BSc, MSc* (*Hons)*

Ed Atkin *BSc, HND*

Executive Summary

Oceania Dairy have proposed to dispose of treated wastewater at an oceanic outfall just north of the Waitake River, offshore of Archibald Road. This report provides information on the physical oceanography of the site and describes the utilisation of a calibrated numerical model to help determine the offshore location and outfall arrangement to achieve satisfactory dilution and dispersion of wastewater at the site; i.e., it is a component of the assessment of environmental effects (AEE) for resource consent application

Field data were collected for the development of a calibrated hydrodynamic numerical model for the investigation of dilution scenarios for the proposed Oceania outfall. A local bathymetry survey was undertaken, and a wave/current/water level instrument was deployed for 28-days for the development of the nearshore model domain and model calibration, respectively. Long-term coincident wind and wave data were analysed to determine the average and worst case metocean scenarios. These conditions were found to be:

- Calm conditions (no wind and small offshore wave conditions – 1 m waves at 12 seconds) worst-case 2% of the time in total;
- Light NE (onshore) winds (2 m/s wind speed with average offshore waves – 2 m at 12 seconds) 2nd worst-case 11% of the time in total;
- Light SW winds and average offshore waves (2 m/s wind speed, 2 m waves at 12 seconds) 2% of the time in total, and;
- Light NE winds with average NE offshore waves (2 m/s wind speed, 2 m waves at 12 seconds) 3% of the time in total.

The rest of the time (i.e., 80%) more energetic wind and wave conditions occur. As noted by Hicks *et al*. (2015), the South Canterbury coastline is very exposed and subject to frequent winter storms. As a result, oceanic outfalls in this region are not uncommon because of the ability of the coastline to rapidly mix treated wastewater in ambient sea water, in turn reducing ecological impacts.

The maximum daily outfall volume of 10,000 m^3/day was applied as the outfall boundary condition in the model simulations. The modelling results are considered conservative (i.e. greater/faster dilution will likely occur) since:

- The calibrated model slightly underestimated significant wave heights (i.e., a physical factor that aids mixing/dilution);
- A neap tide was used for all scenarios in order to minimise tidal currents and therefore mixing (although there is no inter-dependence between tides and metocean conditions), and;

- The outfall water was released into the top layer of the model providing a conservative approach to initial mixing that occurs as the buoyant plume rises through the water column.

Through an iterative approach where the outfall distance was first increased offshore and then divided into 3 outfalls that split the volume at each discharge point (i.e., 3,000, 3,000 and 4,000 m3/day at each), a split outfall configuration discharging at 3 locations between 450 and 500 m offshore was found to result in the fastest dilution for all of the metocean scenarios. Due to the split configuration, dilution of 300x or greater occurs within 10-50 m of the outfall in all 4 metocean scenarios. The exception to this is when calm conditions occur for >6 hours. However, it is likely that this scenario very rarely, if ever, occurs. This is due to a) the models inherent conservatism, and b) the likely occurrence of calm conditions for 6 hours or greater (i.e. on average only once every 2 years or less).

Once the split outfall had been found to result in efficient dilution of the outfall discharge, a representative year-long discharge was simulated, and hourly dilution time-series data were extracted from the 8 sites identified by Greenaway (2018) that were used to consider health impacts along the coast.

Contents

Figures

Tables

1 Background

Oceania Dairy have proposed to dispose of treated wastewater at an oceanic outfall just north of the Waitake River, near Archibald Road (Figure 1.1). This report provides information on the physical oceanography of the site and describes the utilisation of a calibrated numerical model to help determine the offshore location and outfall arrangement to achieve satisfactory dilution and dispersion of wastewater at the site; i.e., it is a component of the assessment of environmental effects (AEE) for resource consent application.

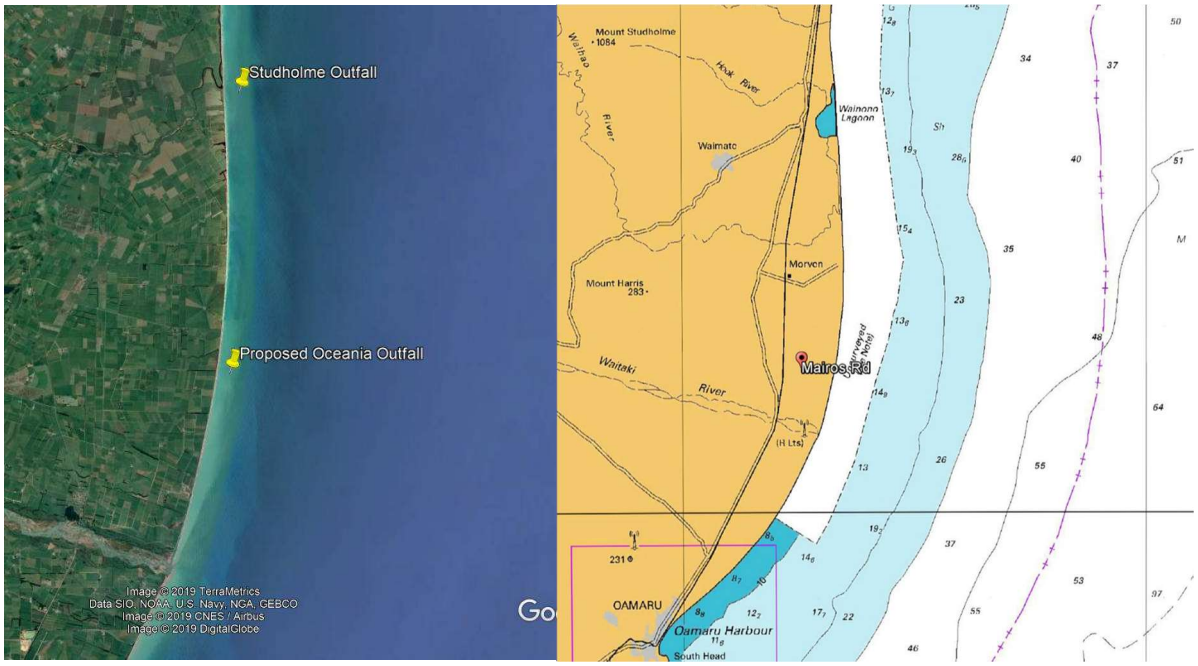

Figure 1.1. A Google Earth image (left) indicating the approximate location of the proposed outfall at Archibald Road. (Right) the available nautical chart (LINZ Chart No. 64) has not nearshore depths at the proposed outfall location, hence the need for a bathymetry survey.

2 Site Information Review

The South Canterbury coastline is very exposed and subject to frequent winter storms (Hicks *et al*., 2015). Oceanic outfalls in this region are not uncommon because of the ability of the coastline to rapidly mix treated wastewater in ambient sea water, in turn reducing ecological impacts. A literature review with respect to the coastal processes of the coast was undertaken to provide a basic setting and understanding of the area. This section of the report presents a summary of relevant literature.

In September 2016, Fonterra Limited (Fonterra) were granted consent to dispose of treated wastewater, stormwater and condensate that had been treated to a secondary biological standard at the Studholme Factory about 10 km north of the proposed site (Figure 1.1). Fonterra were also granted consent to carry out similar disposal activities at their Clandeboye location, which is about 75 km north of the proposed outfall, ~24 km north-east of Timaru. The ocean outfall from Fonterra's Studholme Dairy Factory was to accommodate the proposed plans to increase the processing capacity at the factory (Figure 2.1). The studies undertaken for the Studholme Dairy outfall provide useful background information for the proposed Oceania outfall.

As part of the consent application for the assessment of environmental effects, Cawthron Institute (Cawthron) were engaged to assess environmental effects associated with the construction and operation of the outfall, whilst NIWA were engaged to access the coastal processes and hazards assessment. The reports covered characterisation of the existing receiving environment, assessment of the potential effects of the proposed construction and operation on key components, and coastal processes. This included; water quality and seabed ecology, marine fish and fisheries; marine mammals, birds, and adjacent freshwater habitats.

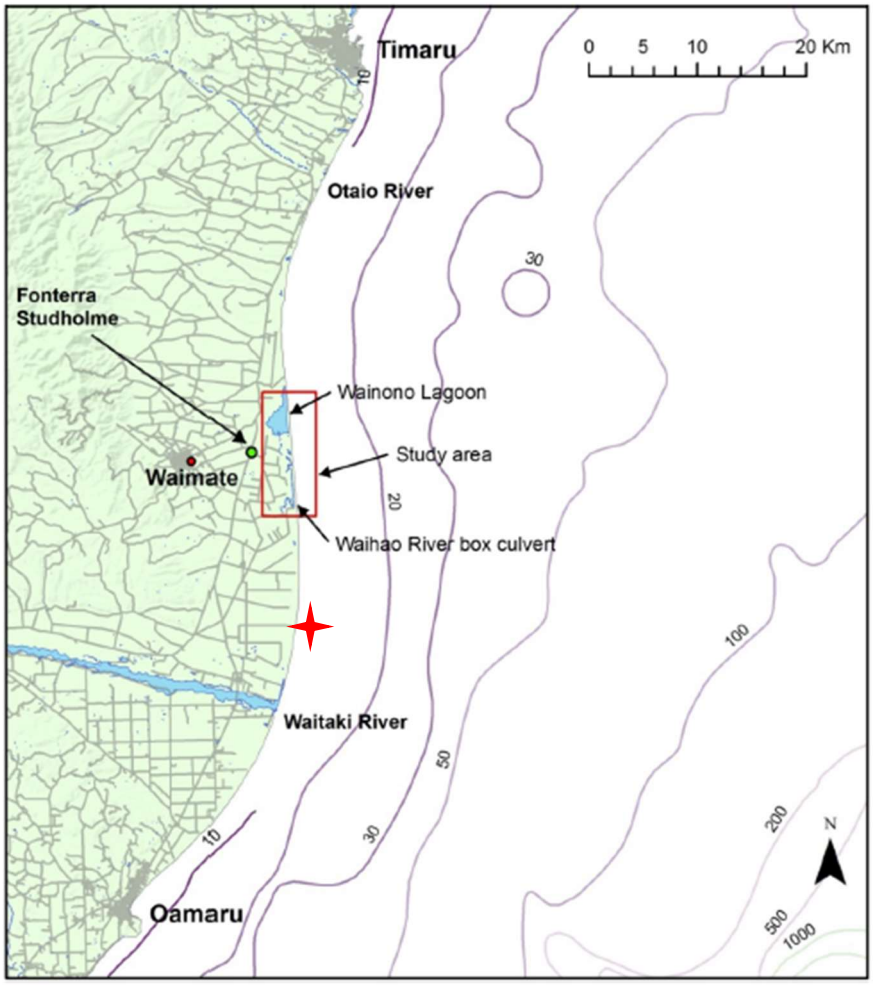

Figure 2.1. Location of the Fonterra Studholme factory and locality of general study area carried out for the Cawthron report (Sneddon *et al*., 2015). The approximate location of the proposed Oceania outfall is shown by the red star.

2.1 Beach Morphology

Hicks *et al*. (2015) characterised the coastline as being a very dynamic, wave-exposed environment comprising steep greywacke sand and coarse gravel beaches (Figure 2.3 and Figure 2.4). Satellite imagery shows suspended/resuspended sediments in the nearshore environment. Sediment inputs from the Waitake River and coastal erosion processes are transported north by the predominant southerly swell. Hicks *et al*. (2015) observed that the South Canterbury coastline is almost entirely erosional with the study site having an estimated long-term rate of erosion of the shoreline between 0.19 and 0.73 m/y (cited in Sneddon *et al*., 2015). The beach profile was noted to be characterised by a steep foreshore and backshore, as can be seen in Figure 2.3 and Figure 2.4, and comprised of flattened gravel. This is very similar to the coastline at Archibald Road, which is also backed by low eroding cliffs (Figure 2.5).

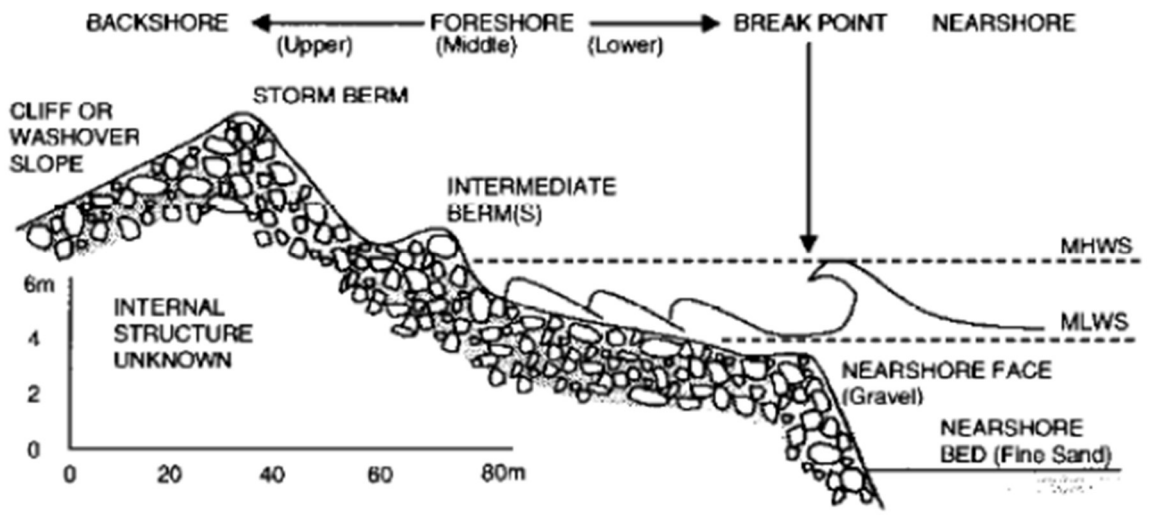

Figure 2.2. The morphology of a typical mixed sand and gravel beach profile (updated from Kirk (1980) by Stapleton (2005), cited in Jenner & Swaffield, 2015).

Figure 2.3. View south of along the barrier and old Waihao Arm channel. Note driftwood line showing extent of relative recent (2014) wave over-wash, steep backshore slope and gravel riffle in channel formed in breach deposits. Near-field crest elevation is 5.5 m and rises to 7.0 m in the distance (Hicks et al., 2015).

Figure 2.4. Barrier backshore-slope 200 m of the then proposed outfall location for Studholme. Driftwood line and cobble colours shows the extent of wave overwash in recent years (2014). Lichen on the cobbles in the lower backshore-slope indicate older deposits. Ridge crest elevation is 7.0 m AMSL (Hicks *et al*., 2015).

Figure 2.5. The similar coastline at Archibald Road, which is backed by low eroding cliffs (the left hand image shows the Aquadopp wave/current/water level meter deployed some 200 m offshore at Archibald Road for model calibration).

2.2 Sediment Characteristics

In the nearshore, permanent hard substrate features, such as bedrock reefs are notably absent. At the 100 m depth contour line, the substrate is comprised of gravel and shell, whereas the nearshore (<10 m depth) is shown as un-surveyed on hydrographic chart NZ64, likely due to the difficulties of nearshore survey because of the exposed nature of the coast (Figure 1.1). The alluvial fan from the Waitake River extends as far north as the Waihao River, between which lies Archibald Road, Morven. Single (2006) reports that the alluvial fan extends more than 50 km out to sea and comprises sands and gravels, which are poorly consolidated

and within the nearshore region are covered by a thin layer of fine sand; this was confirmed during the field data collection (Section 3).

The lack of nearshore data available resulted in Seddon *et al*. (2015) conducting two surveys to characterise the nearshore seabed and water column (Figure 2.6). The first survey was carried out near the Waihao River Box culvert and the second at the proposed outfall location, which was 4 km north (Figure 2.6). The surveys involved sampling of benthic sediment and associated macrofaunal communities, as well as the collection of seawater samples and *in situ* profiling of the water column. Furthermore, a temporary mooring was deployed at the first site to collect time-series data on current and water-quality parameters. Sneddon *et al*., (2015) reported that there were no clear spatial gradients in benthic macrofaunal communities, sediment characteristics or water quality parameters. The nearshore substrate comprised of a “thin mobile sand/silt layer (1-10 cm thick) overlying shingle material, similar to that of the adjacent beach”. Macrofaunal communities were reportedly sparse with low taxa richness and very low total abundances. The water samples indicate high suspended sediment concentrations (particularly in the nearshore). The nutrient and metal concentrations, however, were not reported to be high (Sneddon *et al*., 2015).

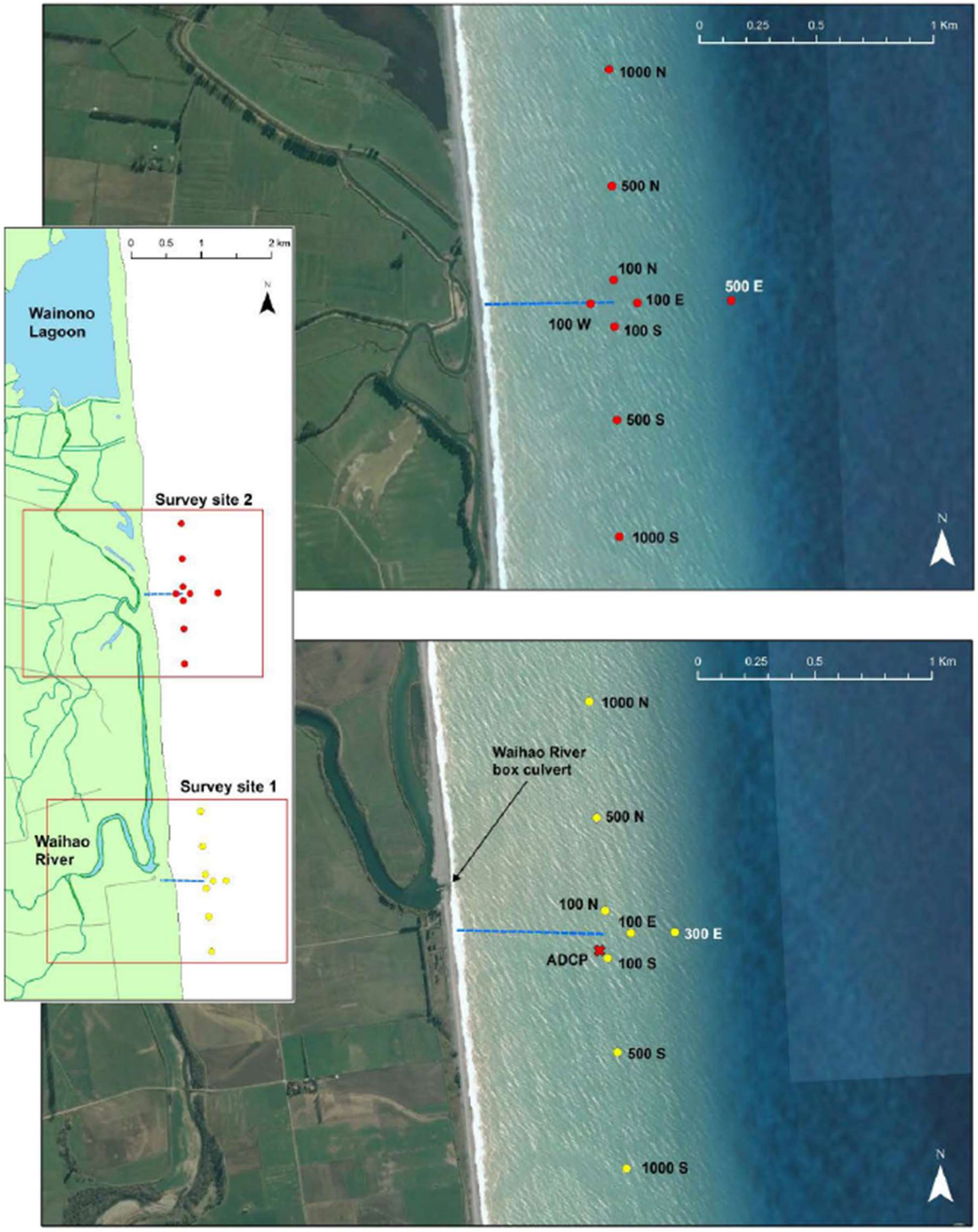

Figure 2.6. Sampling station locations for the two surveys relative to the proposed outfall locations (Sneddon *et al*., 2015

2.3 Wind Climate

The wind rose plot (Figure 2.7), indicates that the predominant wind direction is from the north-west and north-north-east. Interestingly, wind appears to arrive from almost all other directions for equal amounts the time. This wind data is from the Oamaru Airport, which is approximately

5 km south of the Waitake River. The study site is situated just north of the Waitake River approximately 10 km away from the Oamaru Airport. Both the Oamaru Airport and Archibald Road site are situated close to the coast. The strongest wind are easterlies and westerlies.

The wind rose plot (Figure 2.8) for the Waimate CWS location indicates that the predominant wind direction is from the south-west-west to south-west. The secondary dominant wind direction is from the north-north-west. This wind data is from the Waimate Cws location, which is approximately 18 km north of the Archibald Road location and some 10 km inland. The strongest winds are south-westerlies. Generally, the wind speeds observed at both the Waimate and Oamuru airports are reports are quite low.

Golder (2015) also generated a rose plot of the wind for direction and speed for Studholme, which indicated that the dominant wind directions were from the south-west and north-east, with the strongest winds from south west through to west (Figure 2.9). This local wind summary is similar to the offshore wind climate (Section 2.5), and more in agreement with observations at the coast at Archibald Road than the inland wind records.

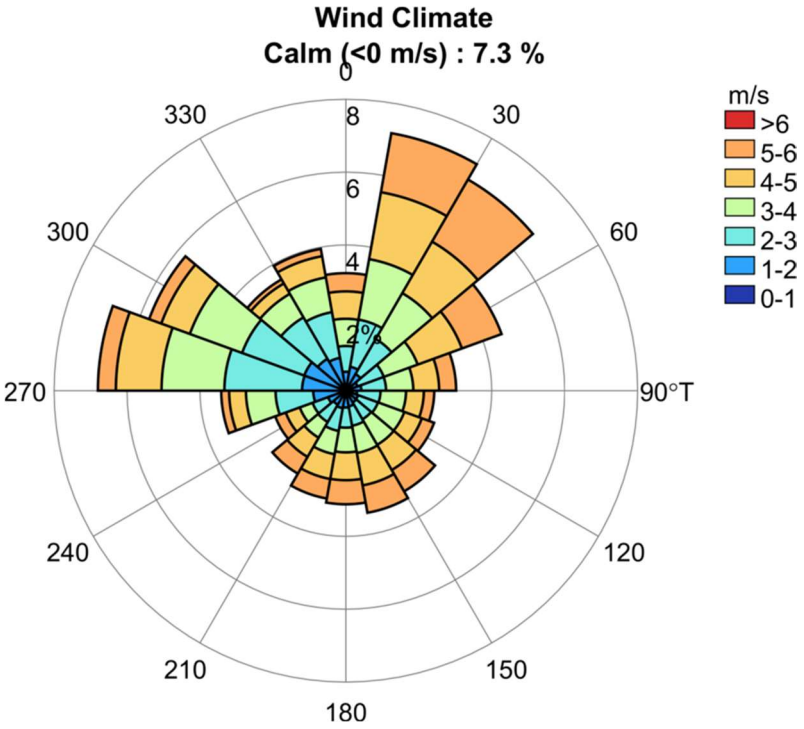

Figure 2.7. Rose plot indicating the direction (DegT) and speed (m/s) of wind at the Oamaru Airport from 1960-2011 (some 13 km south of the proposed outfall at Archibald Road). The colour bar represents the wind speed (m/s) and the bars on the plot indicate the wind origin and percentage occurrence. Data was obtained from the National Climate Database via NIWA.

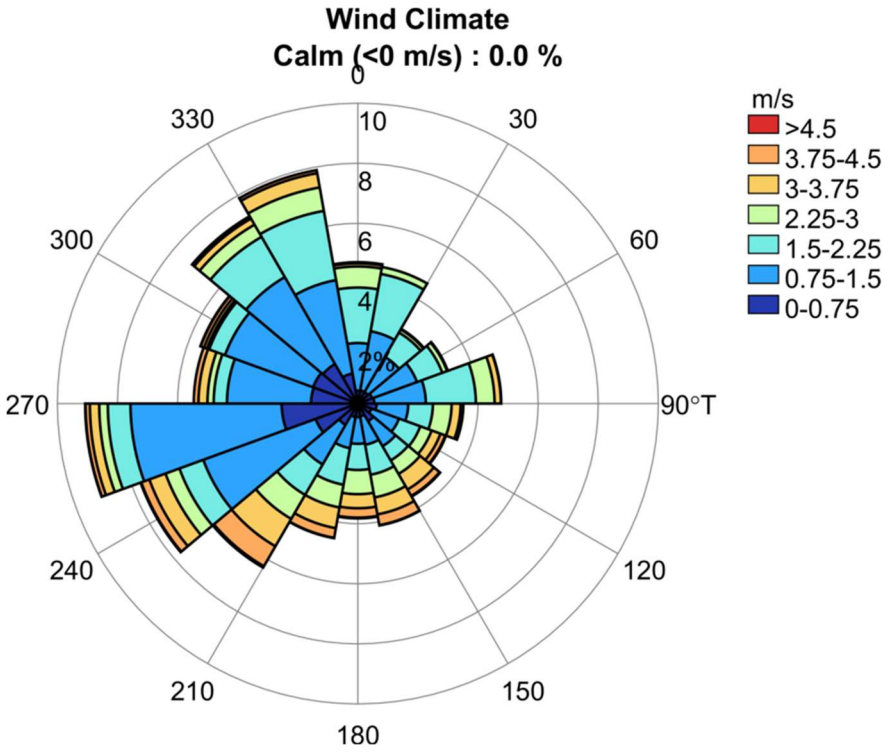

Figure 2.8. Rose plot indicating the direction (DegT) and speed (m/s) of wind at the Waimate CWS from 2009-2011 (some 10 km north of the proposed Archibald Road outfall). The colour bar represents the wind speed (m/s) and the bars on the plot indicate the wind origin and the percentage of occurrence. Data was obtained from the National Climate Database via NIWA.

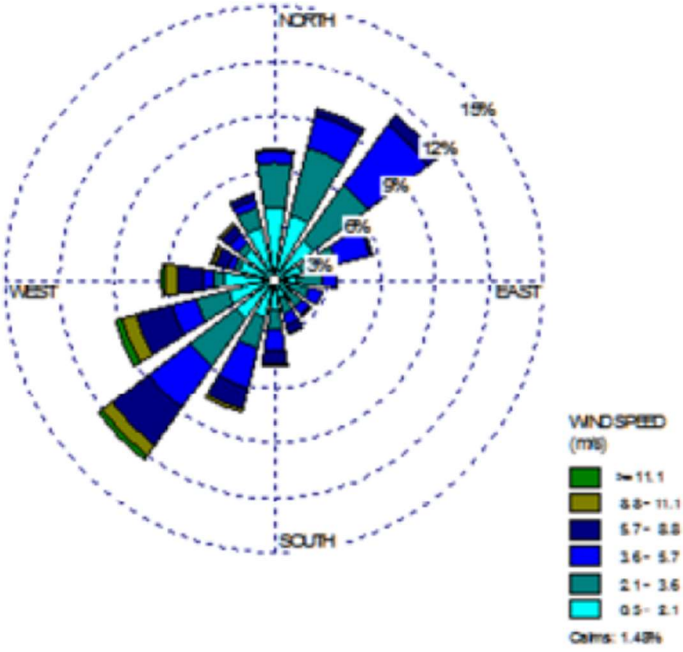

Figure 2.9. Rose plot of wind direction and speed (m/s) of Studholme Factory (Golder Associates, 2015; cited in Jenner & Swaffield, 2015). The colour bar represents the wind speed (m/s) and the bars on the plot indicate the wind origin. Time frame of data not provided.

2.4 Wave Climate

Davies (1972) have reported that the South Canterbury wave climate is one of an east coast type swell (cited in Hicks *et al*., 2015). Most swell energy incident on this coastline is generated by Southern Ocean storms (Hicks *et al*., 2002; cited in Hicks *et al*., 2015). These storm waves typically approach the coast at angles of between 45 – 90 degrees and waves are often not shore-normal by the time they reach the shoreline. Northward longshore transport is attributed to these obliquely breaking waves at the shore. Wave data at the 10 m isobath off Wainono Lagoon was analysed by Stapleton (2005) from Gorman *et al*. (2002) hindcast study, which covered the period between 1979 – 1998. The analysis revealed that 80% of the time waves arrived from the south-east quadrant, whilst the highest waves arrived from the south-south-east (2-4 m) (refer to Figure 2.10). Furthermore, an overall average significant wave height of 1.09 m was recorded, and as might be expect due to winter storms, there is a seasonal pattern with monthly average heights peaking in June and July (1.35 m), whilst the lowest were recorded during December and January (0.9 m) (Figure 2.11).

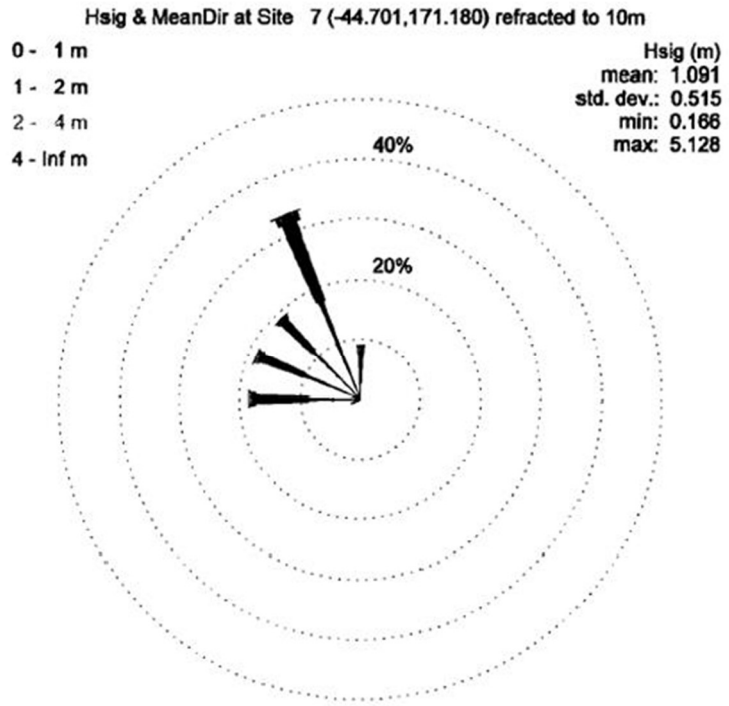

Figure 2.10. Rose plot of wave directions generated in 10 m of water off the Wainono Lagoon (From Stapleton, 2005, using Gorman *et al*., 2002 data; cited in Hicks et al, 2015). Wave climate data between 1979 and 1998. Note: directions are the direction of wave travel, contrary to the usual practice.

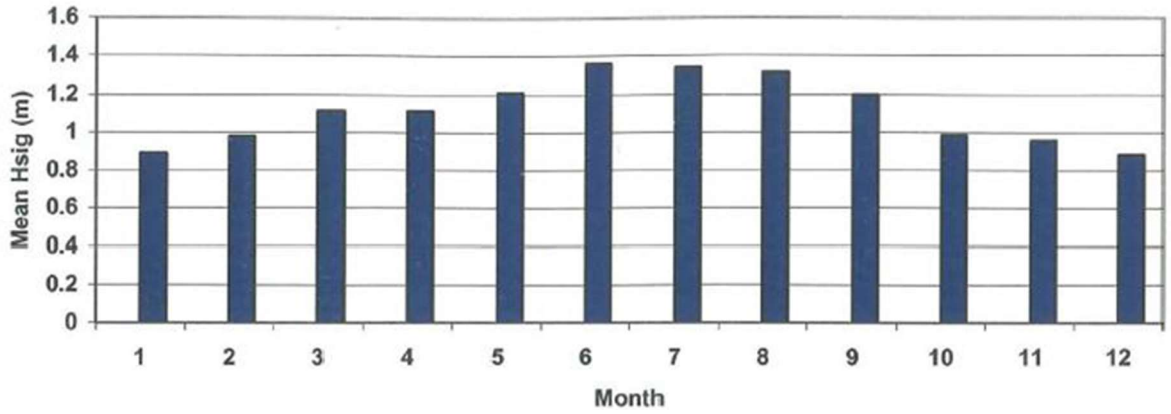

Figure 2.11. The monthly mean significant wave heights generated in 10 m of water off the Wainono Lagoon (From Stapleton, 2005, using Gorman et al., 2002 data; cited in Hicks et al, 2015). Wave climate data between 1979 and 1998.

2.5 Offshore Wind and Wave Climate at Archibald Road

A long-term offshore record of wave statistics was taken from a 0.5-degree by 0.5-degree global model of wind characteristics maintained by NOAA[1]. The 28-year record runs from 1979 until 2017 though there are some gaps. The full record of data was extracted from the model from a point corresponding to -42.5° latitude and 172.5° longitude (Figure 2.12). The wind climate at this location is summarised in the wind rose shown in (Figure 2.13), which indicates that the prevailing winds are predominantly from the south-west with secondary prevailing winds from the north-north-east; this varies from the land-based data sets because the extraction location is over 100 km offshore and not influenced by land. The wave roses indicate that the largest waves with the largest peak periods at the extraction location are derived from the south-west (Figure 2.14). The directions vary from those developed by Stapleton (2005) because they are offshore wave data (Figure 2.13) and have not refracted into the coast to the 10 m mark – transformation modelling of this dataset is presented in Section 4.

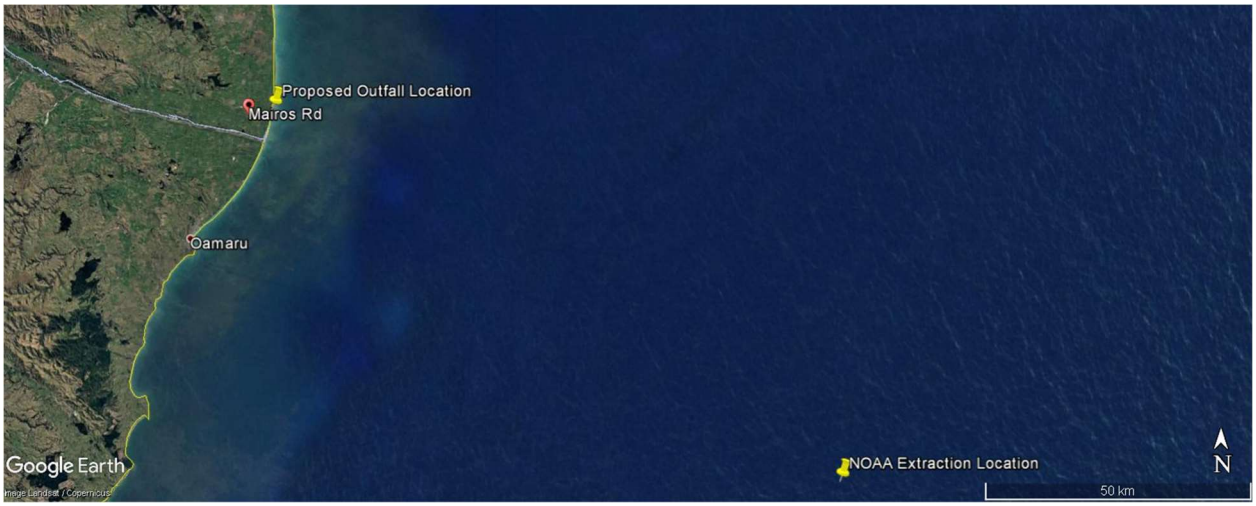

Figure 2.12. NOAA extraction location for long-term wind and wave data (1979 - 2007).

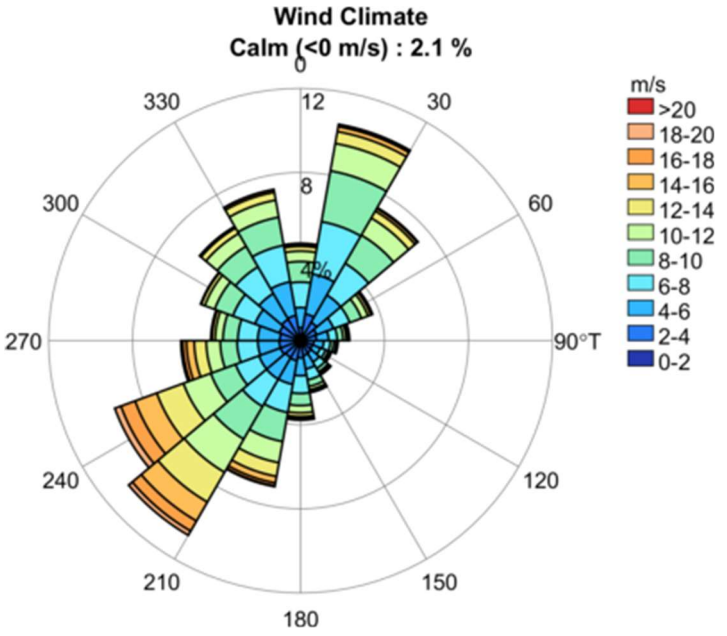

Figure 2.13. Wind rose from the hindcast wind speeds and directions extracted from the NOAA database (1979 - 2017).

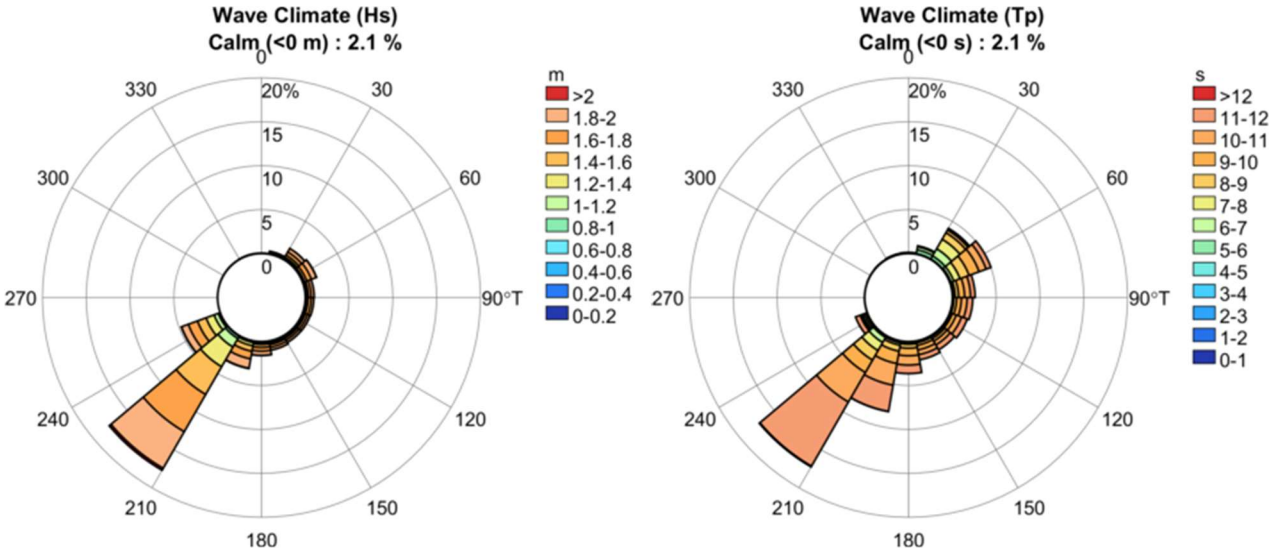

Figure 2.14. Wave roses of Hs and Tp extracted from the NOAA database (1979-2007).

2.6 Tides

The spring tidal range for the Oamaru is approximately 1.8 m. The mean spring and neap tidal ranges for Oamaru are presented in Table 2.1. Note, these are astronomical, or predicted tides. Several metocean factors including wind speed and direction, wave height, period and direction, barometric pressure influence the actual sea level at a given time.

Table 2.1. Oamaru astronomical tidal ranges to chart datum and mean sea level.

	MHWS	MHWN	MLWN	MLWS	MSL
To CD	2.3	1.9	0.8	0.5	0.9
To MSL	1.4	1.0	-0.1	-0.4	0.0

2.7 Storm Surge

Using sea levels records at Green Island and Timaru as representative sites, Goring (2004) estimated the extreme sea level of South Canterbury coast. Through tidal, storm surge and mean sea level analysis, Wainono was estimated to have a 2% annual exceedance probability (AEP) sea level of 1.74 m above Mean Sea Level (MSL) (see Table 2.2). A similar 1 in 50 year storm surge is expected for Archibald Road.

Table 2.2. 2% AEP (50-year return period) sea levels relative to MSL. The rate of sea level rise is taken to be 1.8 mm/yr over 50 years. MLOS = mean sea level from sea (Goring, 2004; cited in Hicks *et al*., 2015).

Item	Green Island	Timaru
Tide + Storm Surge	1.57	1.51
Monthly MLOS fluctuation	0.08	0.08
Present MLOS	0.00	0.03
Rising Sea Level	0.09	0.09
TOTAL m above MSL	1.74	1.71

2.8 Water Column Profile

Sneddon *et al*. (2015) deployed a mooring at about 8.5 m depth from the 25th January to the 29th March 2014. An Acoustic Doppler current profiler (ADCP) was mounted at the base of the mooring, along with a water quality meter. The ADCP was programmed to record data on currents throughout the water column in 0.5 m bins, averaged over 3-minute intervals (sampled at 1 Hz every 10 minutes) for the 63-day period (Figure 2.6).

From the 63-day deployment period, Sneddon *et al*. (2015) found that because the coastline is subject to strong wind and wave action, strong and often sustained along-shore currents, generally between 0.25-0.50 m/s, were present both heading north and south with the strongest currents flowing north of between 0.75-1.40 m/s (Figure 2.15, Figure 2.16, and Figure 2.17). Velocities at the surface reached as high as 1.70 m/s. In general, there were higher portions of currents flowing offshore (north-east and south-east) at the seabed compared to at the surface. This is attributed to “vertical circulation balancing wave-induced onshore flows at the surface”.

The same study also observed a tidal reversing pattern, however, this was ‘easily over-ridden’ by sustained wind fields. A time-series of water quality data revealed that the area is regularly influenced by low salinity surface water events with values frequently decreasing from roughly 33 to 28 PSU possibly due to buoyant freshwater from rainfall or riverine water flowing through the area. Stratification, however, was not evident and oxygen levels were high throughout the water column. Higher turbidity at the seabed was an observed feature and was attributed to benthic resuspension.

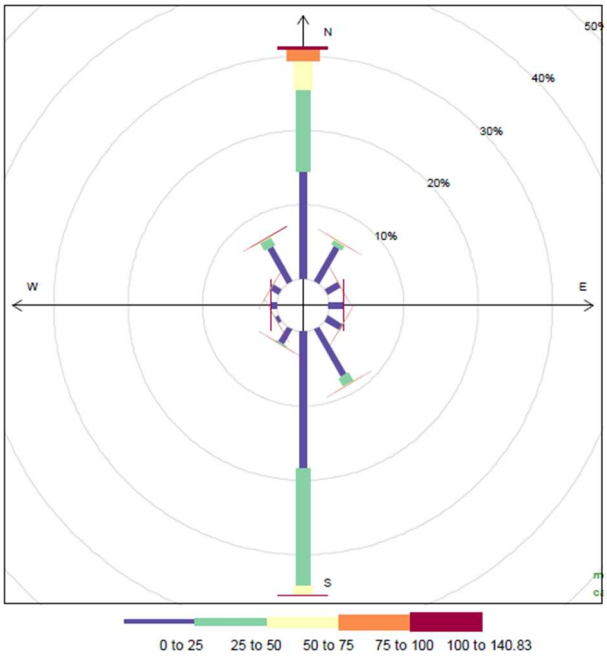

Figure 2.15. Rose plot of the depth averaged current speeds (cm/s) and directions for the period between 25 January to 29 March 2014. The plot shows frequency of counts by current direction. The plot shows the direction the water is moving toward. Each segment represents a 30-degrees direction bin. The segment colours represent the current velocities and the length of the segment represents the percentage of the currents travelling in that direction (source: Sneddon *et al*. (2015)).

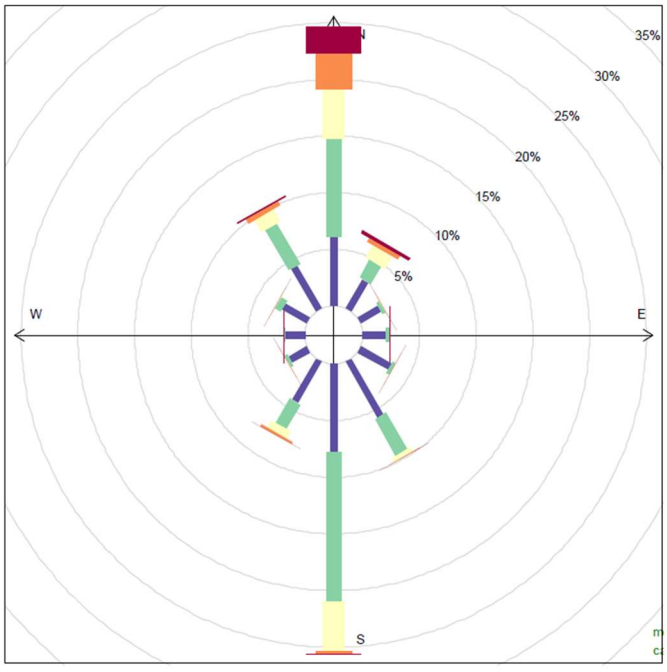

Figure 2.16. Rose plot of current speeds (cm/s) and direction measured at the surface. The plot shows the direction the water is moving toward. Each segment represents a 30-degree direction bin. The segment colours represent the current velocities and the length of the segment represents the percentage of the currents travelling in that direction (source: Sneddon *et al*. (2015)).

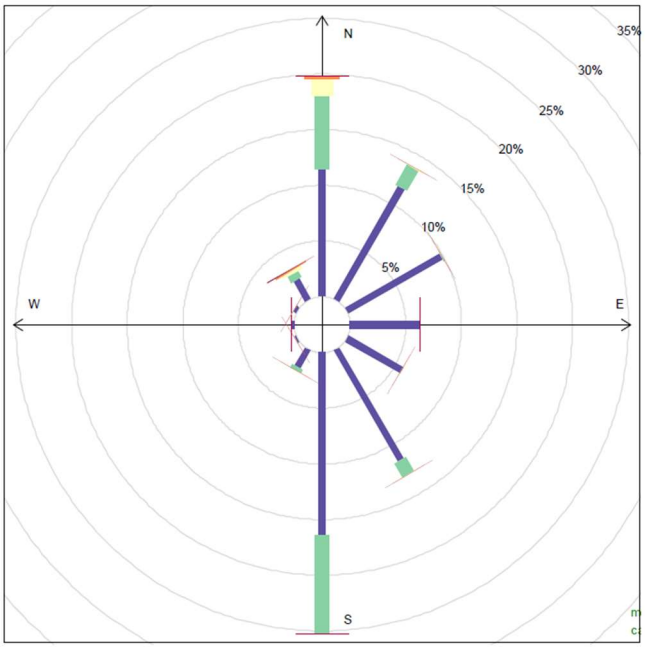

Figure 2.17. Rose plot of current speeds (cm/s) and direction measured at the seabed. The plot shows the direction the water is moving toward. Each segment represents a 30-degree direction bin. The segment colours represent the current velocities and the length of the segment represents the percentage of the currents travelling in that direction (source: Sneddon *et al*. (2015)).

2.9 Clandeboye and Studholme Currents

The Clandeboye and Studholme plots illustrate that the dominant current directions are largely a function of the coastline direction (Figure 2.18). For example, the coastline near Clandeboye is situated on a north-east to south-west axis and so too are dominant current directions. In contrast, the Studholme outfall coastal location is situated on a north to south axis and so too are the dominant current directions. This suggests that if a new ocean outfall were to be located at coastal location adjacent to the Archibald Road, the dominant coastal currents would likely be in a north-north-east to south-south-west direction.

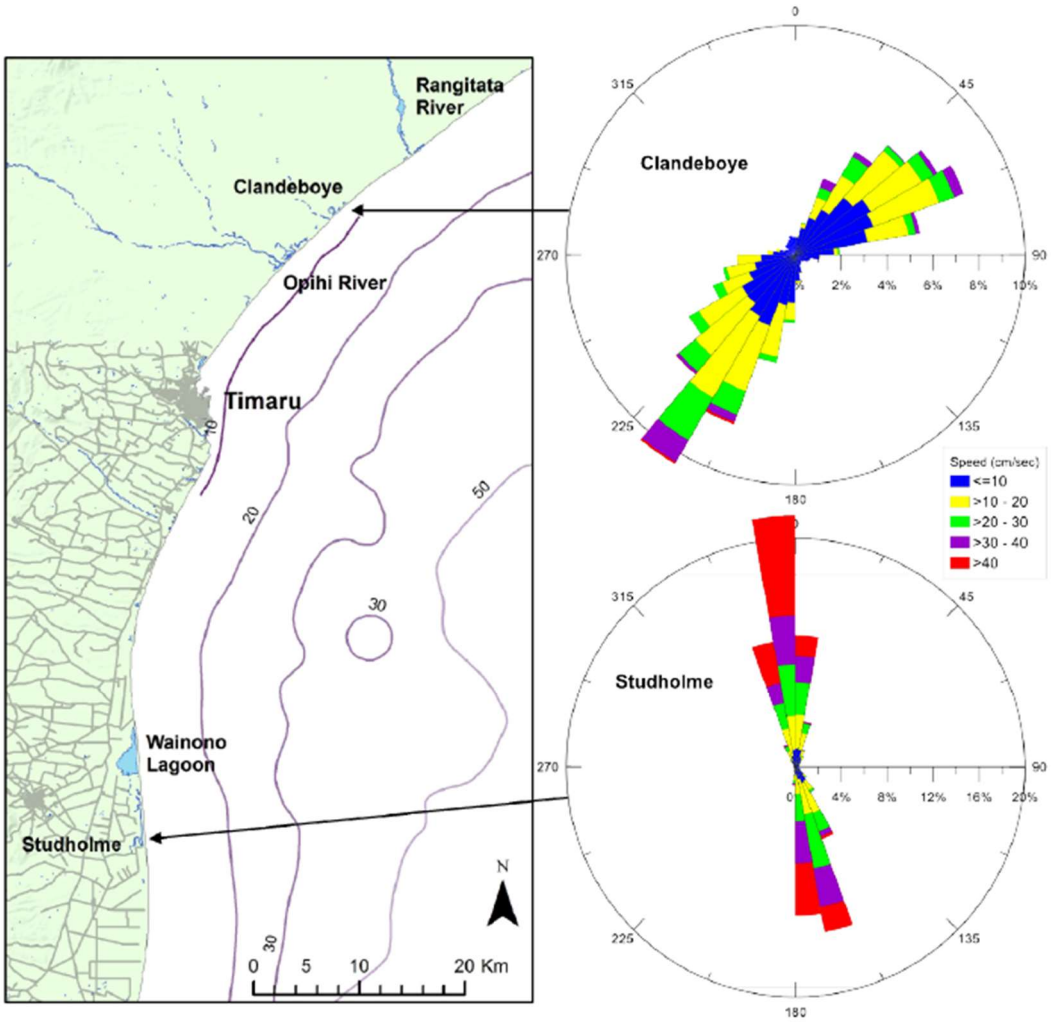

Figure 2.18. Comparison of current rose plots for 2 m depths relative to mean sea level at the Clandeboye and Studholme outfall locations. Note, both outfalls are in between 8 – 10 m of water and between 500 – 650 m offshore. Data collected for Clandeboye is from 17 January to the 24 March 2003, whereas the data collected from Studholme is from the 25 January to 29 March 2014 (Source: Sneddon *et al*. (2015)).

3 Fieldwork

Fieldwork was undertaken at the proposed outfall location in late December 2018/January 2019, which included:

- Deployment of a wave/current/water level meter ~200 m offshore along the route of the proposed outfall location.
- Beach and nearshore morphology analysis, and;
- Nearshore bathymetry and side-scan survey.

3.1 Field Data Results

3.1.1 Bathymetry Survey and Beach/Nearshore Morphology

As noted by Sneddon *et al.*, (2015), permanent hard substrate features, such as bedrock reefs are notably absent from the nearshore along this coast. Given this featureless bathymetry, it was considered that five shore-normal transects provide sufficient information in order to develop the modelling grids/domains in the absence of any chart data. The transects were surveyed out to ~600 m offshore at ~100 m intervals (Figure 3.1), the data were corrected to MSL and further data (GEBCO offshore data and digitised chart data) were added to develop the nearfield model grid (see Figure 4.1 below).

Figure 3.1. Approximate locations of bathymetry survey runlines; ~600 m offshore and ~100 m apart.

As described above, the coastline is a very dynamic, wave-exposed environment comprising steep greywacke sand and coarse gravel beaches, backed by low eroding cliffs (Figure 2.5). This results in a distinctive beach/nearshore interface, where the steep coarse gravelled intertidal beach and shallow subtidal zone becomes a relatively flat fine sand seabed. As a result, the bathymetry along this coast includes the very steep gravel beach gradient (~1:5 (V:H)) that results in water depths of ~4.5 m (to MSL) only ~20 m from the shore at low tide, where the seabed is comprised of fine sand and has a very gentle gradient offshore (~1:300 in the nearshore zone) (Figure 3.2).

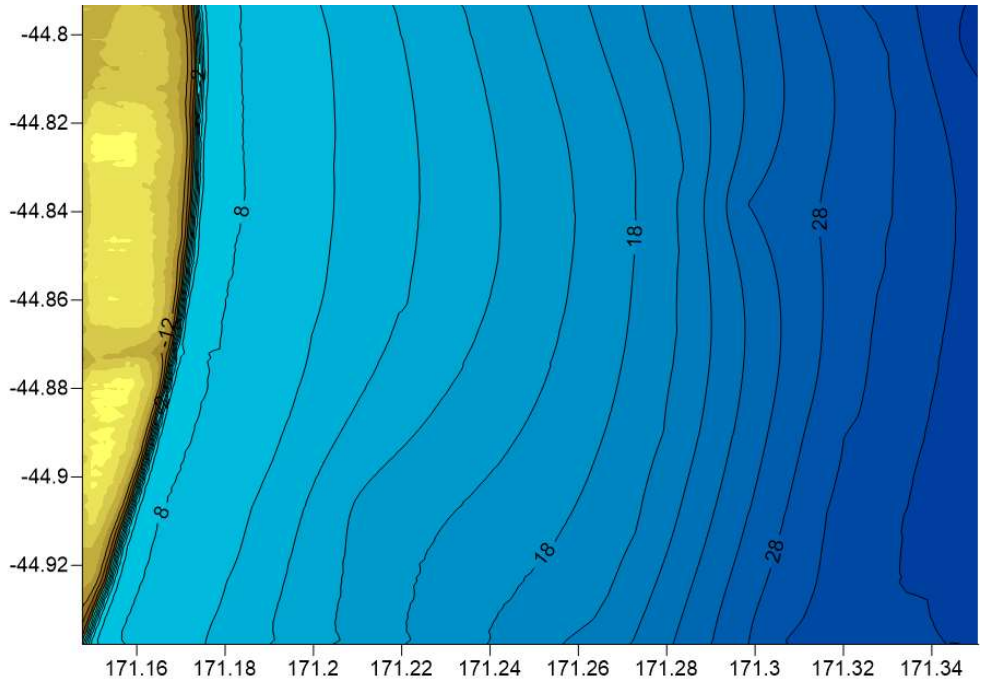

Figure 3.2. A distinct feature of the bathymetry along this coast is the very steep gravel beach gradient (~1:5 (V:H)) that results in water depths of ~4.5 m (to MSL) only ~20 m from the shore at low tide, where the seabed is comprised of fine sand and has a very gentle gradient offshore (~1:300) in the nearshore zone).

When the site was revisited to retrieve the instrument, a side-scan sonar unit was used to determine the extent of sand cover versus gravel cover in the nearshore – the underwater visibility at the site ranges from 0.3 cm at the surface to complete blackness on the seabed making it difficult to determine the seabed make-up other than by feel. The side scan confirmed that the gravel cover becomes very patchy some 10-20 m offshore of the low tide mark, and featureless fine sand comprises the seabed offshore of this. Even so, the flat nearshore seabed is comprised of a fine sand/gravel mix, with a shallow layer of fine sand at the surface. This coast is very exposed and as a consequence very dynamic, which was evident when retrieving the instrument which had been buried some 0.5 m into the seabed by mobile seabed material (a mix of sand and gravel) during high wave events.

3.1.2 Instrument Deployments

The wave/current/water level instrument (a single point Nortek Aquadopp) was deployed from 17th December 2018 to 30th January 2019. The instrument was deployed for model calibration and collection of site-specific data.

Currents speeds 0.5 m above the seabed were found to be mostly under 0.3 m/s (Figure 3.3), and were mostly shore-parallel (Figure 3.4 and Figure 3.5). As found at Studholme to the north, although the tidal currents also run shore-parallel and reserve with each change of the tide, because this coastline is subject to strong wind and wave action, strong and often sustained along-shore currents, generally between 0.25-0.50 m/s (Figure 3.3), were present both heading north and south with the strongest currents flowing north (i.e. Figure 3.5 compared to Figure 2.18). These data and the measured water level data (Figure 3.6) were used to calibrate the numerical model (Section 4).

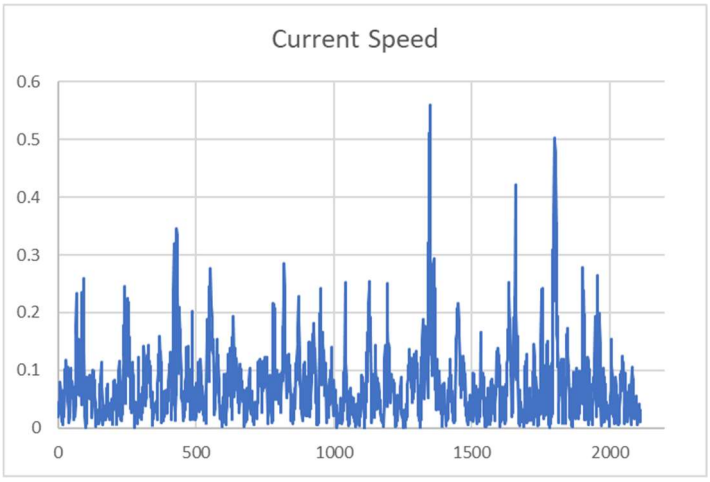

Figure 3.3. Measured current speeds offshore of Archibald Road from 17 December 2018 to 30 January 2019.

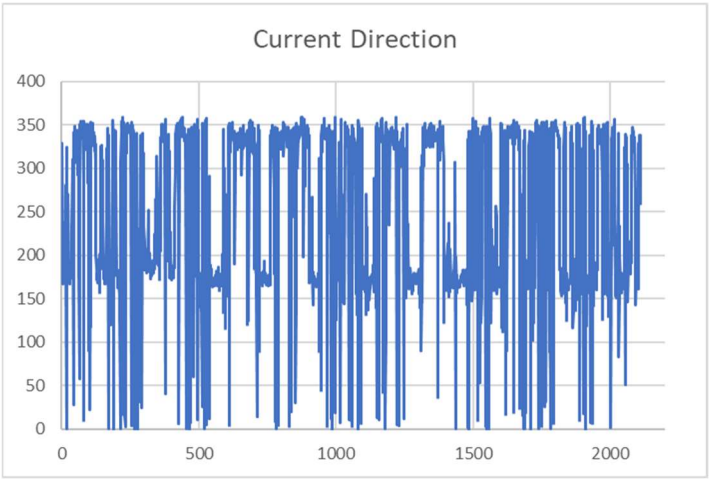

Figure 3.4. Measured current directions offshore of Archibald Road from 17 December 2018 to 30 January 2019.

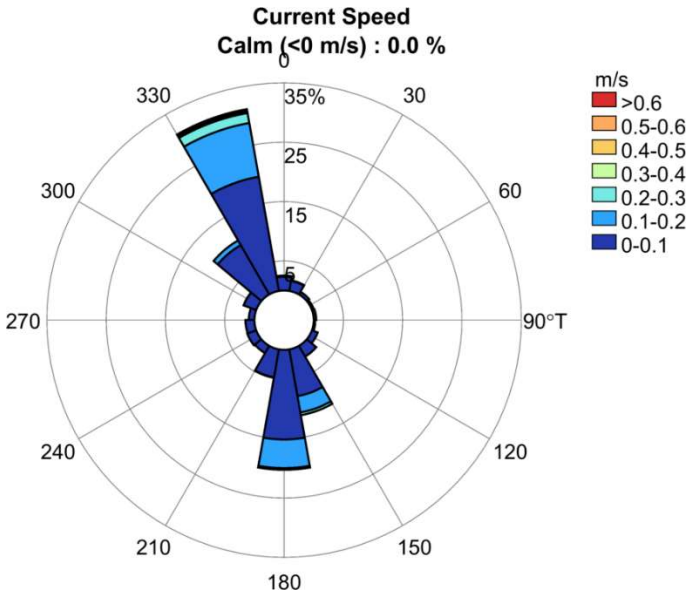

Figure 3.5. Current rose of speed/direction/occurrence measured offshore of Archibald Road from 17 December 2018 to 30 January 2019.

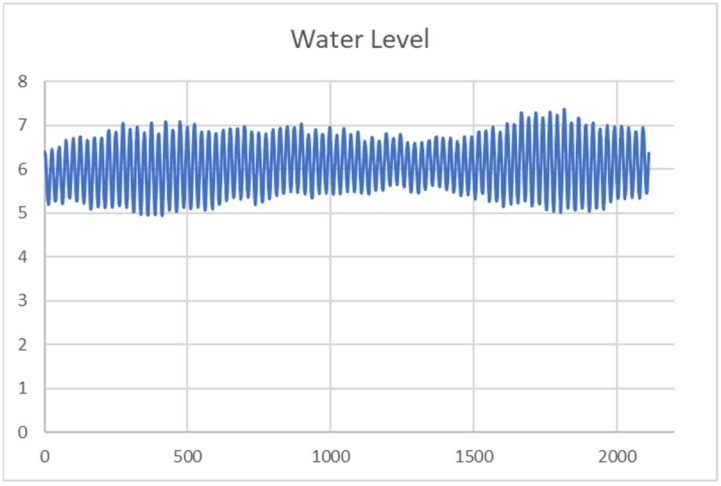

Figure 3.6. Water level showing the tidal signal measured offshore of Archibald Road from 17 December 2018 to 30 January 2019.

During the deployment, significant wave heights[1] were rarely less than 0.6 m and peaked at 1.8 m (Figure 3.7), which demonstrates the exposed nature of the site. Wave direction at the inshore site was dominantly from the southeast (Figure 3.8 and Figure 3.10), which is similar to that derived by Stapleton (2005) (Figure 2.10 - note, this figures shows wave direction towards, which is contrary to the to the usual practice). Wave period ranged from <4 to >14

[1] Significant wave height refers to the average height of the top 1/3rd of waves – maximum wave heights are approximately 1.8x significant wave height.

seconds during the deployment (Figure 3.9 and Figure 3.10), indicating the bimodal wave climate with local winds generating short period waves and the almost constant underlying long period swell. These data were also used to calibrate the numerical model (Section 4).

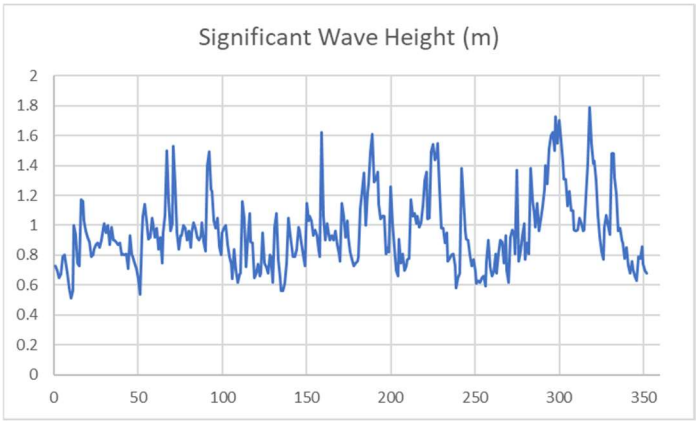

Figure 3.7. Measured significant wave height offshore of Archibald Road from 17 December 2018 to 30 January 2019.

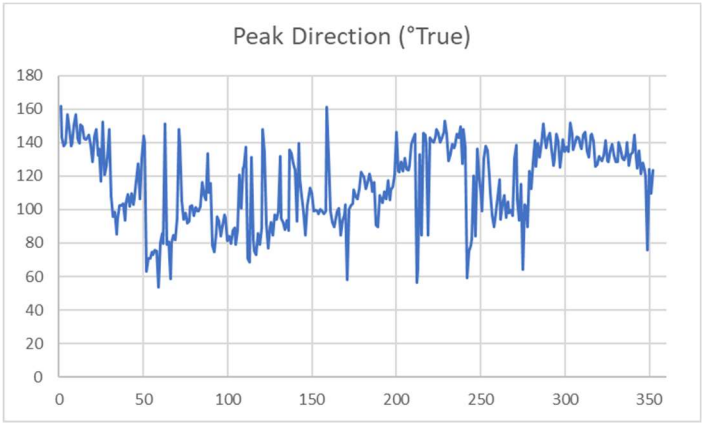

Figure 3.8. Measured wave direction offshore of Archibald Road from 17 December 2018 to 30 January 2019.

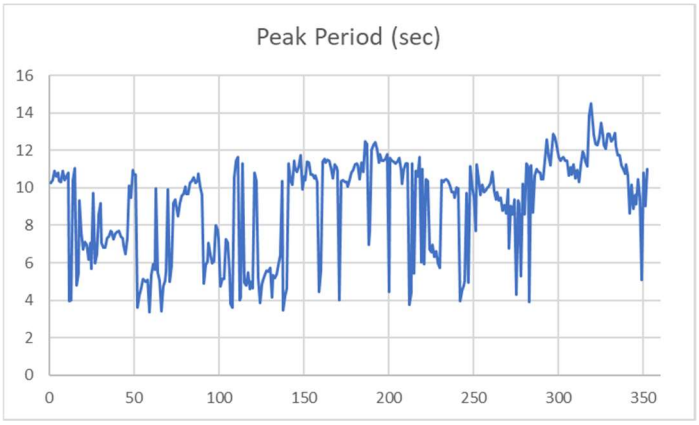

Figure 3.9. Measured wave period offshore of Archibald Road from 17 December 2018 to 30 January 2019.

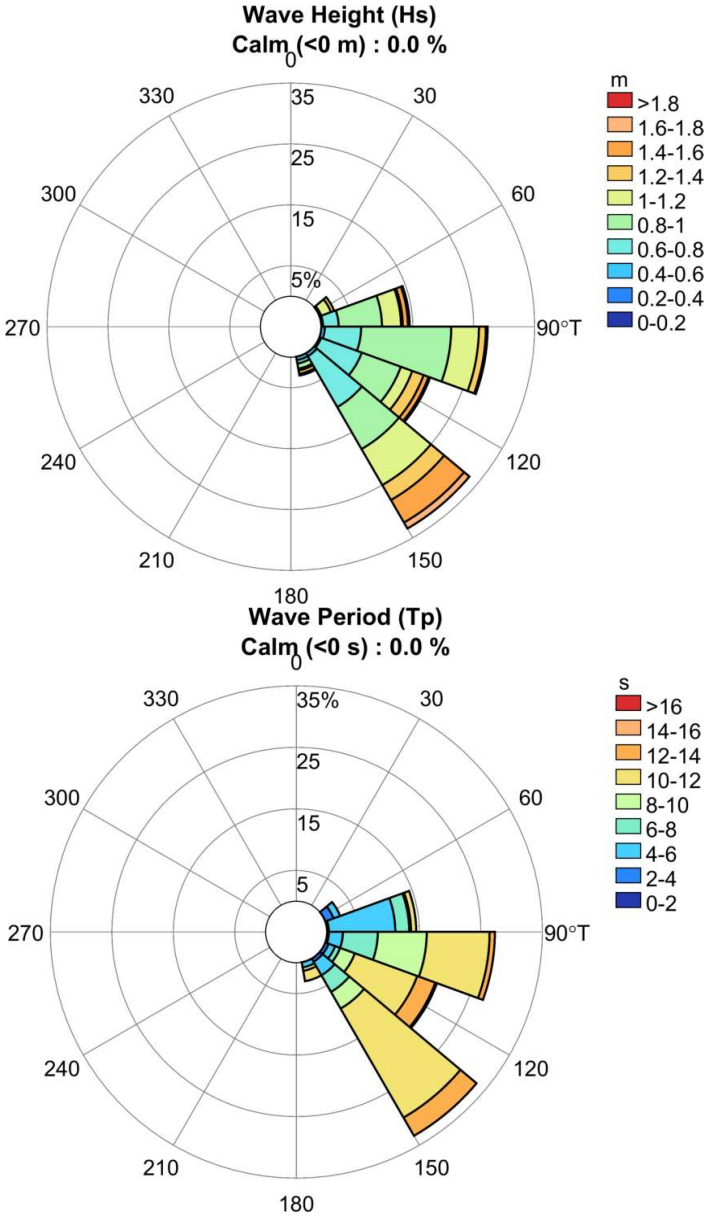

Figure 3.10. Wave roses of significant wave height/direction and occurrence (top) and wave period/direction and occurrence (bottom) measured offshore of Archibald Road from 17 December 2018 to 30 January 2019.

4 Model Development and Calibration

4.1 Model Overview

Numerical models Delft Flow and Delft Wave modules from the Delft3D Model Suite were utilised for this project, which is an industry-standard for hydrodynamic numerical modelling. Delft3D is an open source project meaning that improvements in the software come from a large-scale collaborative effort including internal developers as well as a broad base of users worldwide.

The modelling setup used a system of nested model grids using a process known as Domain Decomposition (DD). Standard nesting procedures use a coarse model run over a large model domain, and nested boundary conditions are extracted from this to run higher resolution models covering a smaller area contained within the domain of the coarse grid. DD is a dynamically coupled nesting system whereby the coarser and finer grids are run simultaneously, and information is passed between the domains (Deltares, 2013). This means that trace substances can pass seamlessly between the two grids in a way that is not possible using standard nesting. Furthermore, information pertaining to other hydrodynamic processes is not lost between domains in the nesting process as it is using standard nesting.

Since the discharge plume is buoyant, models were run with two sigma layers, a 13% surface layer and an 87% bottom layer. These numbers were chosen to obtain a 1 m surface layer thickness at the outfall location, which was modelled at depths of approximately 7-8 m.

Results from the modelling are shown as dilution by ambient water, all plots show up to 1,000-fold dilution.

4.2 Bathymetry Grids

The model was set up using a series of 4 nested rectilinear grids with increasing resolution closer to the outfall, with the coarsest grid having a cell spacing of 1,500 m and the finest 8.6 m. The bathymetry grids were developed using depth data from LINZ hydrographic charts (LINZ, 2008) and GEBCO (General Bathymetric Chart of the Oceans) data for the offshore grids in conjunction with the bathymetry survey data for the finest grid. The point cloud data was converted to gridded depths using a kriging method for all 4 grids. The final bathymetry grids are shown in Figure 4.1.

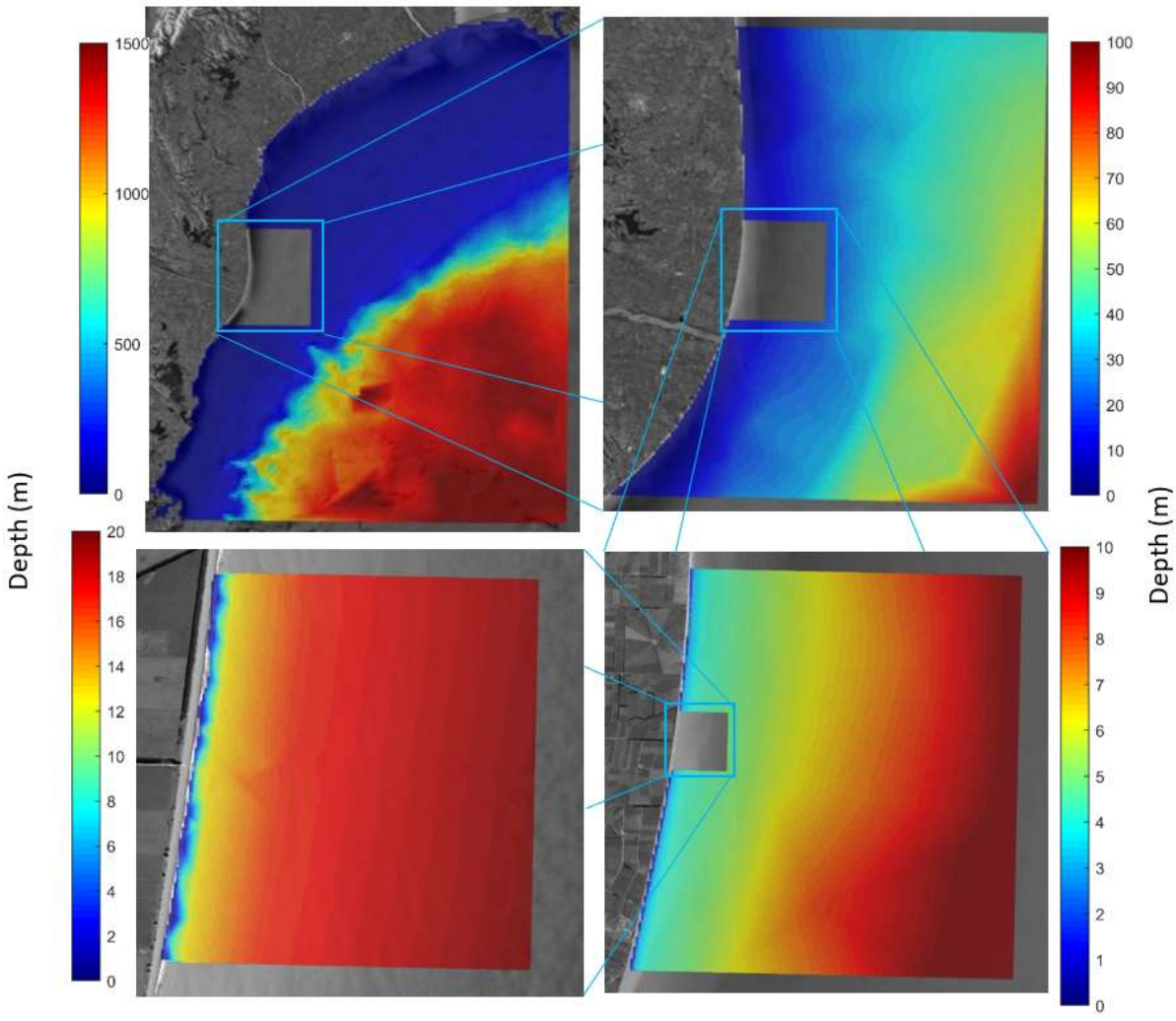

Figure 4.1. East coast of Canterbury/Otago showing nested bathymetry grids used in the hydrodynamic model with increasing resolution clockwise from top left.

4.3 Boundary Conditions

Tidal boundary conditions on the open ocean boundaries of the model were extracted from the TPXO wave atlas (Egbert and Erofeeva, 2002). This model was developed by the Oregon State University, who created a global model of ocean tides which uses along track averaged altimeter data from the TOPEX/Poseidon and Jason satellites since 2002. The methodology applied in the global tide models has been refined to create regional models at higher resolution modelling here. For this project, the Pacific Ocean model with a resolution of 1/12 degree was utilised. The model provided the 11 most influential constituents, as well as two long period (Mf, Mm) harmonic constituents. Each constituent is a sinusoid which represents the gravitational influence of a particular aspect of a planetary body or of several bodies. Each sinusoid was described in the model by a phase and amplitude of the sinusoid and these were extracted at regular intervals along the model boundary.

Wave boundary conditions for calibration were input into Delft-Wave as 2D spectra, extracted from the ECMWF ERA-Interim global atmospheric reanalysis (Berrisford et al., 2011). These spectra were applied to 12 locations around the largest model grid as 6-hourly time series. The wave model was coupled to the hydrodynamic model and used the same 4 nested grids (Figure 4.1). For the scenarios, wave parameters were entered as constants based on ECMWF data if available, and long-term NOAA Wavewatch III Reanalysis data (Tolman, 2002) otherwise. The wave parameters used were significant wave height, peak period, wave direction and directional spreading.

Wind boundary conditions for the outer 3 grids were extracted from the NCEP Climate Forecast System (Saha *et al*. 2011), which has a grid resolution of 1/5 degree. Because wind direction and magnitude were relatively homogenous throughout the model domains spatially uniform wind time series were used, extracted from a location near the model boundary. For the innermost grid, recorded wind data from Oamaru Airport Aws (NIWA, 2005) was applied over the entire domain. Long term data at Oamaru Airport was used to determine worst case and average wind conditions for modelled scenarios.

For the modelled scenarios the initial and boundary salinity in the model was set to a uniform value of 35 PSU. The outfall salinity was set to 0 PSU at a constant flow rate of 10,000 m^3/day for single outfall scenarios (Figure 4.2) and flow rates of 3,000 m^3/day, 3,000 m^3/day and 4,000 m^3/day for split outfall scenarios (Figure 4.3).

Figure 4.2. Discharge locations for the 300, 400 and 500 m offshore modelling scenarios (source, Google Earth, 2019).

Figure 4.3. Split in-line outfall discharging 3,000 m^3/day, 3,000 m^3/day and 4,000 m^3/day at distances of 300, 350 and 400 m offshore, respectively.

4.4 Model Calibration

The model calibration simulation was run for the duration of the instrument deployment with a 3-day lead in time from 14 December 2018 until 24 January 2018. This period includes a full spring-neap cycle and captures some strong wind events, with a range of 0-20 m/s predominately from the south-west (Figure 4.4, Figure 4.5 and Figure 4.6). Offshore waves were from the south-east with a mean significant wave height (Hs) and mean peak period (Tp) of 0.95 m and 9 s, respectively (Figure 4.7 and Figure 4.8).

The model accurately reproduced the Aquadopp water level record, with only a few periods of slight deviation (Figure 4.4). Current speeds were more difficult to reproduce, due to the currents being more sensitive to small scale nearshore processes (as described by Sneddon *et al*. (2015), Section 2.8). Current speeds were generally underestimated, but were reproduced well during strong wind events on January 14 and 23. Current directions on the other hand were more accurately reproduced by the model and were also strongly wind driven.

Hs was generally underestimated in the model (Figure 4.7), which will lead to reduced mixing and more conservative results. Both Tp and peak wave direction (Dp) calibrated well considering the 6-hourly boundary conditions which do not completely capture detailed dynamics.

Sensitivity testing was undertaken for both bottom roughness and horizontal eddy viscosity (Figure 4.9 and Figure 4.10). Current speeds were relatively insensitive to changes in both parameters within sensible ranges, current directions however, were more sensitive in both cases. For bottom roughness, a Chezy formula was chosen with U and V values of 65. Horizontal eddy viscosity had values increasing from outer to inner grids, the values selected were 1,000 m^2/s, 500 m^2/s, 200 m^2/s and 50 m^2/s for lowest to highest resolution grids.

In summary, model calibration is considered to be reasonably good and provides confidence in dispersion modelling results, with slightly lower wave heights, which adds some conservatism to the model outputs.

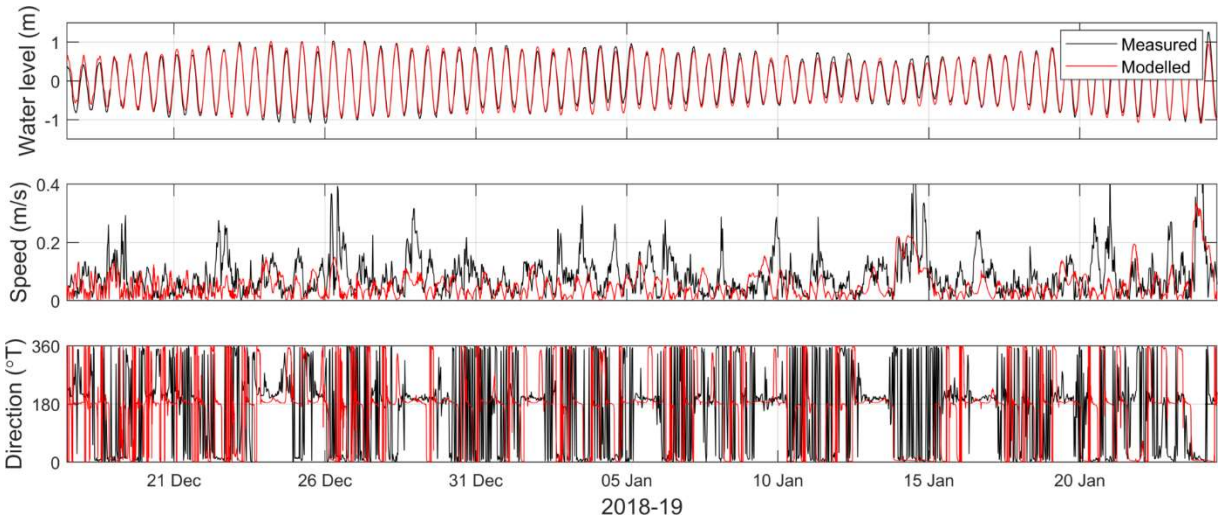

Figure 4.4. Measured and modelled water level and currents for the calibration period.

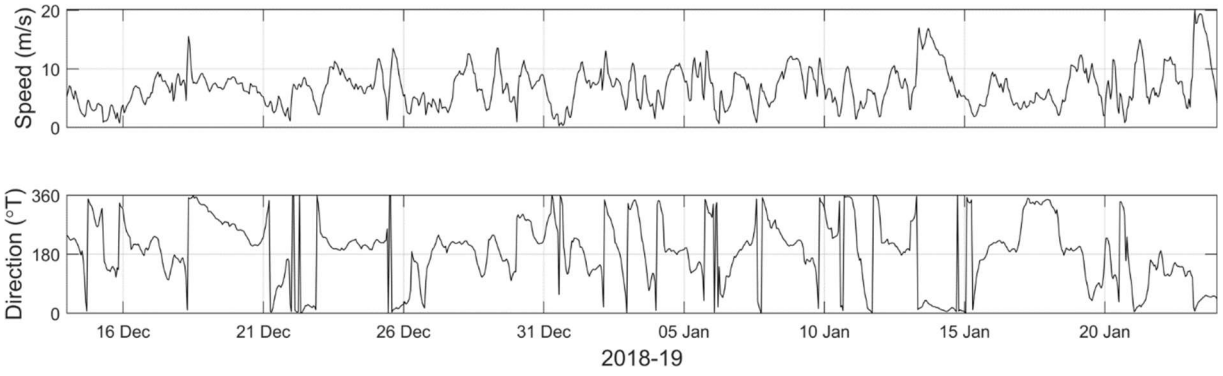

Figure 4.5. Input wind speed and direction time series for the calibration model run.

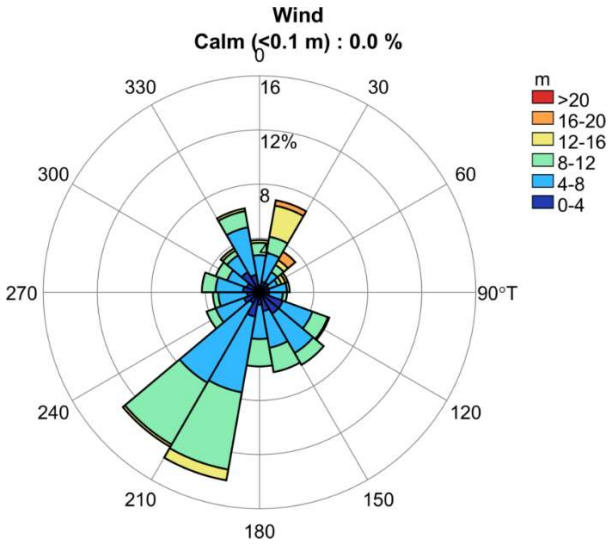

Figure 4.6. Wind rose for the calibration period.

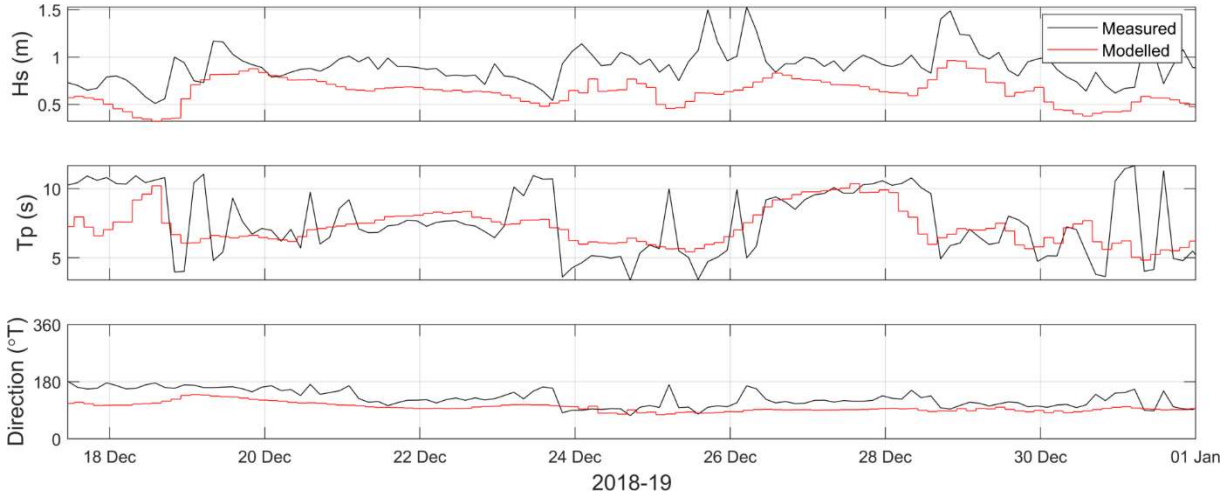

Figure 4.7. Measured and modelled significant wave height (Hs), peak period (Tp) and peak direction for the calibration period.

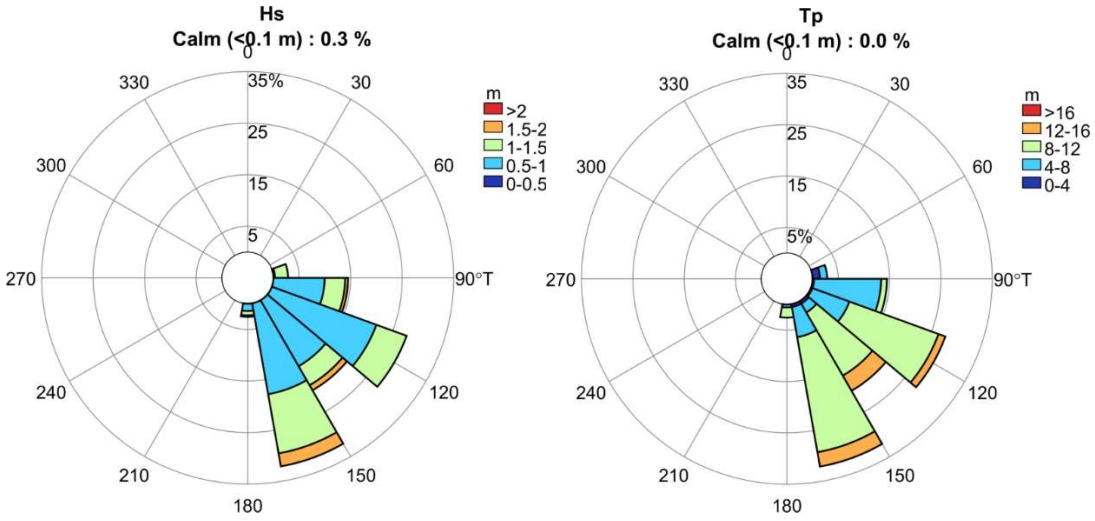

Figure 4.8. Wave roses for Hs and Tp over the calibration period.

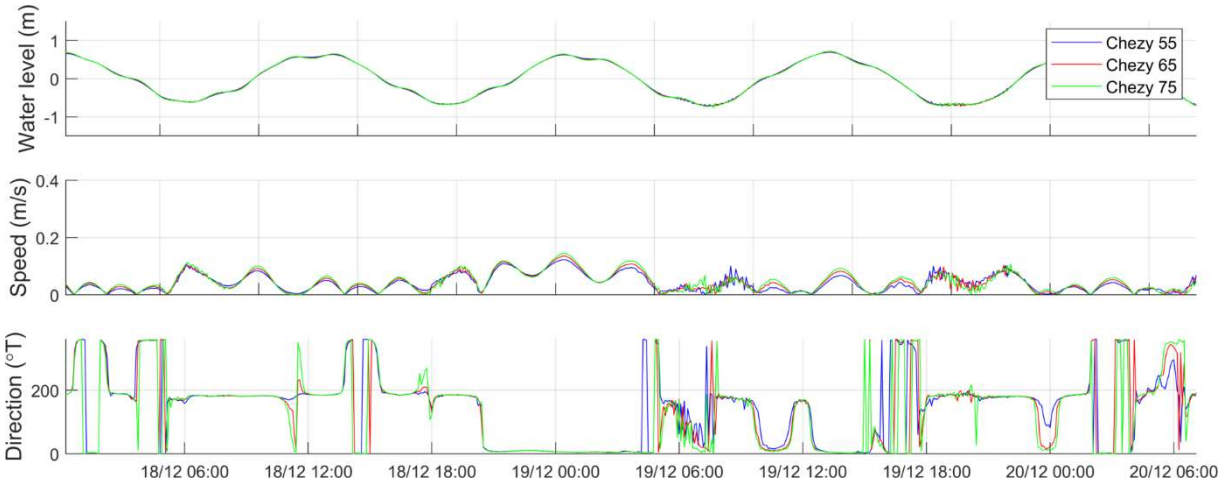

Figure 4.9. Sensitivity testing on bottom roughness using the Chezy formula.

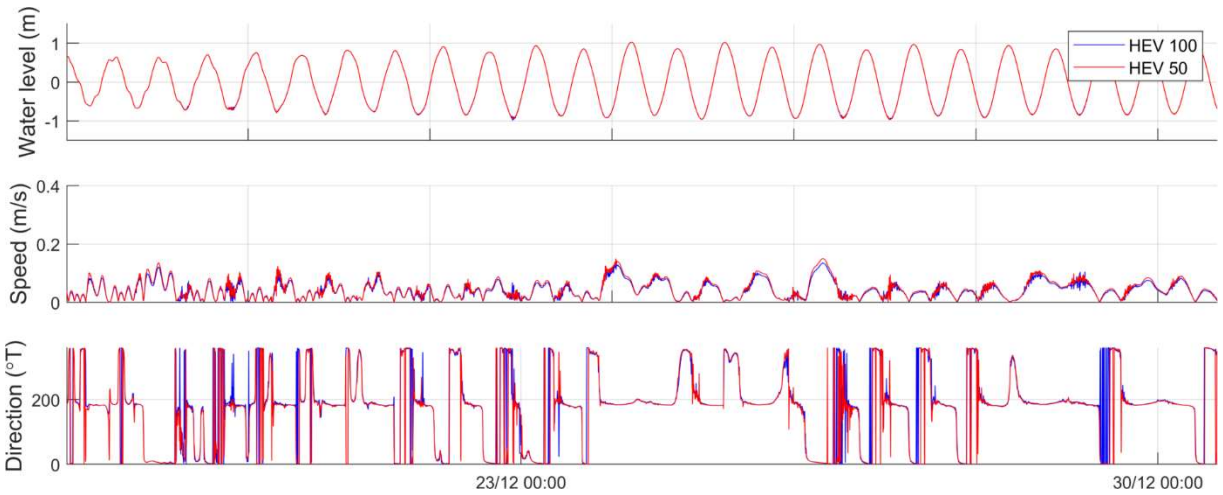

Figure 4.10. Sensitivity testing on horizontal eddy viscosity for the inner grid.

5 Discharge Modelling

In the absence of more detailed diffuser designs, the outfall water was released into the top layer of the model providing a conservative approach to initial mixing that occurs as the buoyant plume rises through the water column. Note, the cell sizes for the local model grid are 8 x 8 m, which represents 64 m^3 and results in the initial dilution value presented in the dilution transects (Figure 5.1).

To determine the extent, concentration and orientation of the outfall plumes under different scenarios, surface-layer dilution was calculated as follows:

$$d = \frac{35}{35 - s}$$

where 35 (ppt) is the background salinity and s is the salinity in the model. Dilution was calculated throughout the model domain for all timesteps after the spin up period and percentiles of dilution were calculated at each model cell. It is important to note that the dilution plots show the surface layer of the model as this is where the buoyant outfall water is expected to be most concentrated (low salinity water is less dense than sea water for a constant temperature).

Shore-normal and shore-parallel transects of surface dilution were produced, both intersecting the outfall (Figure 5.1). Finally, a representative year dilution time-series at sites of local and national recreational use (Greenaway, 2019) were produced (See Figure 5.2 for site locations).

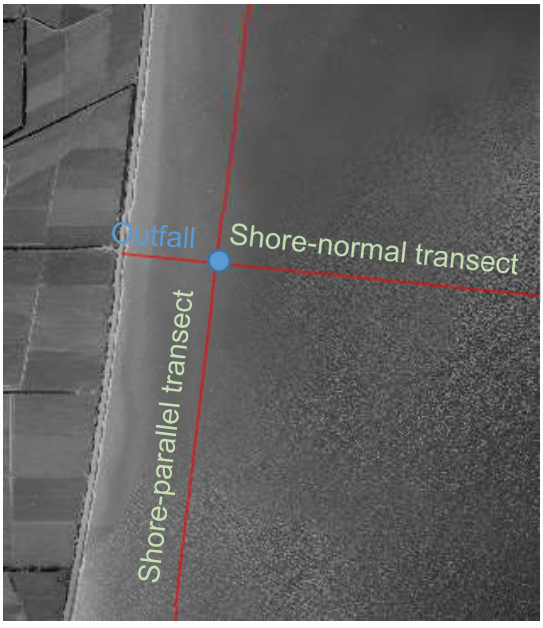

Figure 5.1. Shore-normal and shore-parallel transects used to analyse dilution. Note that in this case the outfall is 500 m from the high tide line, but in all scenarios the shore-parallel transect is moved in line with the outfall.

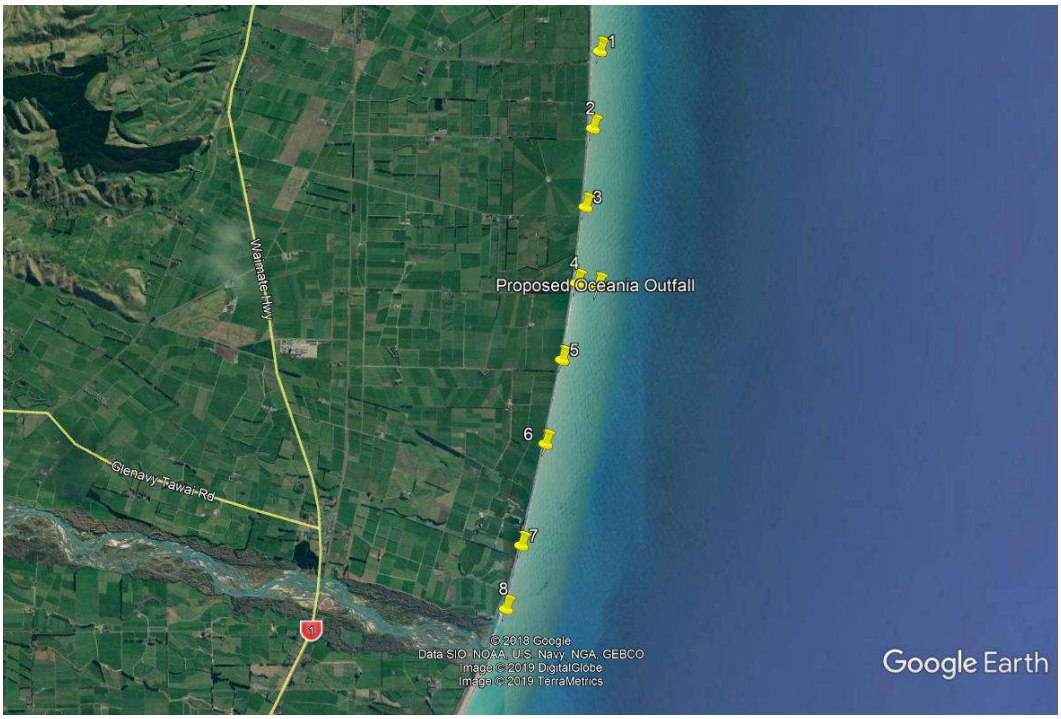

Figure 5.2. Locations of the 8 exposure sites where representative year-long dilution time series were extracted from to consider health impacts on recreational use (Greenaway, 2019).

5.1 Discharge Scenarios

The model was used to explore a range of scenarios under varying outfall locations and meteorological conditions. Initially, 12 simulations were run to represent worst-case (i.e. low mixing) and common scenarios, which are described in Table 5.1. There are four meteorological conditions which were each simulated under three outfall locations: 300 m, 400 m and 500 m from the high tide line at a flow rate of 10,000 m^3/day.(i.e. 4 conditions by 3 outfall locations = 12 scenarios).

Next, a multiple outfall design with the discharge split into three locations was also simulated for the 4 metocean conditions. The multiple outfall consists of discharges of 3,000 m^3/day at 300 m from the high tide line, 3,000 m^3/day at 350 m from the high tide line and 4,000 m^3/day at 400 m from the high tide line (Figure 4.2). Finally, a multiple outfall design was simulated for the 4 metocean conditions with a split set-up having a discharge to the north (3,000 m^3/day), to the south (3,000 m^3/day) and straight out (4,000 m^3/day) at approximately 450 m, 400 m and 500 m offshore, respectively (Figure 5.3).

Historical wind and wave data for the period 1980-2013 were used to find worst-case and average meteorological conditions. Wind and wave roses for this period are shown in Figure 5.4 and Figure 5.5. The worst-case and average scenarios modelled occur a total of 20% of the time in total.

Table 5.1: Outfall and metrological model scenarios.

	Outfall scenario	Tp (s)	Hs (m)	Dp (°)	Wind speed (m/s)	Wind dir (°)	Tidal range	Probability of occurrence
Calm	300 m	12	1	220	0	-	Neap	0.02
Calm	400 m	12	1	220	0	-	Neap	0.02
Calm	500 m	12	1	220	0	-	Neap	0.02
Calm	Multiple1	12	1	220	0	-	Neap	0.02
Calm	Multiple2	12	1	220	0	-	Neap	0.02
NE wind	300 m	12	2	220	2	40	Neap	0.13
NE wind	400 m	12	2	220	2	40	Neap	0.13
NE wind	500 m	12	2	220	2	40	Neap	0.13
NE wind	Mulitple1	12	2	220	2	40	Neap	0.13
NE wind	Multiple2	12	2	220	2	40	Neap	0.13
SW wind	300 m	12	2	220	2	200	Neap	0.02
SW wind	400 m	12	2	220	2	200	Neap	0.02
SW wind	500 m	12	2	220	2	200	Neap	0.02
SW wind	Multiple1	12	2	220	2	200	Neap	0.02
SW wind	Multiple2	12	2	220	2	200	Neap	0.02
NE waves	300 m	12	2	60	2	40	Neap	0.03
NE waves	400 m	12	2	60	2	40	Neap	0.03
NE waves	500 m	12	2	60	2	40	Neap	0.03
NE waves	Multiple1	12	2	60	2	40	Neap	0.03
NE waves	Multiple2	12	2	60	2	40	Neap	0.03

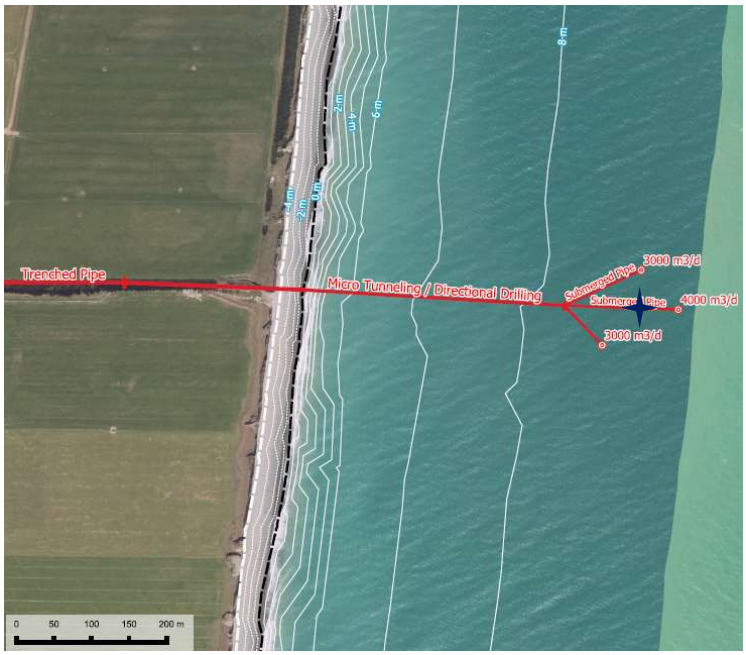

Figure 5.3. The split multiple outfall design. The star indicates the central discharge point from where the dilution transects have been plotted.

The calm condition is a realistic worst-case scenario, with no wind and low significant wave height (1 m). Non-exceedance persistence for this condition was calculated in terms of number of non-exceedance events per year (Figure 5.6). It is clear that these no wind with low significant wave height conditions are infrequent and when they do occur, they rarely persist longer than 3 hours; only some 2% of the time, or approximately 7 days out of 365 days. Mean peak direction (Tp) and peak period (Dp) during these events were determined and applied to the model. Mean Tp was approximately 12 s for all conditions, so this value was applied to all scenarios (Table 5.1). Mean Dp was found to be south-westerly for the calm condition, which was consistent with the prevailing Dp (Figure 5.5). A neap tide was used for all scenarios in order to minimise tidal currents and therefore mixing – which applies further conservation to the results.

The wind record shows that the predominant wind direction is north-easterly (Figure 5.4), so this was one of the conditions that was deemed important to simulate. The next most predominant wind direction is west-north-westerly, which as an offshore wind would push the discharge plume offshore, therefore this boundary condition was not simulated. Although south-westerly winds are not nearly as common as north-easterly winds, they make up 19% of the total wind record, which was considered enough to simulate south-westerly wind scenarios. For each scenario average Tp, Hs, Dp and wind speed were used (Table 5.1).

Although the historical record was clearly dominated by south-westerly waves (Figure 5.5), north-easterly waves (directly onshore waves) make up approximately 14% of the record.

Because this condition could potentially drive the plume shoreward, it was considered important to model as another potential worse-case scenario. Mean Tp, Hs, wind speed and direction for this condition was determined (Table 5.1).

Each of the scenarios were run over three tidal cycles with a two day spin up time. However, Following the prior scenario modelling, the calm scenario was treated differently for the final split multiple outfall design (Figure 5.3) due to the decreasing probability of persistence, as shown in Figure 5.6.

Since calm conditions rarely persist for more than 3 hours (i.e. ~2.5 events per year), and very rarely persist over 15 hours (Figure 5.6), to provide more realistic dispersion modelling results, the long-term wind records were analysed to determine the wind conditions for the time period preceding the calm conditions (i.e. the 2-day spin-up period). It was found that the majority of events that preceded calm events were light NE wind conditions, which represent the second ranked worst case scenario after calm conditions (as seen in the results presented in Appendix A).

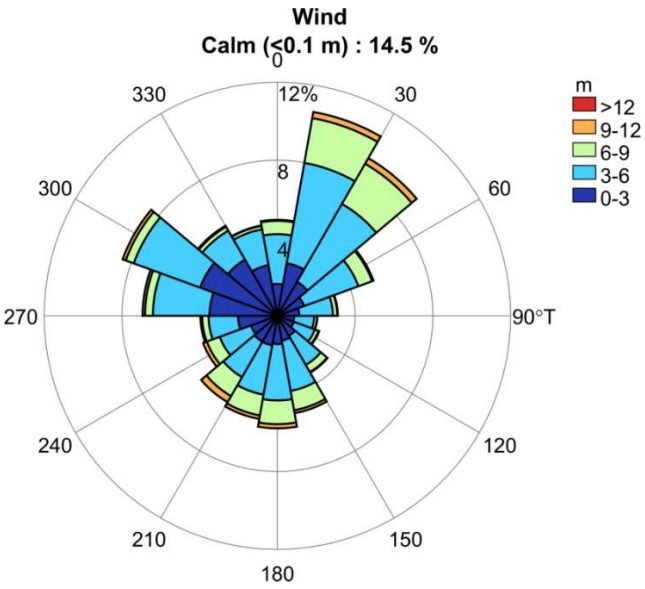

Figure 5.4. Wind rose for the period 1980-2013.

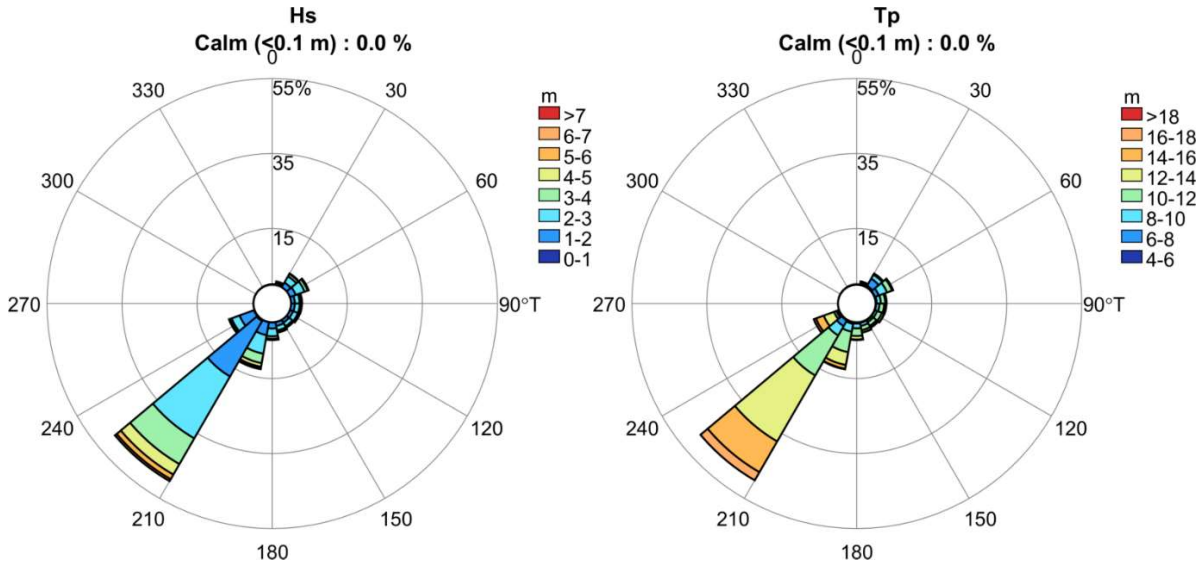

Figure 5.5. Wave roses for the period 1980-2013.

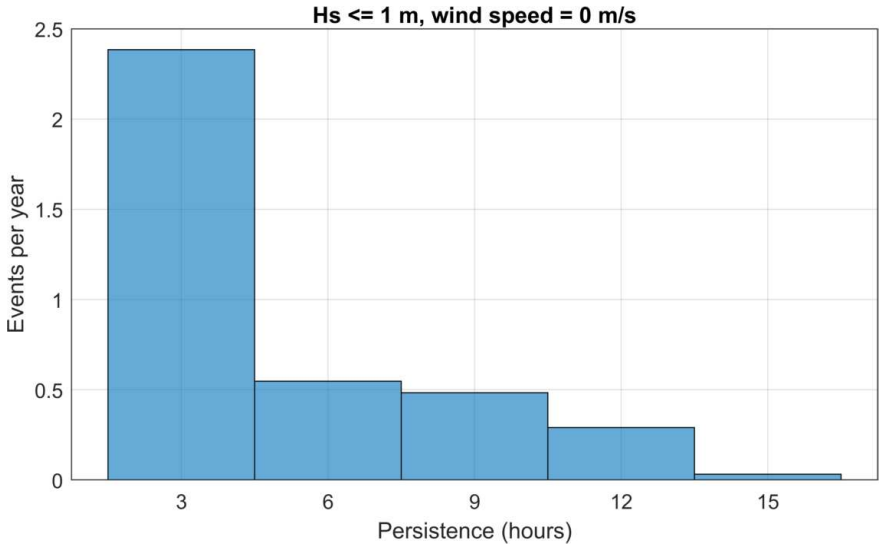

Figure 5.6. Non-exceedance persistence of the condition Hs < 1m and wind speed = 0 m/s in terms of number of non-exceedance events per year.

5.2 Results

The results are displayed in Figure 5.8 to Figure 5.15 provide surface dilution maps and dilution transects (shore-parallel and shore-normal – Figure 5.1) for the final multiple outfall layout (Figure 5.3) for each metocean scenario (Table 5.1). The results for all other outfall simulations that led to the development of the split multiple outfall (Figure 5.3) are presented in Appendix A. As would be expected, the split multiple outfall performs the best in terms of dilution in comparison to all the previous outfalls tested; the mixing zone for the multiple outfall is presented in Figure 5.7.

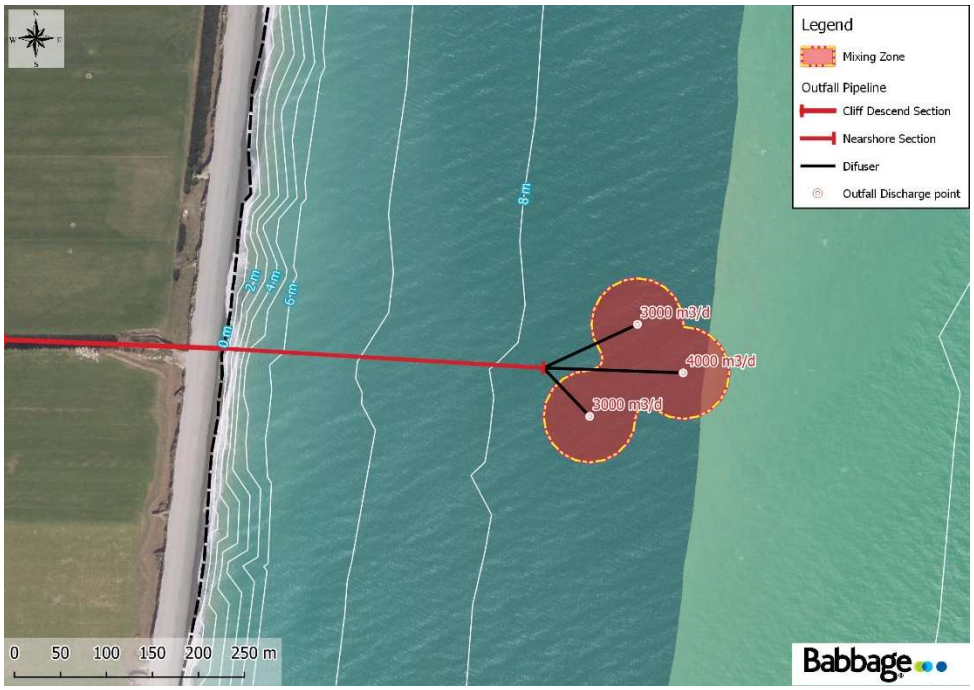

Figure 5.7. The mixing zone for the multiple outfall layout show a 50 m radius around each of the 3 discharges.

The results indicate that the dilution plume of the worst-case calm scenario (occurs 2% of the time in total) following the second-ranked NE wind scenario (occurs 11% of the time in total), which is the usual progression of metocean conditions at the site, slowly increases in size over an 18 hour duration (Figure 5.8 and Figure 5.9).

Due to the separation of the 3 outfalls, dilution of >300x occurs within approximately 30-50 m of the discharge source in all scenarios simulated. With respect to the 4 average and worst-case scenarios simulated, dilution occurs fastest during NE wave conditions, followed by SW wind conditions, NE wind conditions and calm conditions (Figure 5.8 to Figure 5.15). The exception to this is when calm conditions occur for >6 hours (Figure 5.9). However, it is likely that this scenario very rarely, if ever, occurs. This is due to a) the models inherent conservatism, and b) the likely occurrence of calm conditions for 6 hours or greater (i.e. on average only once every 2 years or less – Figure 5.6). A detailed analysis of the dilution during the worst case calm scenario is attached as Appendix B.

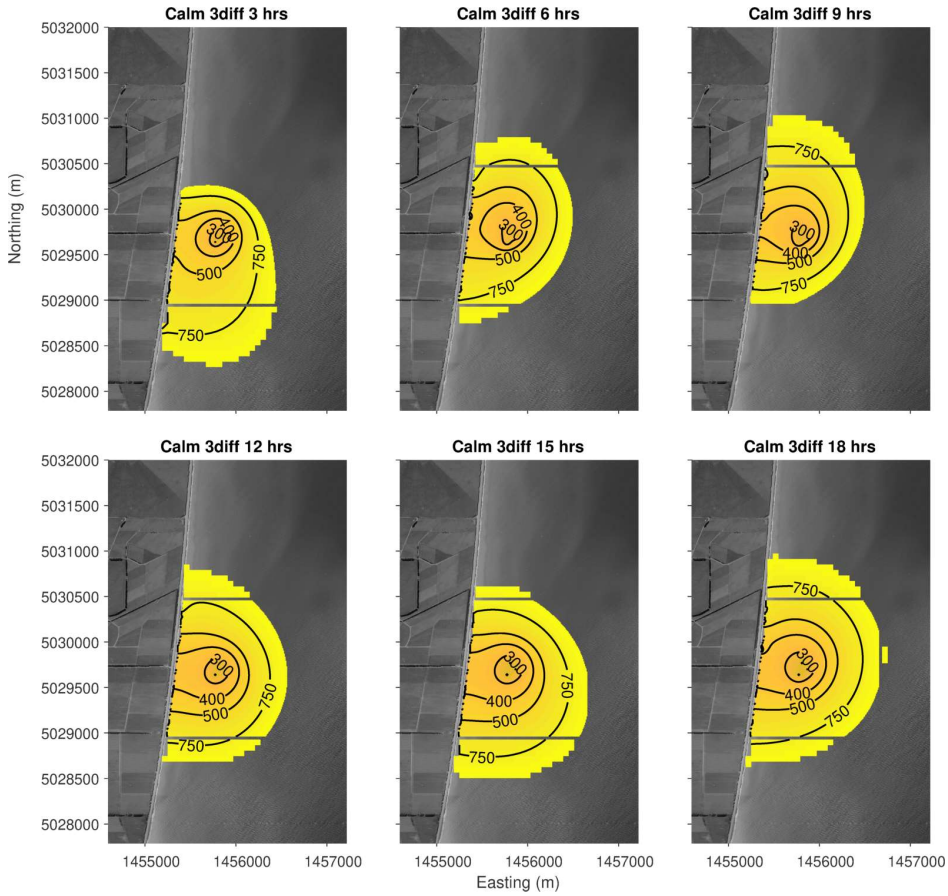

Figure 5.8. Time series (3, 6, 9, 12, 15 and 18 hours – refer to Figure 5.6) maps of the surface dilution for the calm scenario with the split multiple outfall configuration (Figure 5.3) following the most common (and second ranked worst case scenario) conditions preceding calm conditions, which is light NW winds. In the absence of wind, the plume 'wobbles' up and down coast due to reversing shore-parallel tidal currents. Grey lines show the innermost model domain.

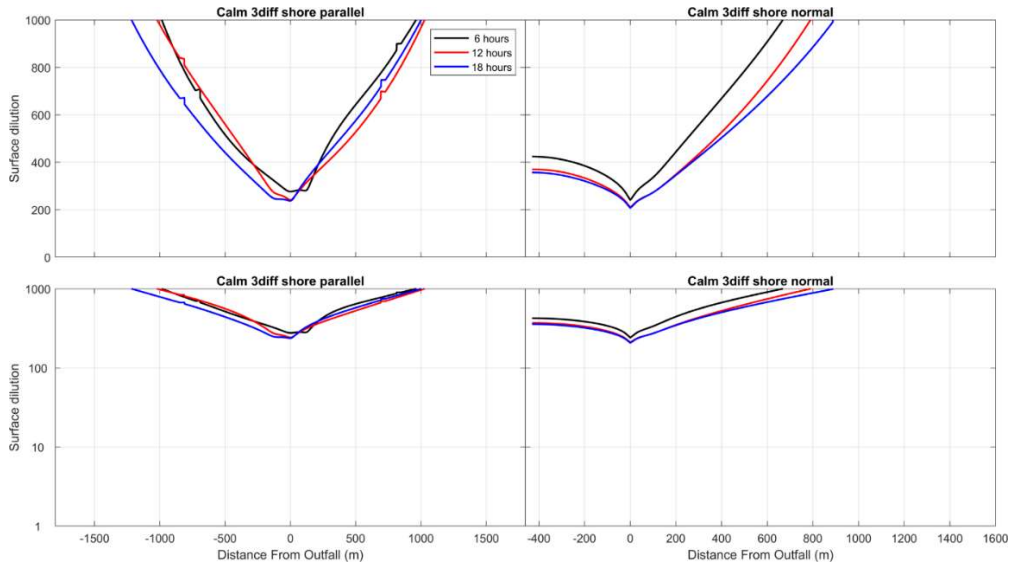

Figure 5.9. Surface dilution transects for the calm scenario with the split multiple outfall configuration (Figure 5.3) 6, 12 and 18 hours after the switch from NE winds to calm conditions. Left plots are the shore normal transects from offshore to onshore while the right plots are shore parallel transects from north-east to south-west. Lower plots are the log transformed version of their corresponding upper plot.

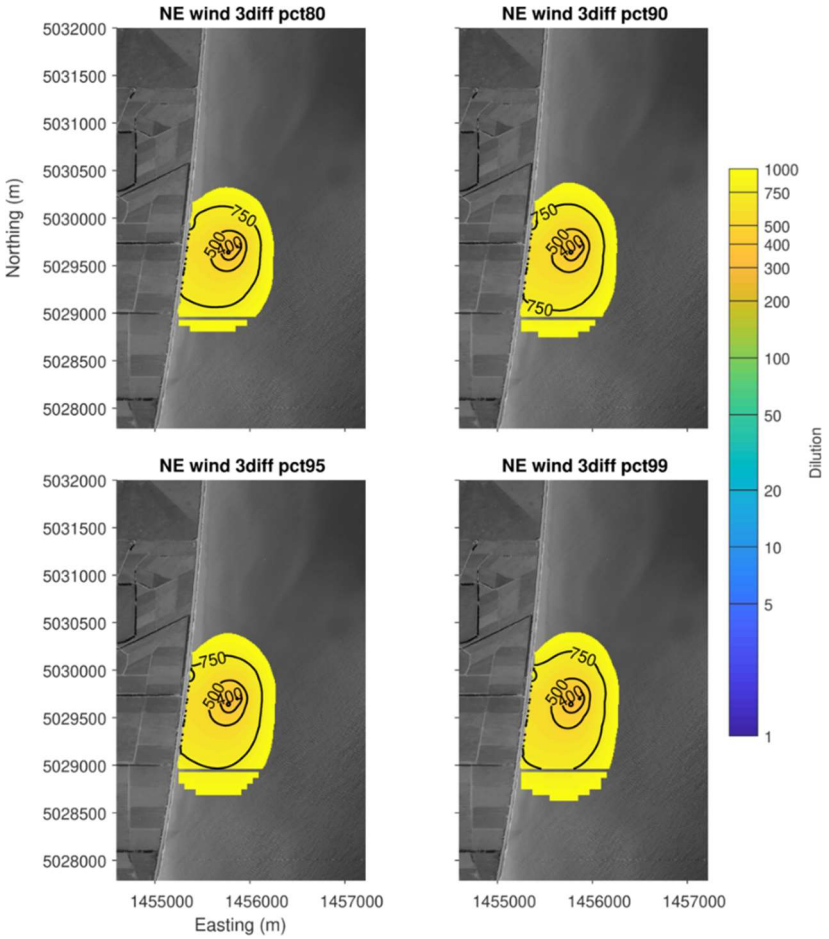

Figure 5.10. Maps of the 80th, 90th, 95th and 99th percentile surface dilution for the NE wind scenario with the split multiple outfall configuration (Figure 5.3). Grey lines show the innermost model domain.

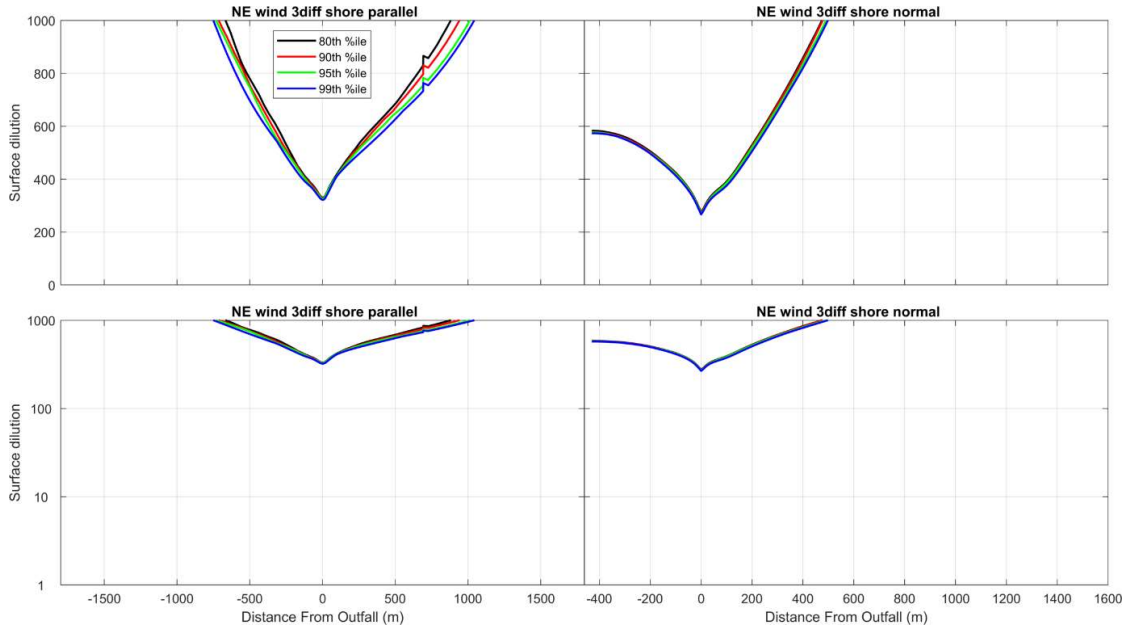

Figure 5.11. 80th, 90th, 95th and 99th percentile surface dilution transects for the NE wind scenario with the split multiple outfall configuration (Figure 5.3). Left plots are the shore normal transects from offshore to onshore while the right plots are shore parallel transects from north-east to south-west. Lower plots are the log transformed version of their corresponding upper plot.

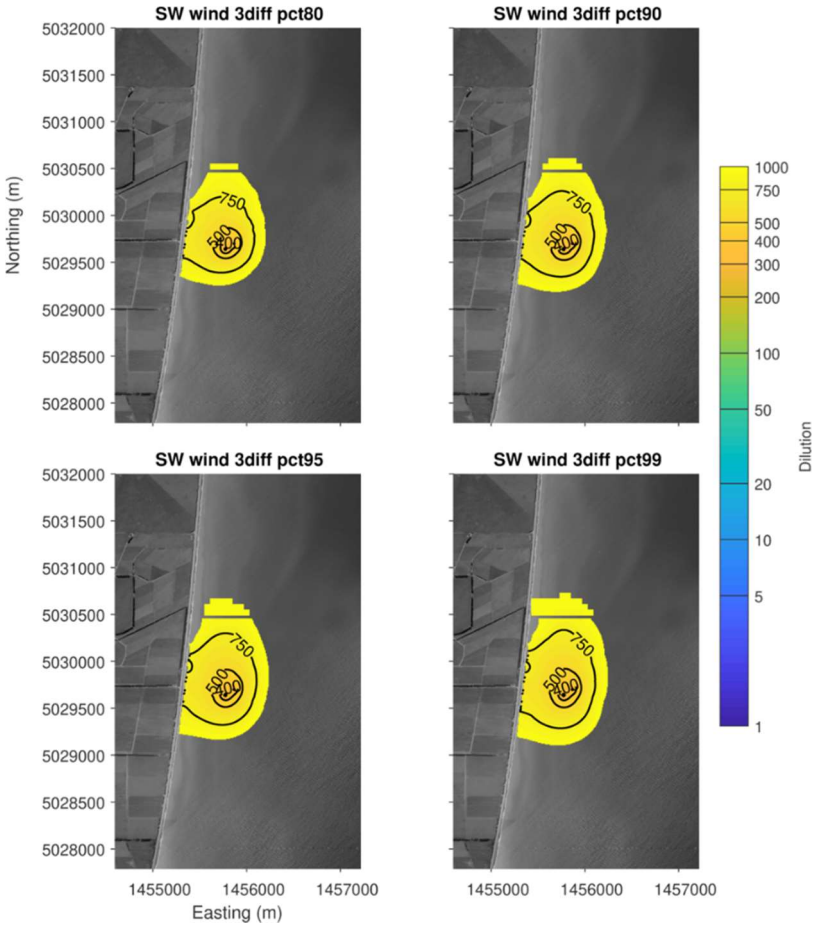

Figure 5.12. Maps of the 80th, 90th, 95th and 99th percentile surface dilution for the SW wind scenario with the split multiple outfall configuration (Figure 5.3). Grey lines show the innermost model domain.

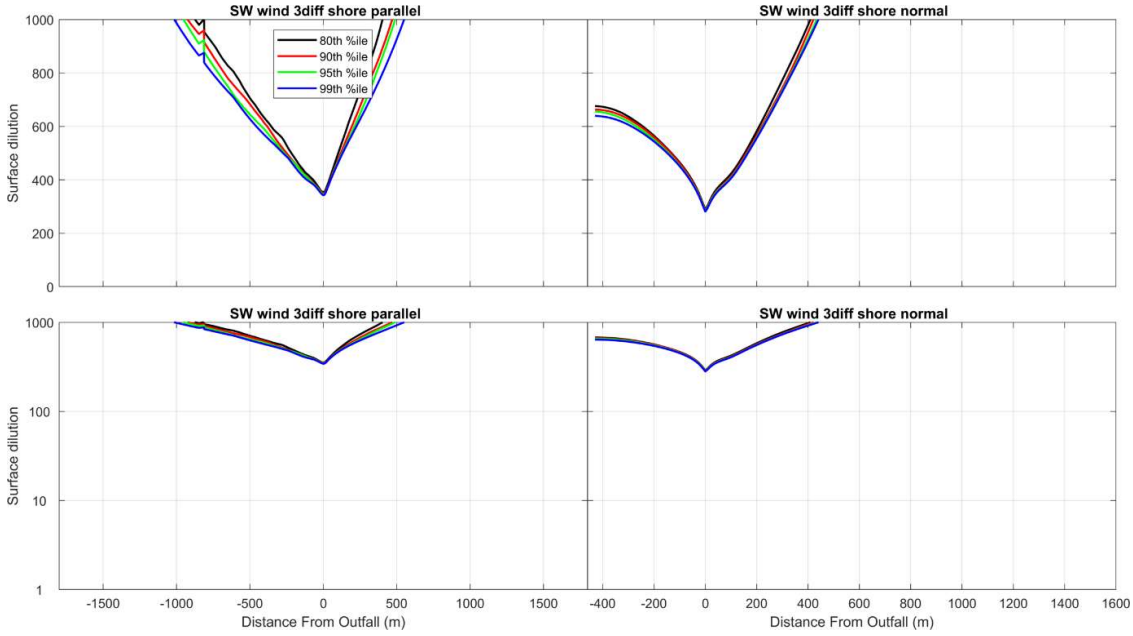

Figure 5.13. 80th, 90th, 95th and 99th percentile surface dilution transects for the SW wind scenario with the split multiple outfall configuration (Figure 5.3). Left plots are the shore normal transects from offshore to onshore while the right plots are shore parallel transects from north-east to south-west. Lower plots are the log transformed version of their corresponding upper plot.

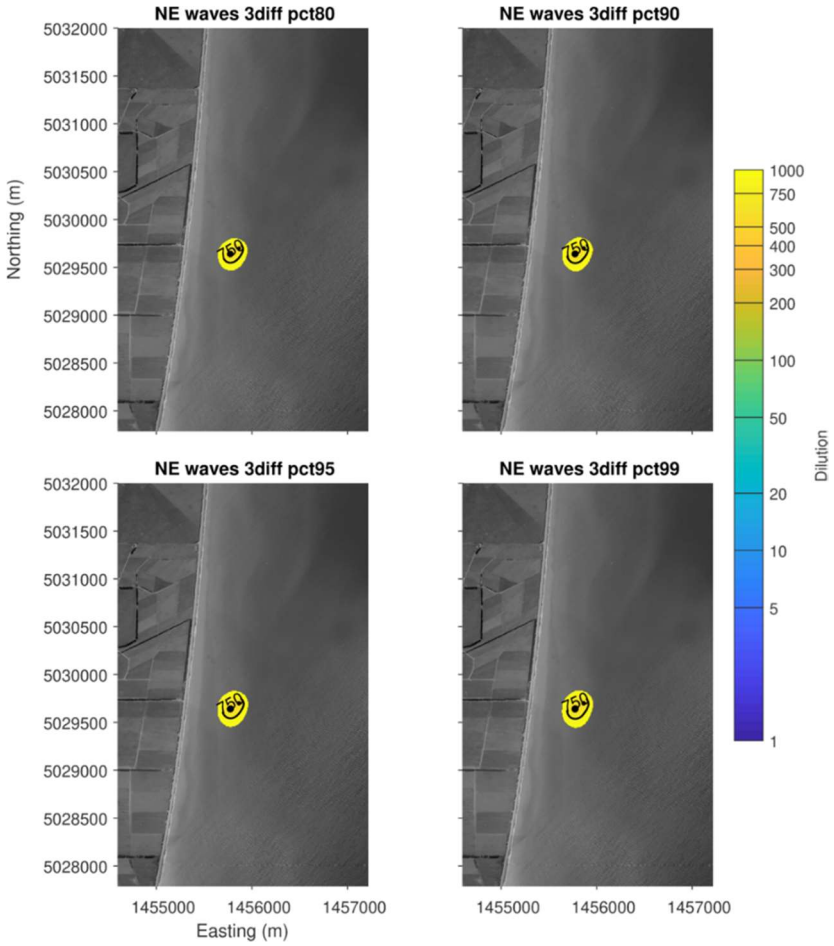

Figure 5.14. Maps of the 80th, 90th, 95th and 99th percentile surface dilution for the NE waves scenario with the split multiple outfall configuration (Figure 5.3). Grey lines show the innermost model domain.

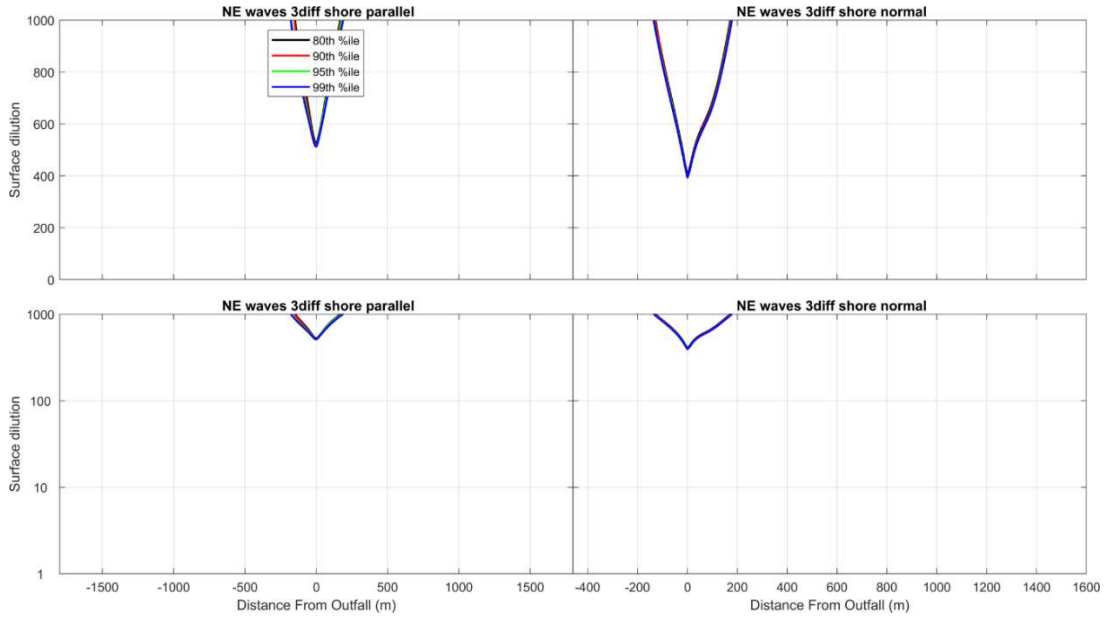

Figure 5.15. 80th, 90th, 95th and 99th percentile surface dilution transects for the NE waves scenario with split multiple outfall configuration (Figure 5.3). Left plots are the shore normal transects from offshore to onshore while the right plots are shore parallel transects from north-east to south-west. Lower plots are the log transformed version of their corresponding upper plot.

5.3 Summary and Conclusions

Field data were collected for the development of a calibrated hydrodynamic numerical model for the investigation of dilution scenarios for the proposed Oceania outfall. Long-term coincident wind and wave data were analysed to determine the average and worst-case metocean scenarios. These conditions were found to be:

- Calm conditions (no wind and small offshore wave conditions – 1 m waves at 12 seconds) worst-case 2% of the time in total;
- Light NE (onshore) winds (2 m/s wind speed with average offshore waves – 2 m at 12 seconds) 2nd worst-case 11% of the time in total;
- Light SW winds and average offshore waves (2 m/s wind speed, 2 m waves at 12 seconds) 2% of the time in total, and;
- Light NE winds with average NE offshore waves (2 m/s wind speed, 2 m waves at 12 seconds) 3% of the time in total.

The rest of the time (i.e., 80%) more energetic wind and wave conditions occur. As noted by Hicks *et al*. (2015), the South Canterbury coastline is very exposed and subject to frequent winter storms. As a result, oceanic outfalls in this region are not uncommon because of the ability of the coastline to rapidly mix treated wastewater in ambient sea water, in turn reducing ecological impacts.

The maximum daily outfall volume of 10,000 m^3/day was applied as the outfall boundary condition in the model simulations. The modelling results are considered conservative (i.e. greater/faster dilution will likely occur) since:

- The calibrated model slightly underestimated significant wave heights (i.e., a physical factor that aids mixing/dilution);
- A neap tide was used for all scenarios in order to minimise tidal currents and therefore mixing (although there is no inter-dependence between tides and metocean conditions), and;
- The outfall water was released into the top layer of the model providing a conservative approach to initial mixing that occurs as the buoyant plume rises through the water column.

Through an iterative approach where the outfall distance was first increased offshore and then divided into 3 outfalls that split the volume at each discharge point (i.e., 3,000, 3,000 and 4,000 m3/day at each), a split outfall configuration discharging at 3 locations between 450 and 500 m offshore was found to result in the fastest dilution for all of the metocean scenarios. Due to the split configuration, dilution of 300x or greater occurs within 10-50 m of the outfall in all 4

metocean scenarios. The exception to this is when calm conditions occur for >6 hours (Figure 5.9). However, it is likely that this scenario very rarely, if ever, occurs. This is due to a) the models inherent conservatism described above, and b) the likely occurrence of calm conditions for 6 hours or greater (i.e. on average only once every 2 years or less – Figure 5.6).

Once the split multiple outfall had been found to result in efficient dilution of the outfall discharge, a representative year-long discharge was simulated, and hourly dilution time-series data were extracted from the 8 sites identified by Greenaway (2018) that were used to consider health impacts along the coast.

References

Abell, J., Jones, H. & Hamilton, D. (2015). Hydrodynamic–ecological modelling to support assessment of water quality management options for Wainono Lagoon. Aquatic Analytics Ltd. Report for Environment Canterbury. 85p.

Berrisford, P., Kallberg, P., Kobayashi, S., Dee, D., Uppala, S., Simmons, A.J., Poli, P. & Sato, H. (2011). Atmospheric conservation properties in ERA-Interim**.** *Quarterly Journal of the Royal Meteorological Society*, 13(659), 1381-1399.

Davies, J. L. (1972). Geographical variation in coastal development. Oliver and Boyd.

Deltares, 2013a. User Manual Delft3D-WAVE. version: 3.05.27794, Published and printed by: Deltares, 222 p. available online: http://oss.deltares.nl/web/delft3d/manuals.

Environment Canterbury. (2004). Waihao River floodplain management strategy: October 2004. Environment Canterbury (Christchurch), in consultation with Waimate District Council.36 p.

Egbert, G.D., & S.Y. Erofeeva, (2002), Efficient inverse modelling of barotropic ocean tides, J. Atmos. Oceanic Technol., 19(2), 183-204.

Goring, D. (2004): Extreme Sea Levels in South Canterbury, Unpublished Report for Meridian Energy Limited.

Greenaway, R. (2019). Oceania Dairy – Proposed Ocean Outfall Recreation Effects Assessment. Prepared for Babbage Consultants Ltd - incomplete draft.

Hicks, D. M., Hoyle., J. & Bind, J. (2015). Studholme outfall: Coastal processes and hazards assessment. Prepared for Fonterra Ltd. NIWA client report No: CHC2015-19. 83p.

Hicks, D.M, Wild, M, Todd, D. (2002): Project Aqua: Coastal and river mouth effects. Report for Meridian Energy Ltd. NIWA Client Report CHC01/112.

Jenner, G. & Swaffeild, M. (2015). Studholme pipeline and outfall: Assessment of Environmental Effects. Prepared for Fonterra Limited. Becca Ltd.

Kirk, R. M. (1980). Mixed sand and gravel beaches: morphology, processes and sediments. *Progress in physical geography*, *4*(2), 189-210.

Land Information New Zealand. (2008). Chart NZ 64 Banks Peninsula to Otago Peninsula. Retrieved from https://data.linz.govt.nz/layer/51256-chart-nz-64-banks-peninsula-to-otago-peninsula.

National Institute of Water and Atmospheric Research (2005). Oamaru Airport Aws. Retrieved from https://cliflo.niwa.co.nz/.

Saha, S., et al. 2011, updated monthly. NCEP Climate Forecast System Version 2 (CFSv2) Selected Hourly Time-Series Products. Research Data Archive at the National Center for Atmospheric Research, Computational and Information Systems Laboratory. https://doi.org/10.5065/D6N877VB.

Sneddon, R., Dunmore, R., Barter, P., Clement, D., Melville, d., Kelly, D. & Elvines, D. (2015). Ecological investigations and effects of the proposed Fonterra Studholme outfall. Prepared for Fonterra Limited. Cawthron Report No. 2666. 141 p. plus appendices.

Stapleton, J. (2005). Form and function of the Waihao – Wainono Barrier, South Canterbury. MSc Thesis; Department of Geography, University of Canterbury.

Tolman H.L. (2002). Validation of WAVEWATCH III version 1.15 for a global domain. NOAA / NWS / NCEP / OMB Technical Note Nr. 213, 33 pp.

Appendix A. Dilution Simulation Results for the single 300 m, 400 m and 500 m outfalls, and the in-line 300/400/500 m multiple outfall for the 4 Metocean Conditions (Average and Worst-Case – 20% of all Conditions that occur at the site).

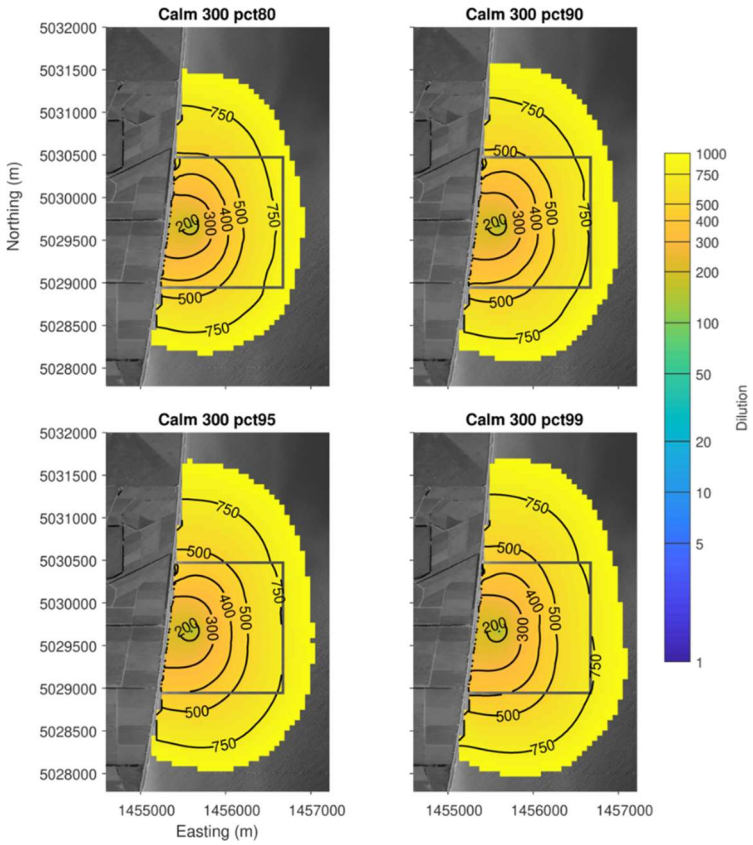

Figure 0.1. Maps of the 80th, 90th, 95th and 99th percentile surface dilution for the calm scenario with the outfall 300 m from the high tide line. Grey lines show the innermost model domain.

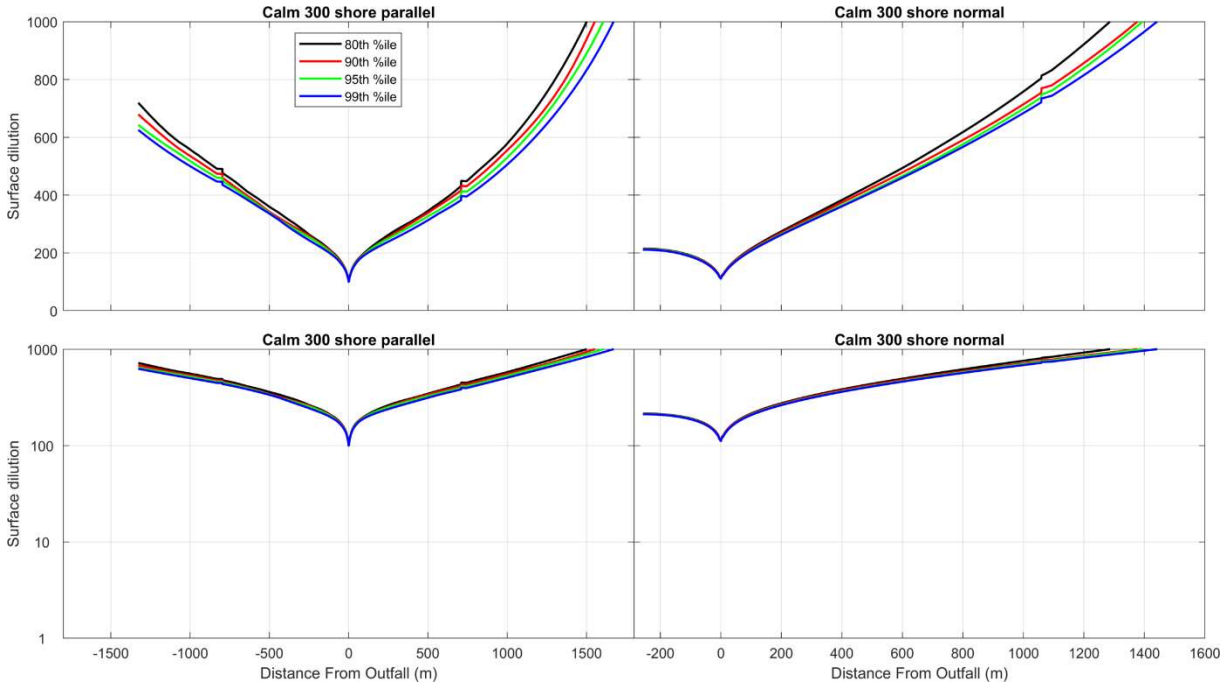

Figure 0.2. 80th, 90th, 95th and 99th percentile surface dilution transects for the calm scenario with the outfall 300 m from the high tide line. Left plots are the shore normal transects from offshore to onshore while the right plots are shore parallel transects from north-east to south-west. Lower plots are the log transformed version of their corresponding upper plot.

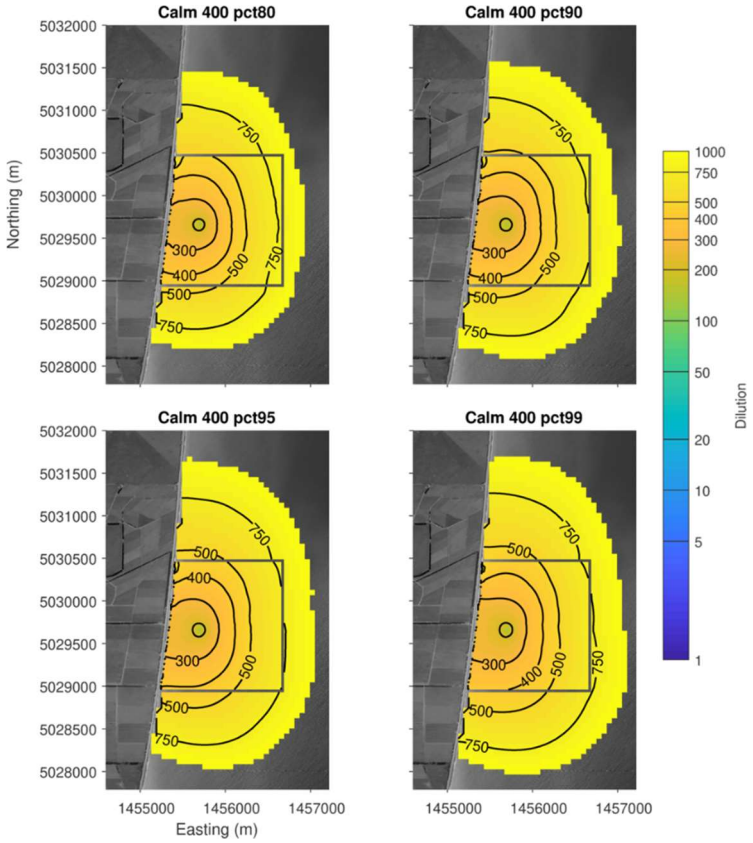

Figure 0.3. Maps of the 80th, 90th, 95th and 99th percentile surface dilution for the calm scenario with the outfall 400 m from the high tide line. Grey lines show the innermost model domain.

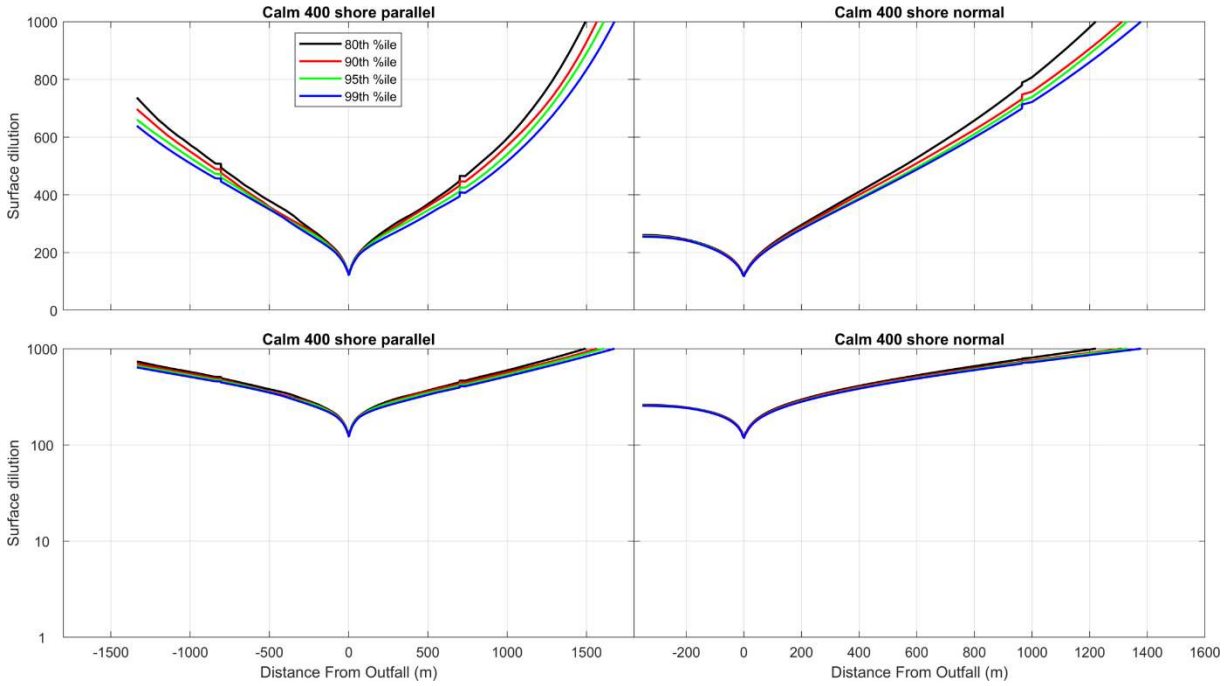

Figure 0.4. 80th, 90th, 95th and 99th percentile surface dilution transects for the calm scenario with the outfall 400 m from the high tide line. Left plots are the shore normal transects from offshore to onshore while the right plots are shore parallel transects from north-east to south-west. Lower plots are the log transformed version of their corresponding upper plot.

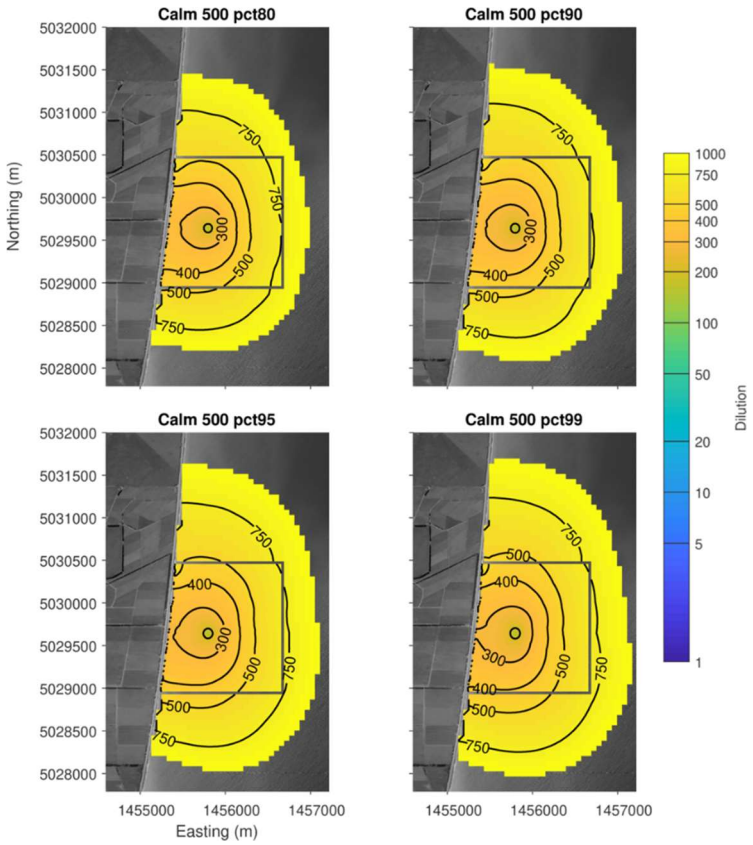

Figure 0.5. Maps of the 80th, 90th, 95th and 99th percentile surface dilution for the calm scenario with the outfall 500 m from the high tide line. Grey lines show the innermost model domain.

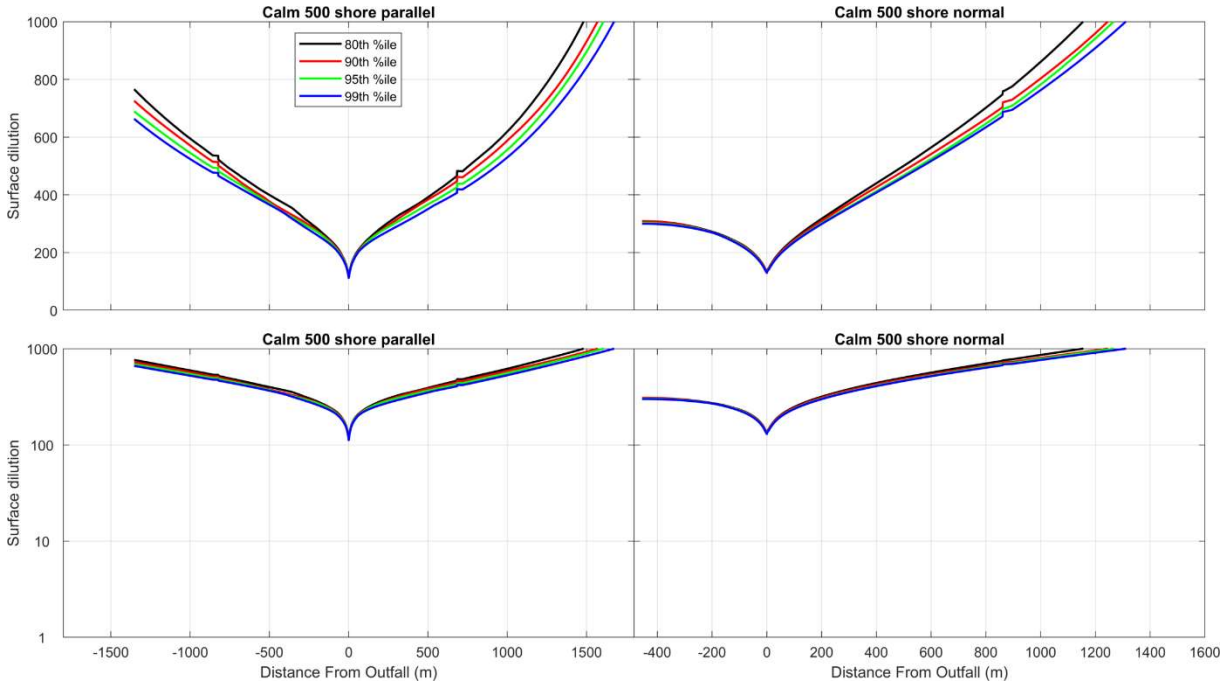

Figure 0.6. 80th, 90th, 95th and 99th percentile surface dilution transects for the calm scenario with the outfall 500 m from the high tide line. Left plots are the shore normal transects from offshore to onshore while the right plots are shore parallel transects from north-east to south-west. Lower plots are the log transformed version of their corresponding upper plot.

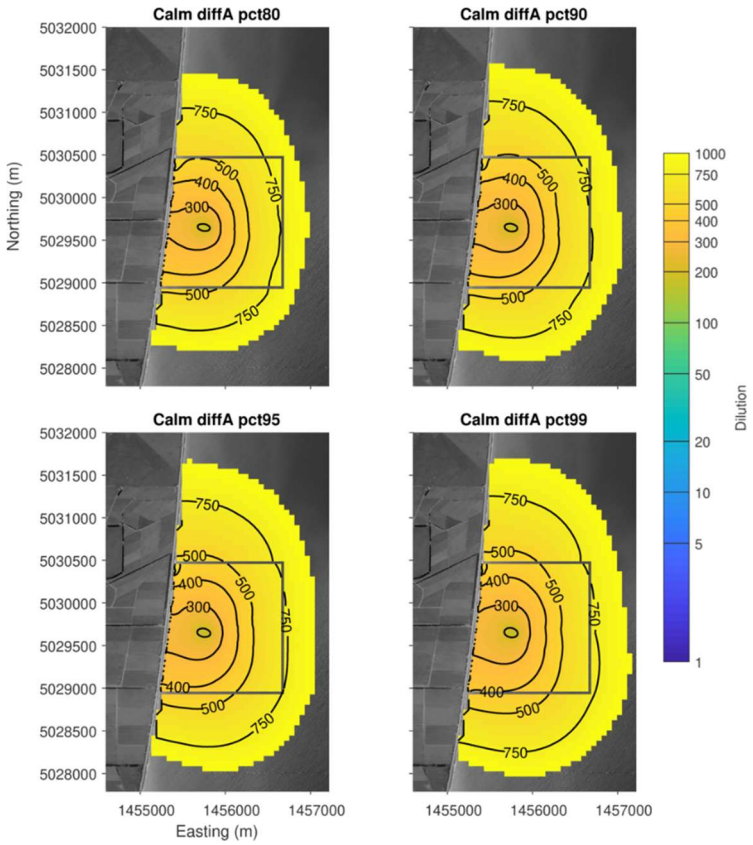

Figure 0.7. Maps of the 80th, 90th, 95th and 99th percentile surface dilution for the calm scenario with the in-line multiple outfall configuration. Grey lines show the innermost model domain.

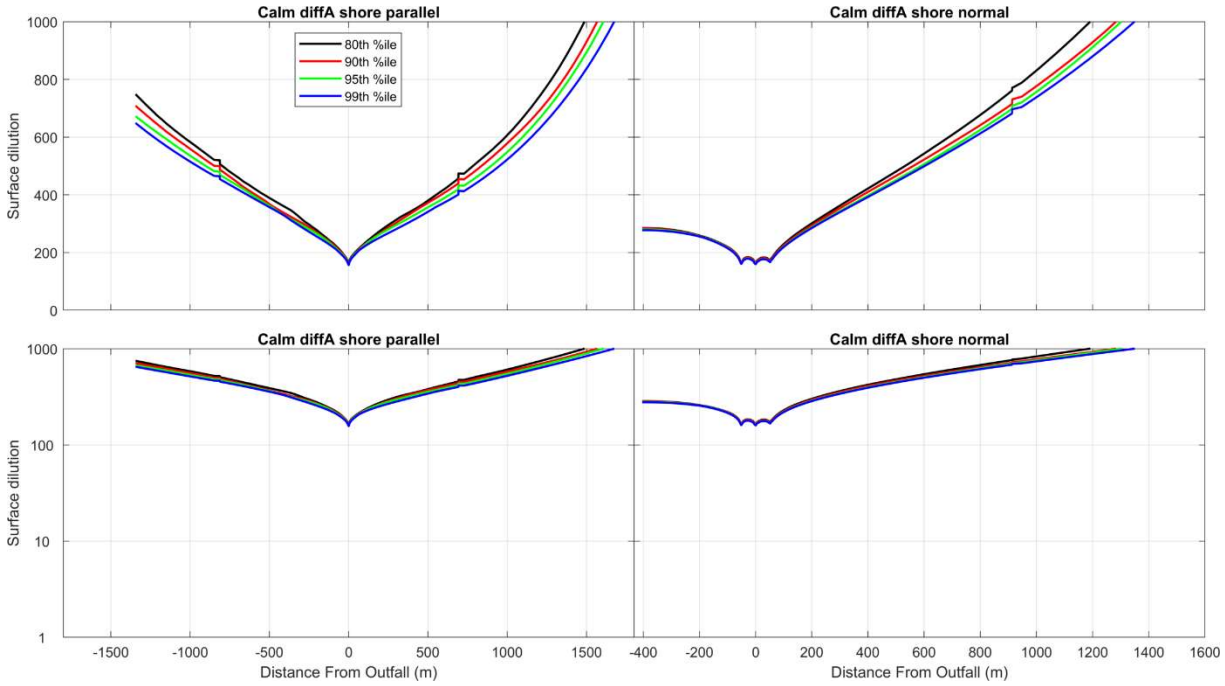

Figure 0.8. 80th, 90th, 95th and 99th percentile surface dilution transects for the calm scenario with the in-line multiple outfall configuration. Left plots are the shore normal transects from offshore to onshore while the right plots are shore parallel transects from north-east to south-west. Lower plots are the log transformed version of their corresponding upper plot.

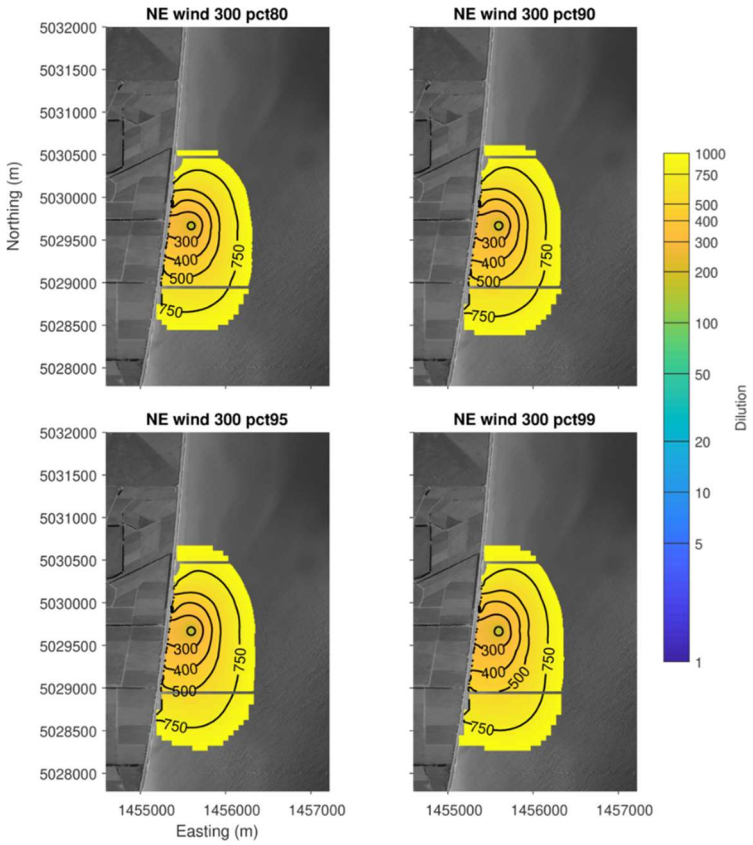

Figure 0.9. Maps of the 80th, 90th, 95th and 99th percentile surface dilution for the NE wind scenario with the outfall 300 m from the high tide line. Grey lines show the innermost model domain.

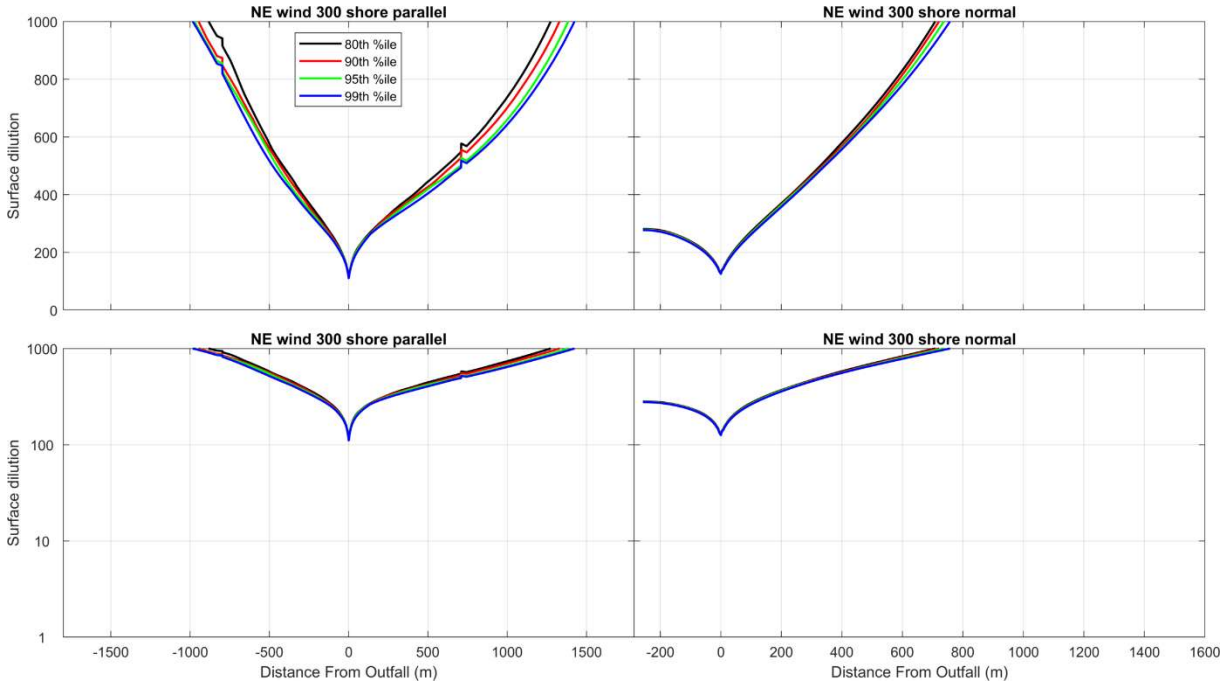

Figure 0.10. 80th, 90th, 95th and 99th percentile surface dilution transects for the NE wind scenario with the outfall 300 m from the high tide line. Left plots are the shore normal transects from offshore to onshore while the right plots are shore parallel transects from north-east to south-west. Lower plots are the log transformed version of their corresponding upper plot.

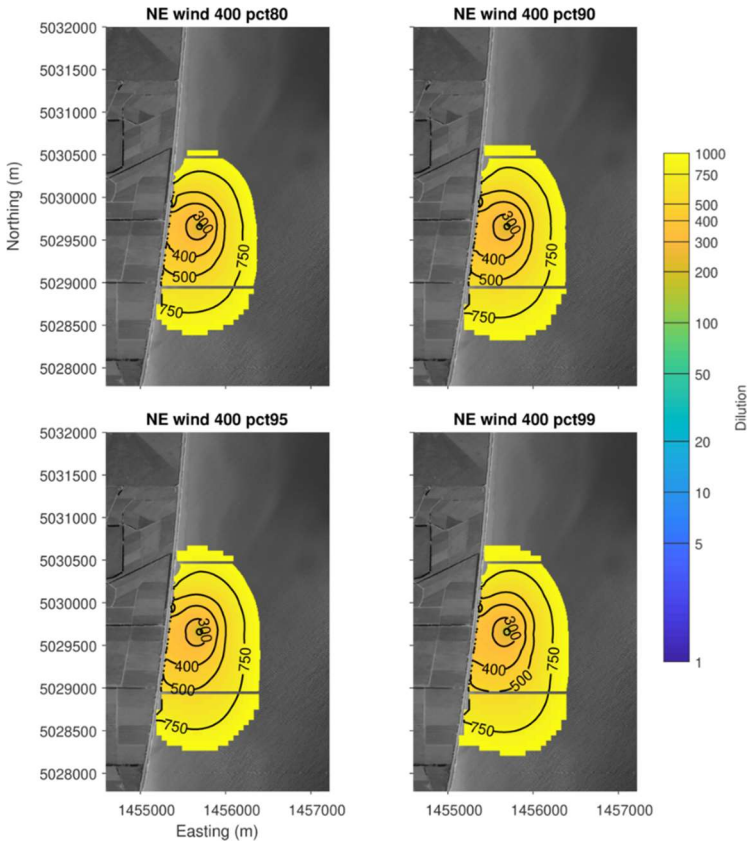

Figure 0.11. Maps of the 80th, 90th, 95th and 99th percentile surface dilution for the NE wind scenario with the outfall 400 m from the high tide line. Grey lines show the innermost model domain.

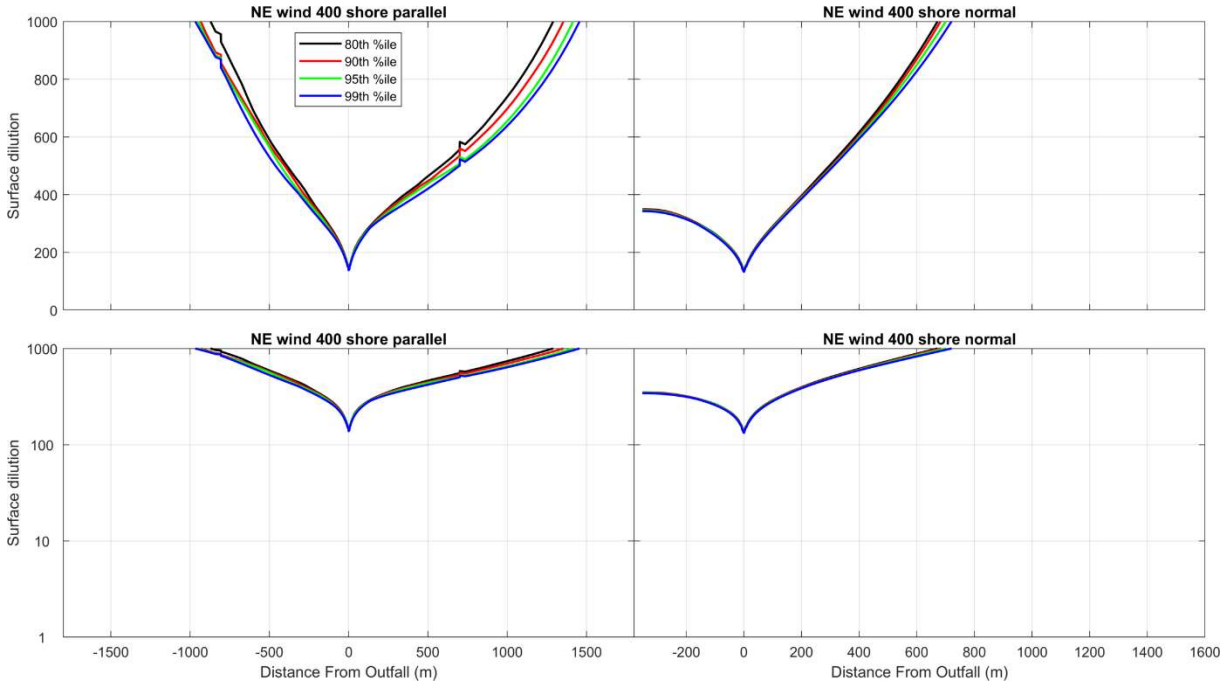

Figure 0.12. 80th, 90th, 95th and 99th percentile surface dilution transects for the NE wind scenario with the outfall 400 m from the high tide line. Left plots are the shore normal transects from offshore to onshore while the right plots are shore parallel transects from north-east to south-west. Lower plots are the log transformed version of their corresponding upper plot.

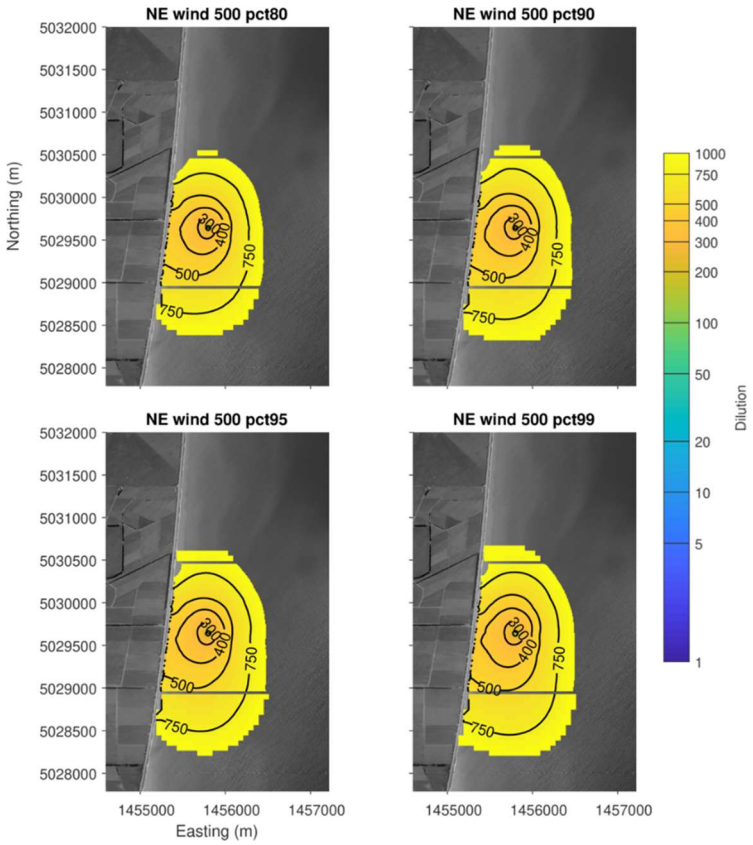

Figure 0.13. Maps of the 80th, 90th, 95th and 99th percentile surface dilution for the NE wind scenario with the outfall 500 m from the high tide line. Grey lines show the innermost model domain.

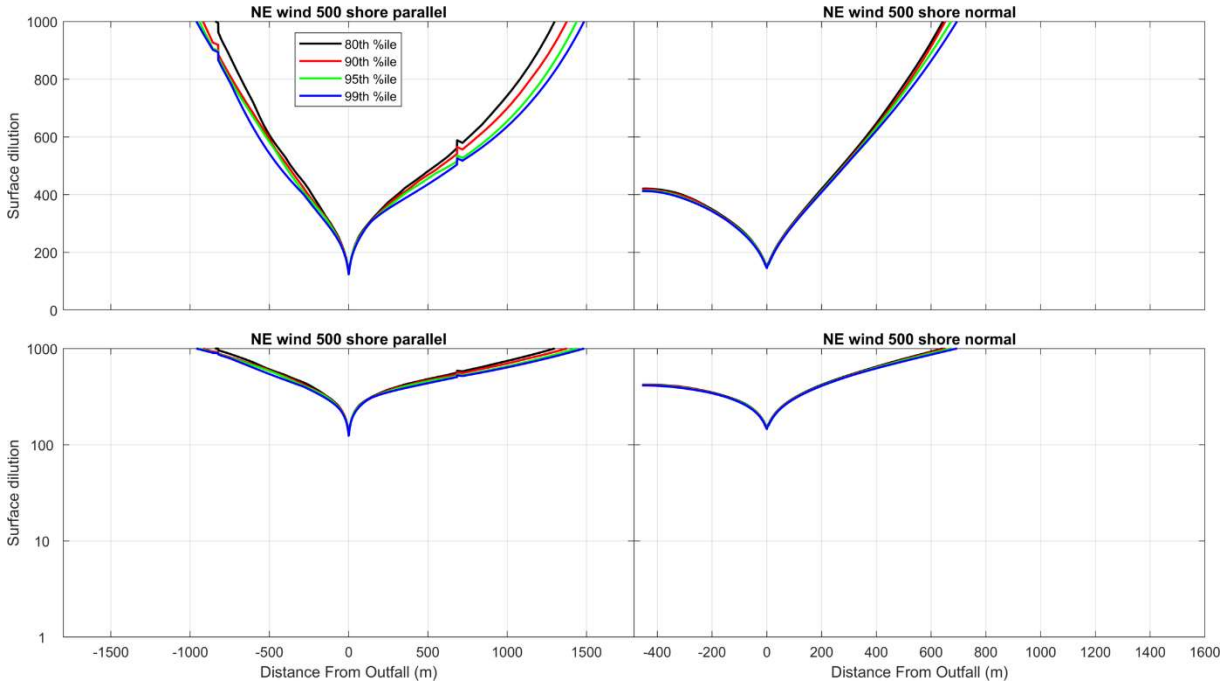

Figure 0.14. 80th, 90th, 95th and 99th percentile surface dilution transects for the NE wind scenario with the outfall 500 m from the high tide line. Left plots are the shore normal transects from offshore to onshore while the right plots are shore parallel transects from north-east to south-west. Lower plots are the log transformed version of their corresponding upper plot.

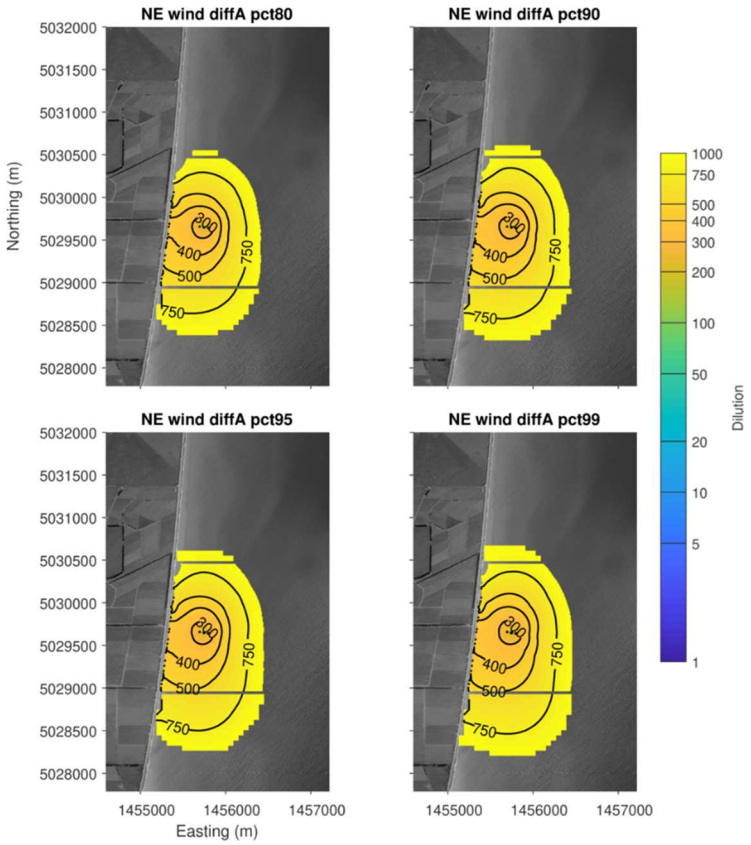

Figure 0.15. Maps of the 80th, 90th, 95th and 99th percentile surface dilution for the NE wind scenario with the in-line multiple outfall configuration. Grey lines show the innermost model domain.

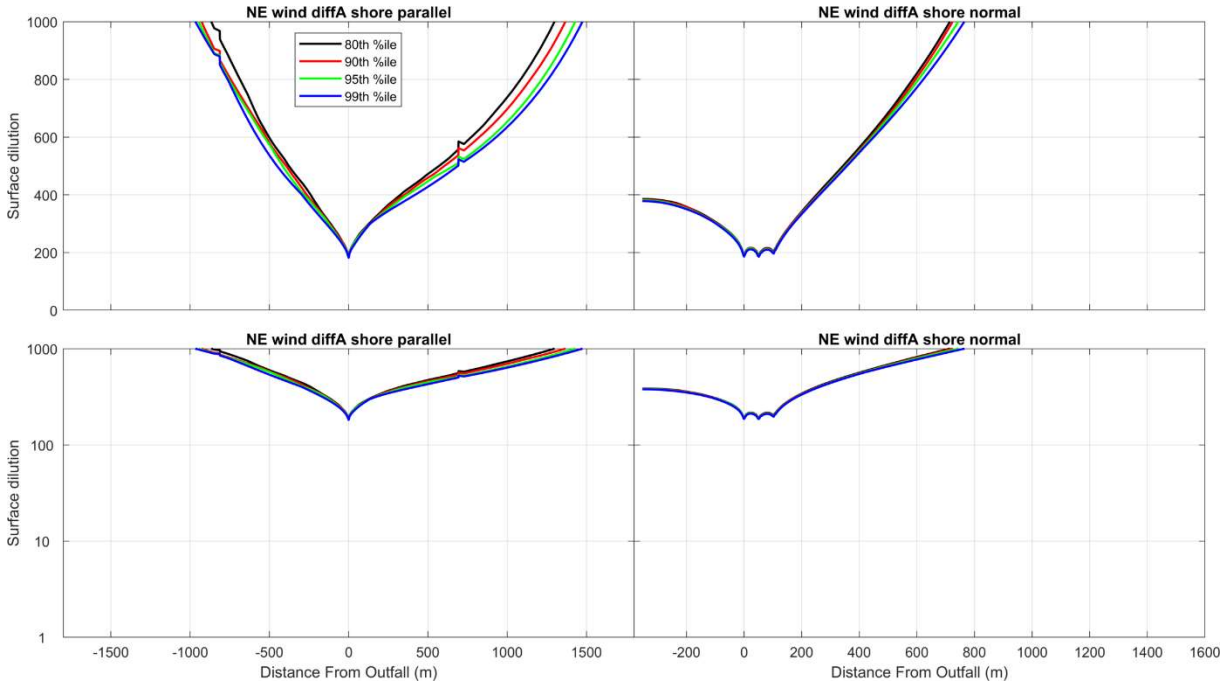

Figure 0.16. 80th, 90th, 95th and 99th percentile surface dilution transects for the NE wind scenario with the in-line multiple outfall configuration. Left plots are the shore normal transects from offshore to onshore while the right plots are shore parallel transects from north-east to south-west. Lower plots are the log transformed version of their corresponding upper plot.

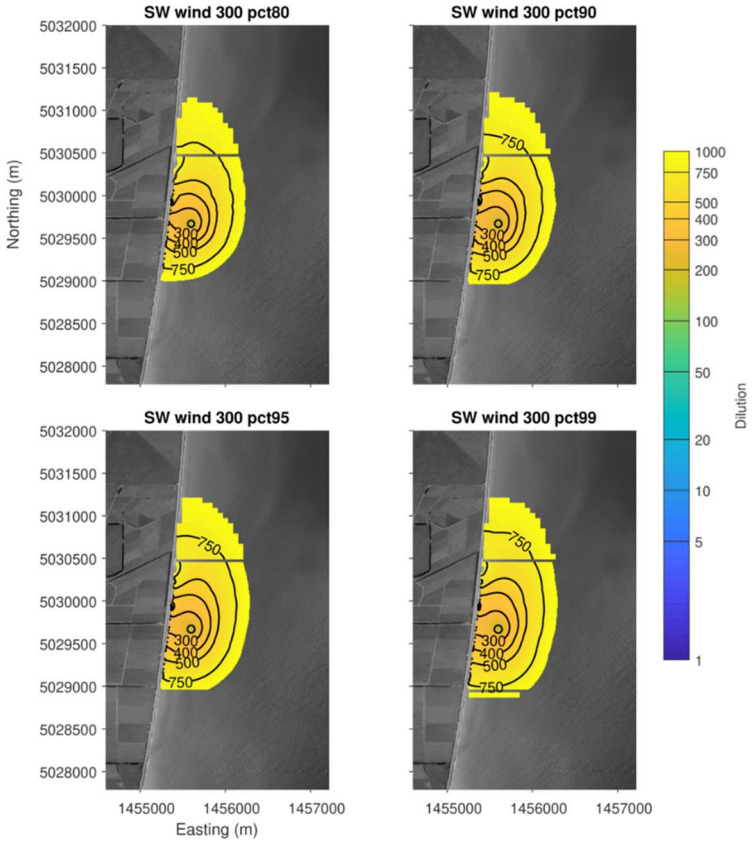

Figure 0.17. Maps of the 80th, 90th, 95th and 99th percentile surface dilution for the SW wind scenario with the outfall 300 m from the high tide line. Grey lines show the innermost model domain.

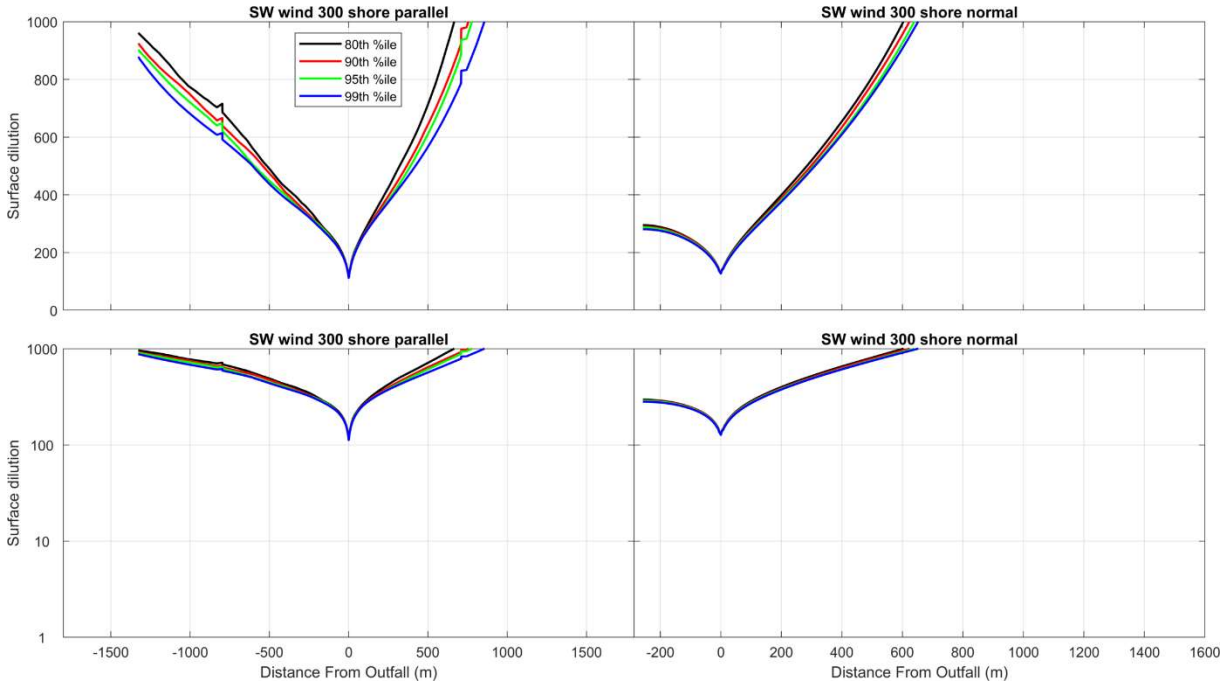

Figure 0.18. 80th, 90th, 95th and 99th percentile surface dilution transects for the SW wind scenario with the outfall 300 m from the high tide line. Left plots are the shore normal transects from offshore to onshore while the right plots are shore parallel transects from north-east to south-west. Lower plots are the log transformed version of their corresponding upper plot.

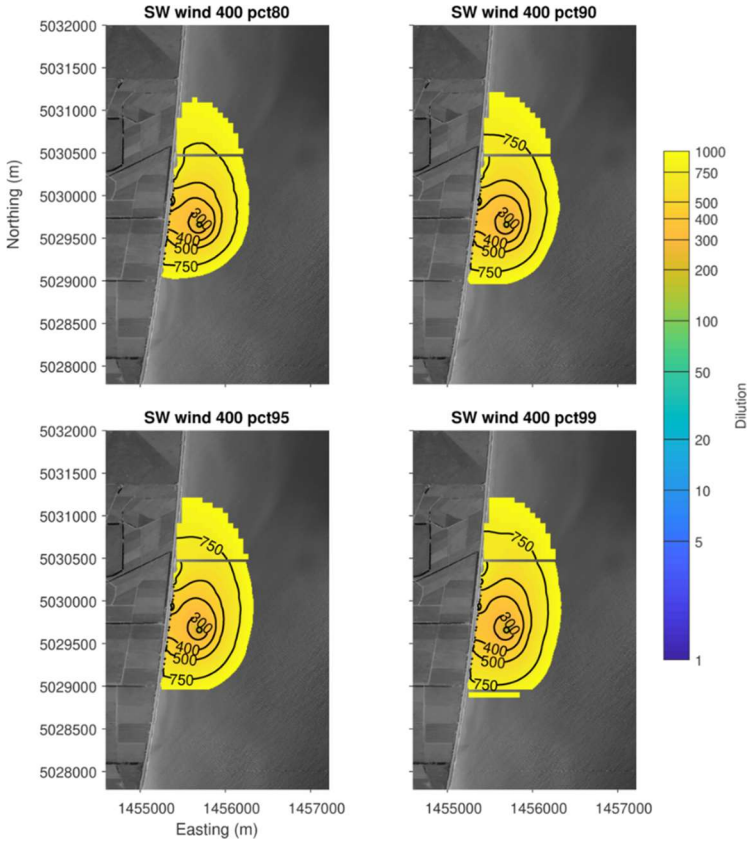

Figure 0.19. Maps of the 80th, 90th, 95th and 99th percentile surface dilution for the SW wind scenario with the outfall 400 m from the high tide line. Grey lines show the innermost model domain.

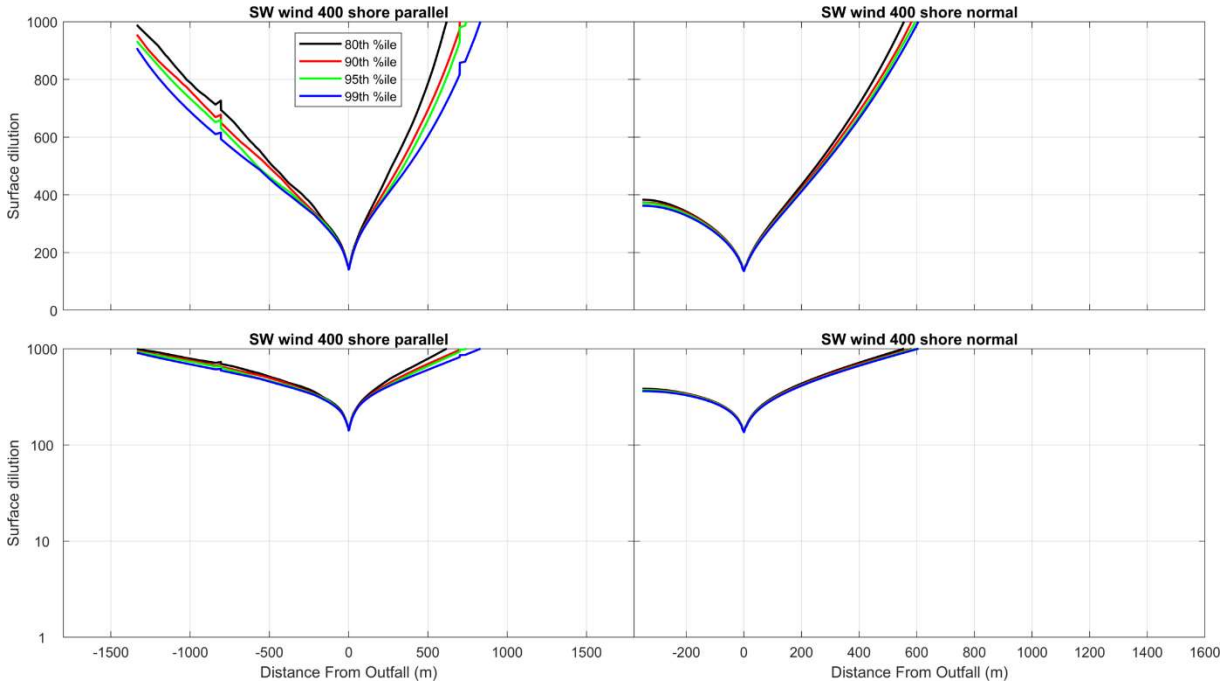

Figure 0.20. 80th, 90th, 95th and 99th percentile surface dilution transects for the SW wind scenario with the outfall 400 m from the high tide line. Left plots are the shore normal transects from offshore to onshore while the right plots are shore parallel transects from north-east to south-west. Lower plots are the log transformed version of their corresponding upper plot.

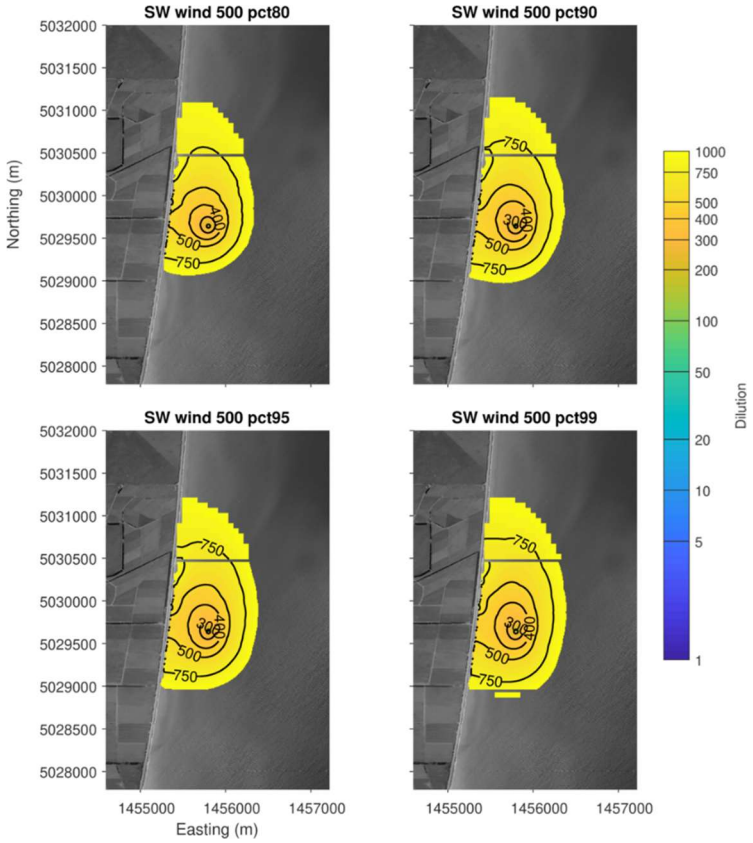

Figure 0.21. Maps of the 80th, 90th, 95th and 99th percentile surface dilution for the SW wind scenario with the outfall 500 m from the high tide line. Grey lines show the innermost model domain.

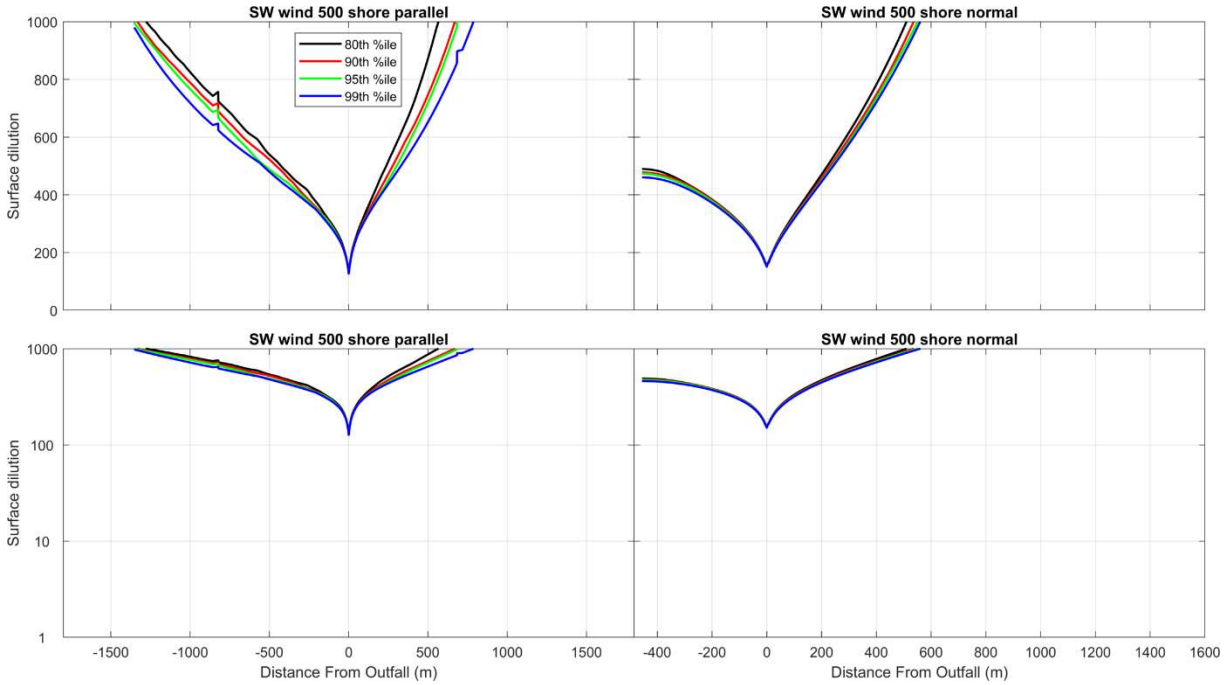

Figure 0.22. 80th, 90th, 95th and 99th percentile surface dilution transects for the SW wind scenario with the outfall 500 m from the high tide line. Left plots are the shore normal transects from offshore to onshore while the right plots are shore parallel transects from north-east to south-west. Lower plots are the log transformed version of their corresponding upper plot.

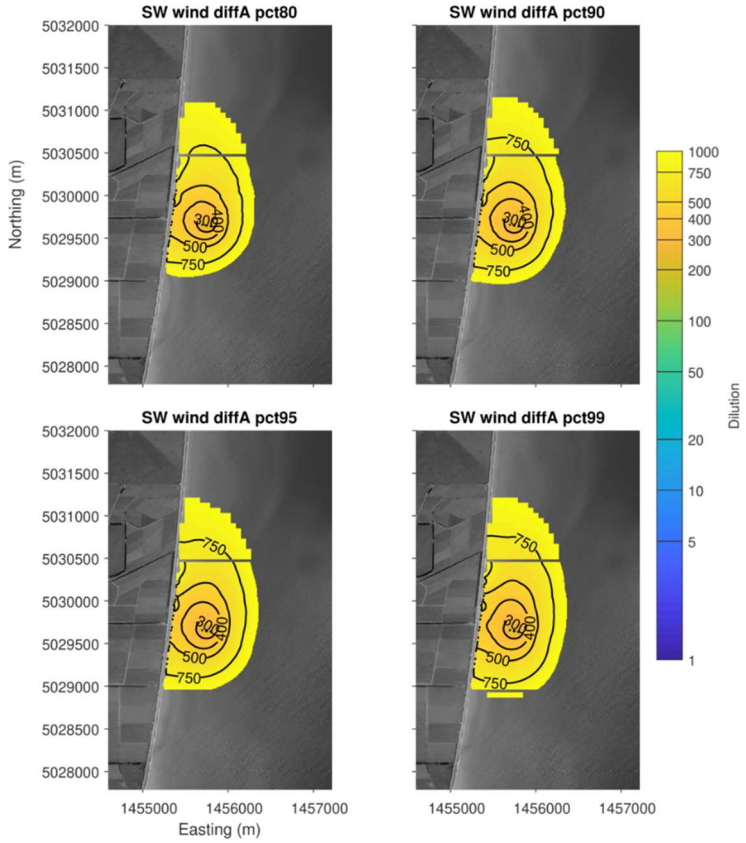

Figure 0.23. Maps of the 80th, 90th, 95th and 99th percentile surface dilution for the SW wind scenario with the in-line multiple outfall configuration. Grey lines show the innermost model domain.

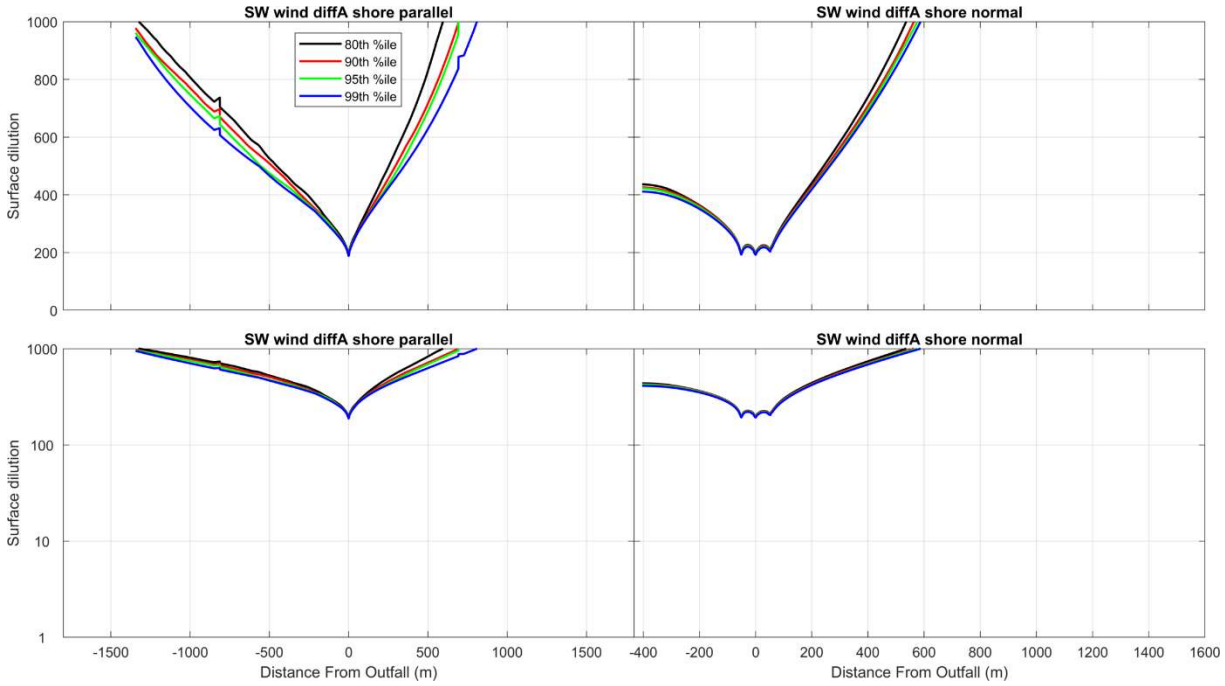

Figure 0.24. 80th, 90th, 95th and 99th percentile surface dilution transects for the SW wind scenario with the in-line multiple outfall configuration. Left plots are the shore normal transects from offshore to onshore while the right plots are shore parallel transects from north-east to south-west. Lower plots are the log transformed version of their corresponding upper plot.

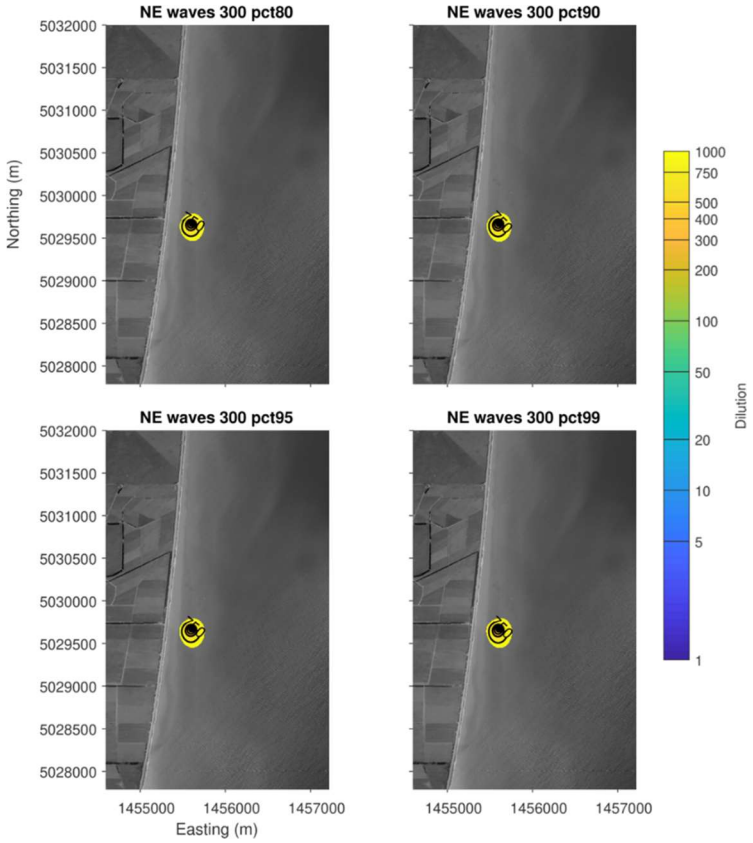

Figure 0.25. Maps of the 80th, 90th, 95th and 99th percentile surface dilution for the NE waves scenario with the outfall 300 m from the high tide line. Grey lines show the innermost model domain.

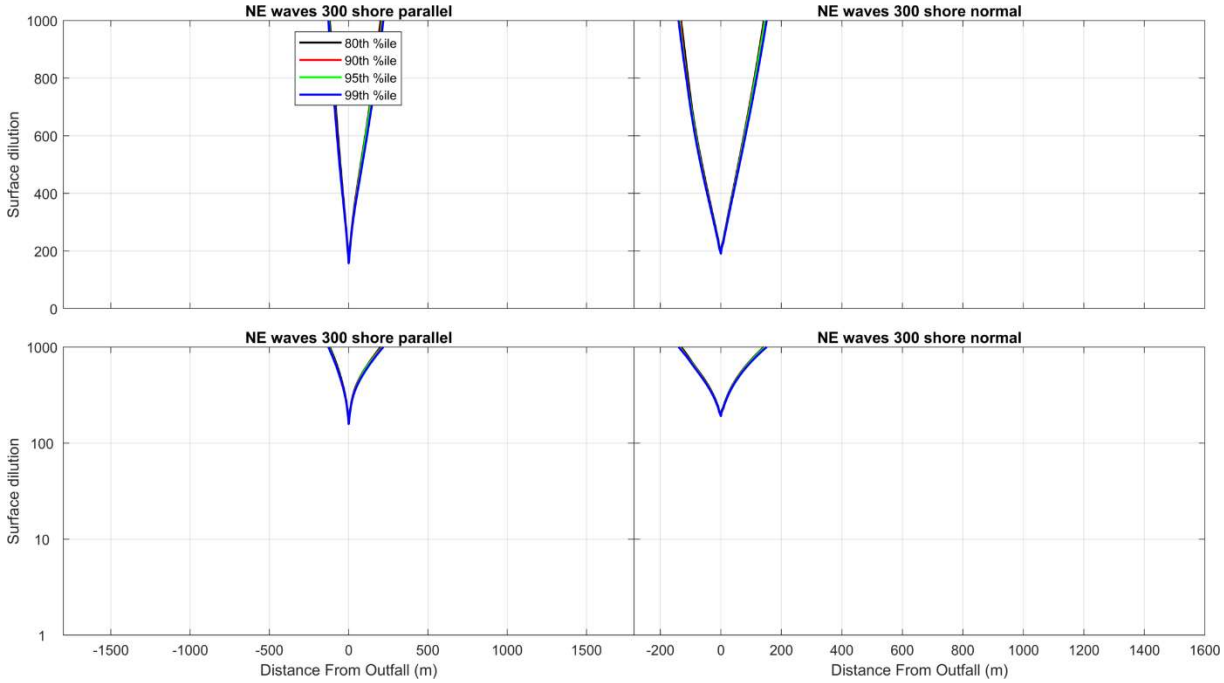

Figure 0.26. 80th, 90th, 95th and 99th percentile surface dilution transects for the NE waves scenario with the outfall 300 m from the high tide line. Left plots are the shore normal transects from offshore to onshore while the right plots are shore parallel transects from north-east to south-west. Lower plots are the log transformed version of their corresponding upper plot.

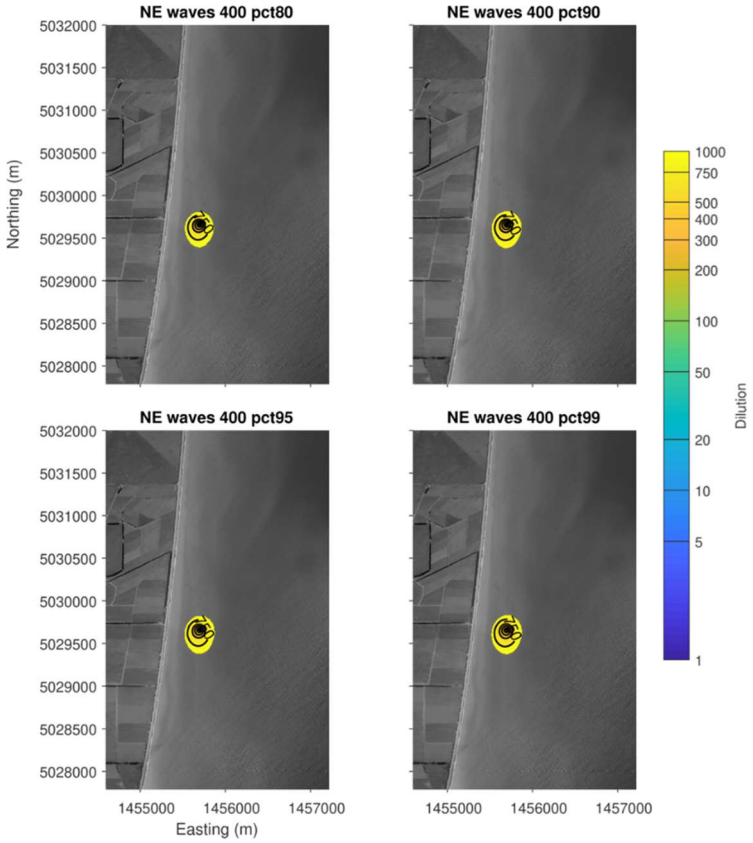

Figure 0.27. Maps of the 80th, 90th, 95th and 99th percentile surface dilution for the NE waves scenario with the outfall 400 m from the high tide line. Grey lines show the innermost model domain.

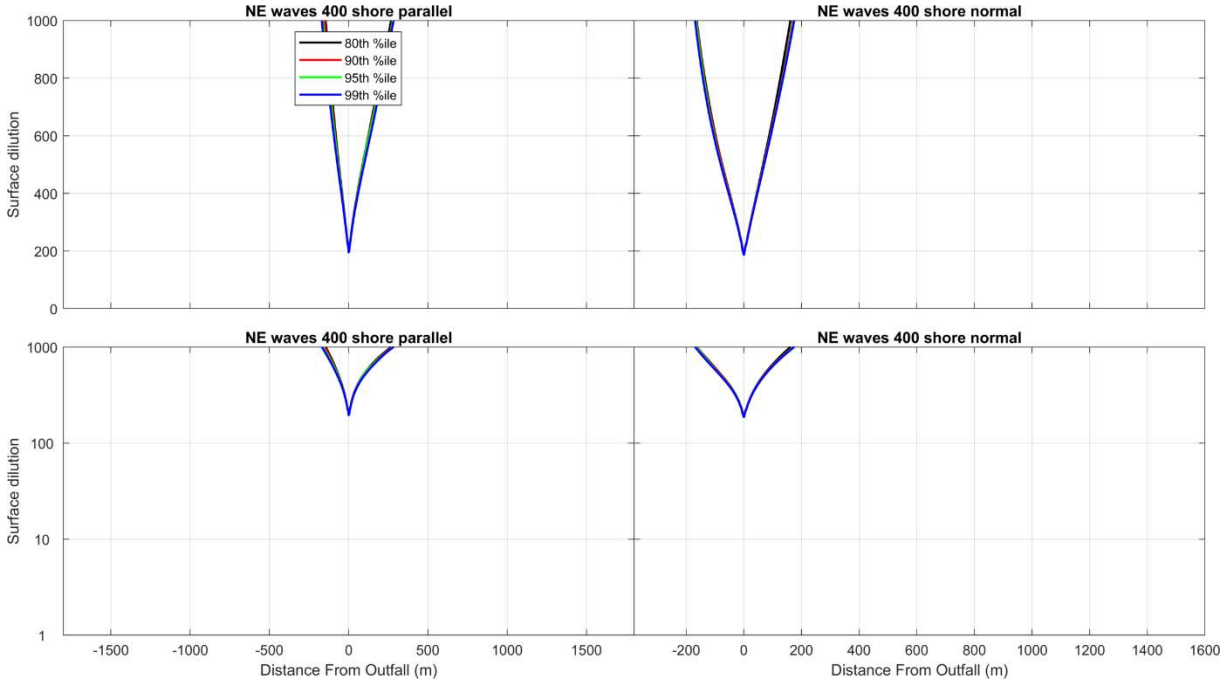

Figure 0.28. 80th, 90th, 95th and 99th percentile surface dilution transects for the NE waves scenario with the outfall 400 m from the high tide line. Left plots are the shore normal transects from offshore to onshore while the right plots are shore parallel transects from north-east to south-west. Lower plots are the log transformed version of their corresponding upper plot.

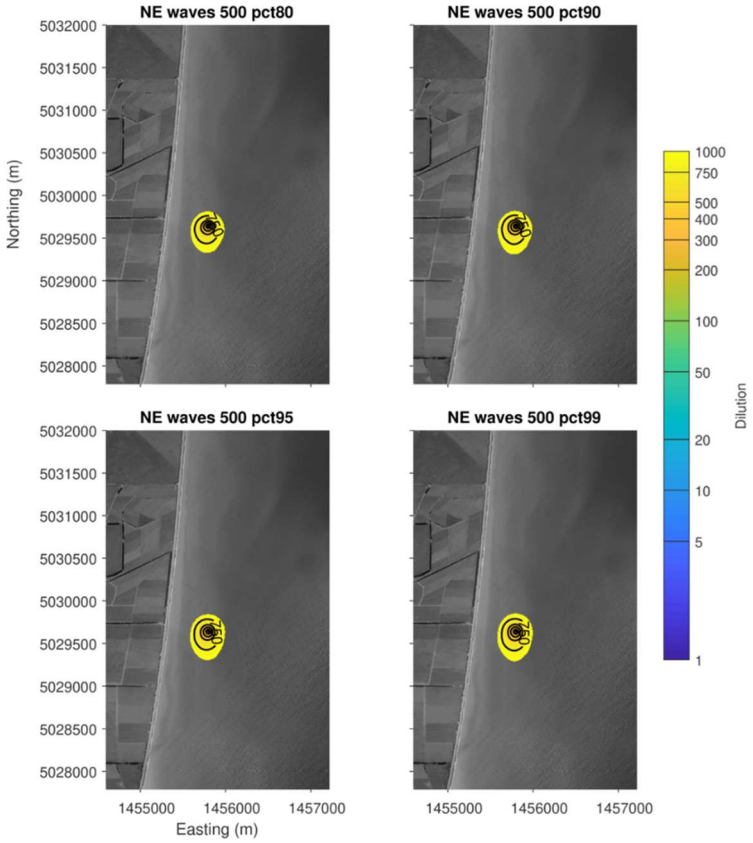

Figure 0.29. Maps of the 80th, 90th, 95th and 99th percentile surface dilution for the NE waves scenario with the outfall 500 m from the high tide line. Grey lines show the innermost model domain.

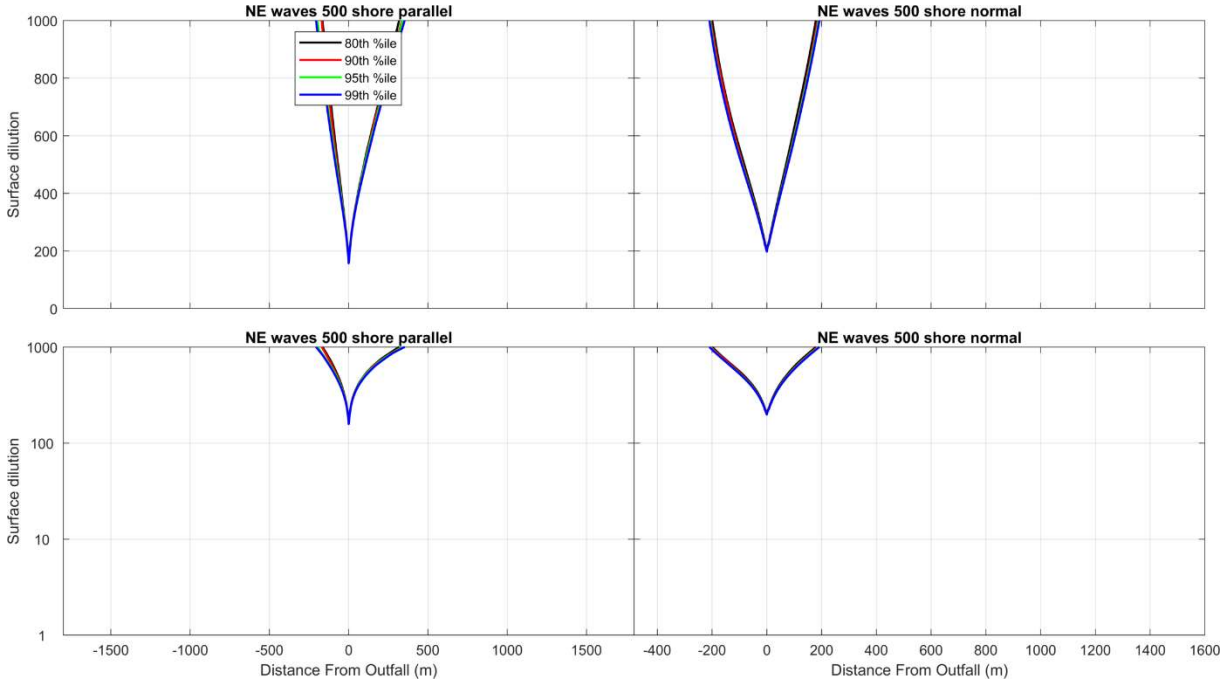

Figure 0.30. 80th, 90th, 95th and 99th percentile surface dilution transects for the NE waves scenario with the outfall 500 m from the high tide line. Left plots are the shore normal transects from offshore to onshore while the right plots are shore parallel transects from north-east to south-west. Lower plots are the log transformed version of their corresponding upper plot.

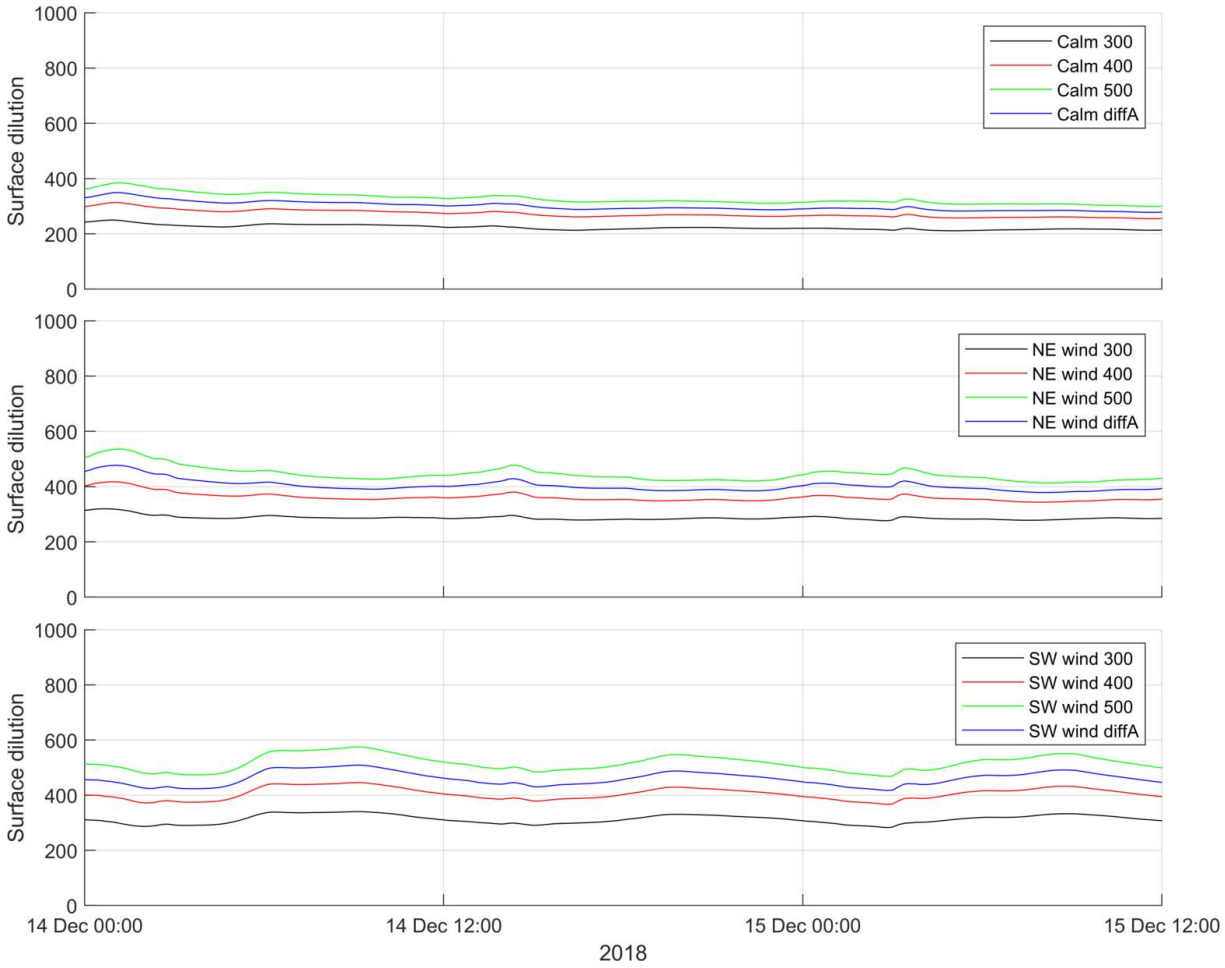

Figure 0.31. Surface dilution at Archibald Road for 300 m, 400 m, 500 m the in-line multiple outfall (diffA) configurations under the calm, NE wind, SW wind scenarios (results for the NE waves condition were >1000 fold dilution and were therefore negligible).

Appendix B. Dilution During the Worst Case Calm Scenario

Since there are 3 discharge points, evaluation of 300x dilution within 50 m of the outfall is more complex than a single discharge point. As was found in the modelling results, the scenario that results in the least mixing is the calm scenario. To get a clearer picture of the dilution around the 3 discharge points, 6x shore-normal and shore-parallel transects were sampled from 6 point sources, and a close-up of the discharges at 3, 6 and 9 hours was also extracted from the calm simulation. It is important to recognise that it is likely that the calm scenario (no wind and small swell) very rarely, if ever, occurs. This is due to a) the models inherent conservatism, and b) the likely occurrence of calm conditions for 6 hours or greater (i.e. on average only once every 2 years or less).

Figure 1 shows the 6 locations where transects of dilution have been extracted:

- At each of the 3 discharge locations – 1, 2 and 3 moving offshore;
- Locations along the central pipeline – Mid1 and Mid2, and;
- The 'worst' case scenario where the 50 m radius mixing zone of discharge points 2 and 3 overlap.

Figure 1. Central points for the 6x shore-normal and shore-parallel transects sampled. The dotted circles indicate a 50 m radius around each discharge point.

The results of this further analysis of dilution from the split outfall configuration(Figures 2-8) are basically the same as reported:

"*Due to the split configuration, dilution of 300x or greater occurs within 10-50 m of the outfall in all 4 metocean scenarios. The exception to this is when calm conditions occur for >6 hours (Figure 5.8). However, it is likely that this scenario very rarely, if ever, occurs. This is due to a) the models inherent conservatism described above, and b) the likely occurrence of calm conditions for 6 hours or greater (i.e. on average only once every 2 years or less – Figure 5.6)*".

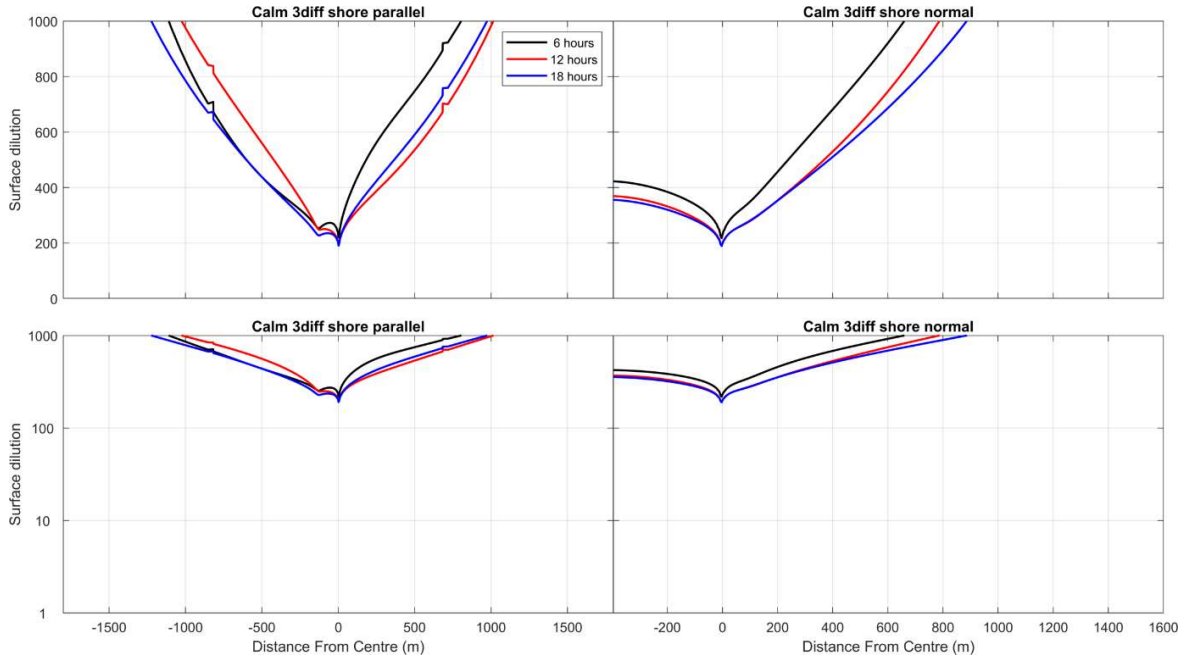

Figure 2. Discharge 1 dilution.

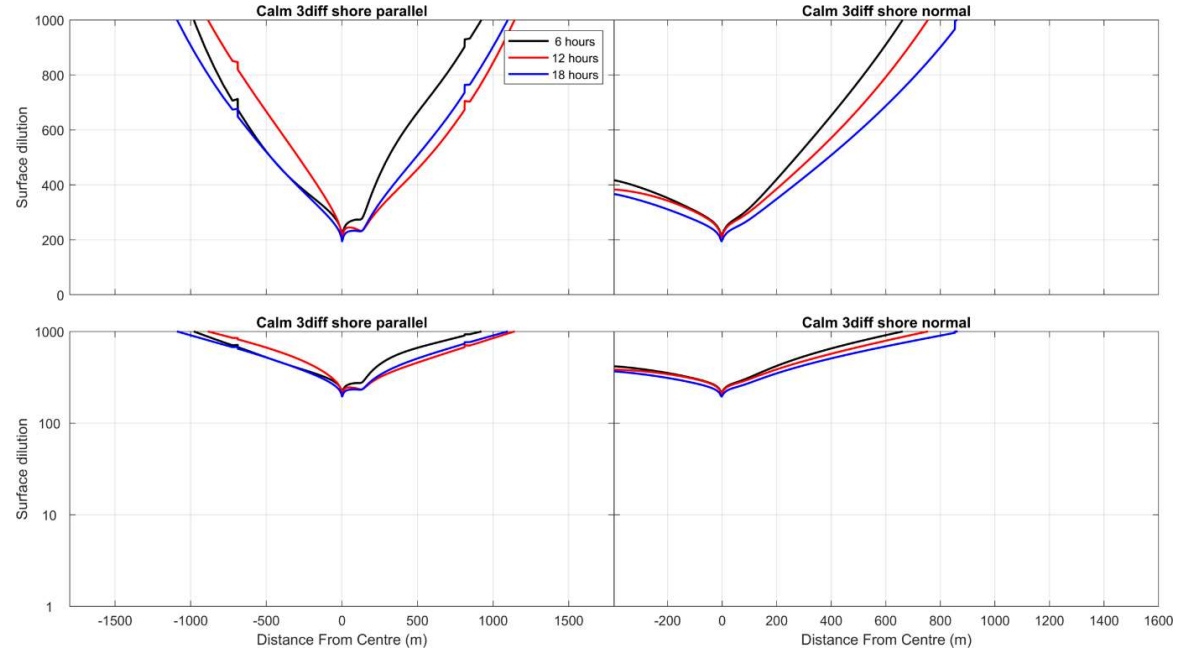

Figure 3. Discharge 2 dilution.

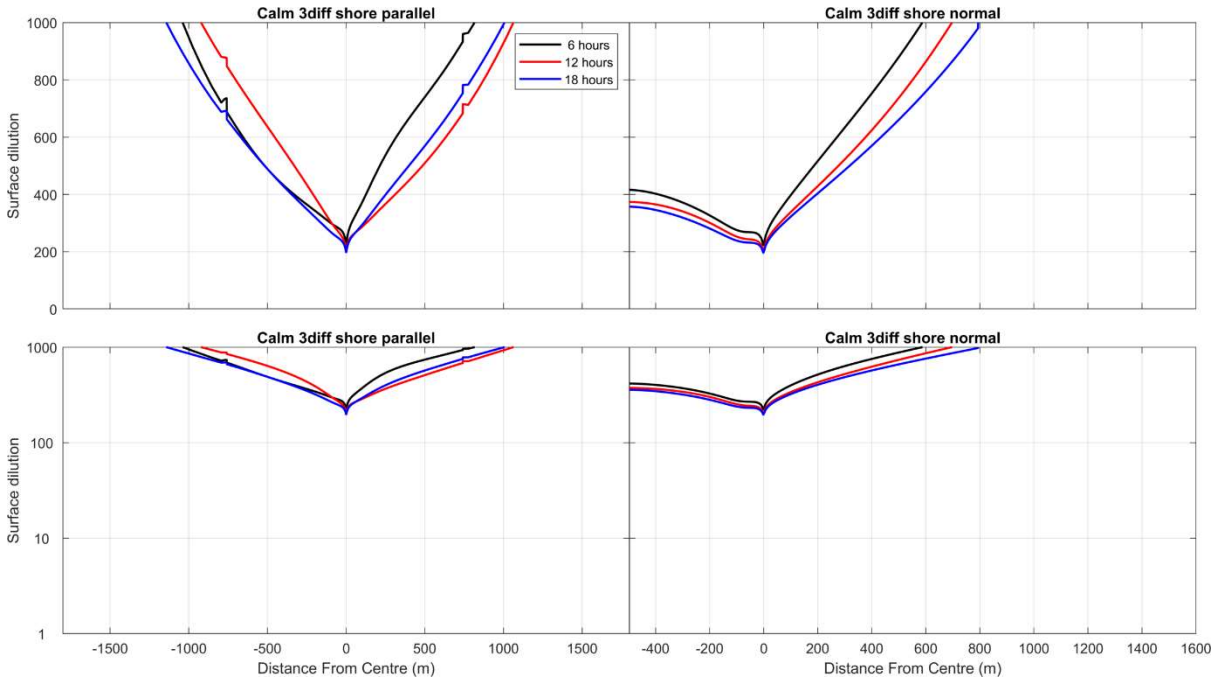

Figure 4. Discharge 3 dilution.

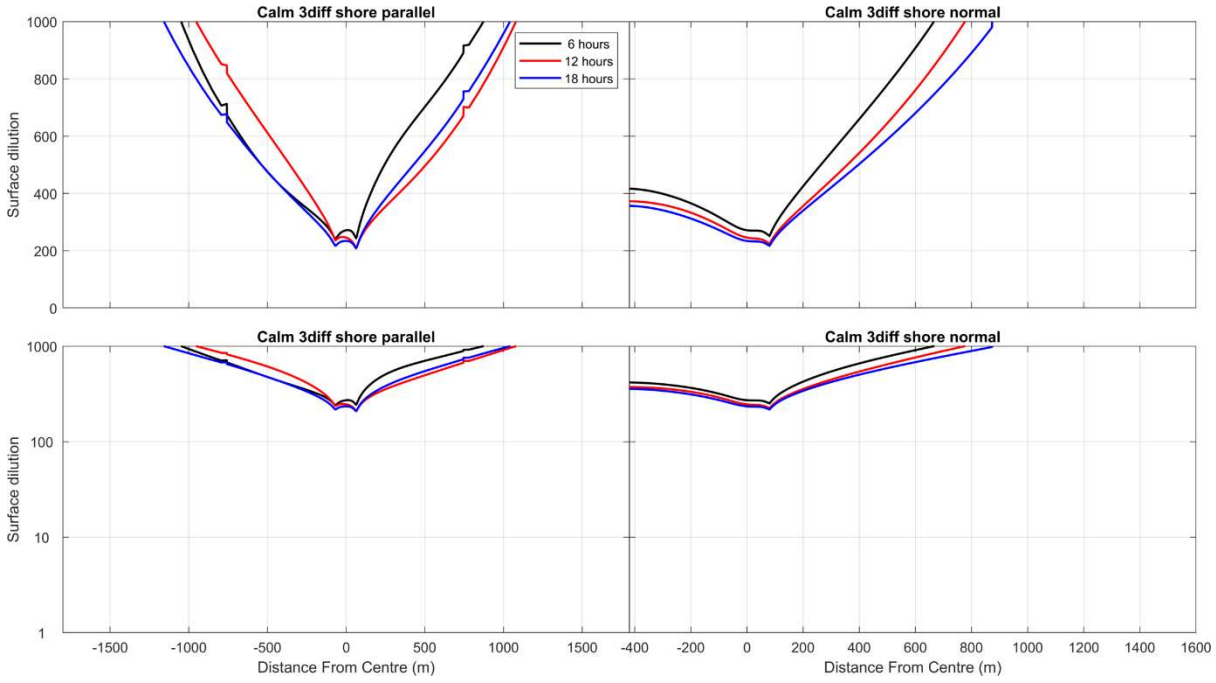

Figure 5. Mid1 Dilution.

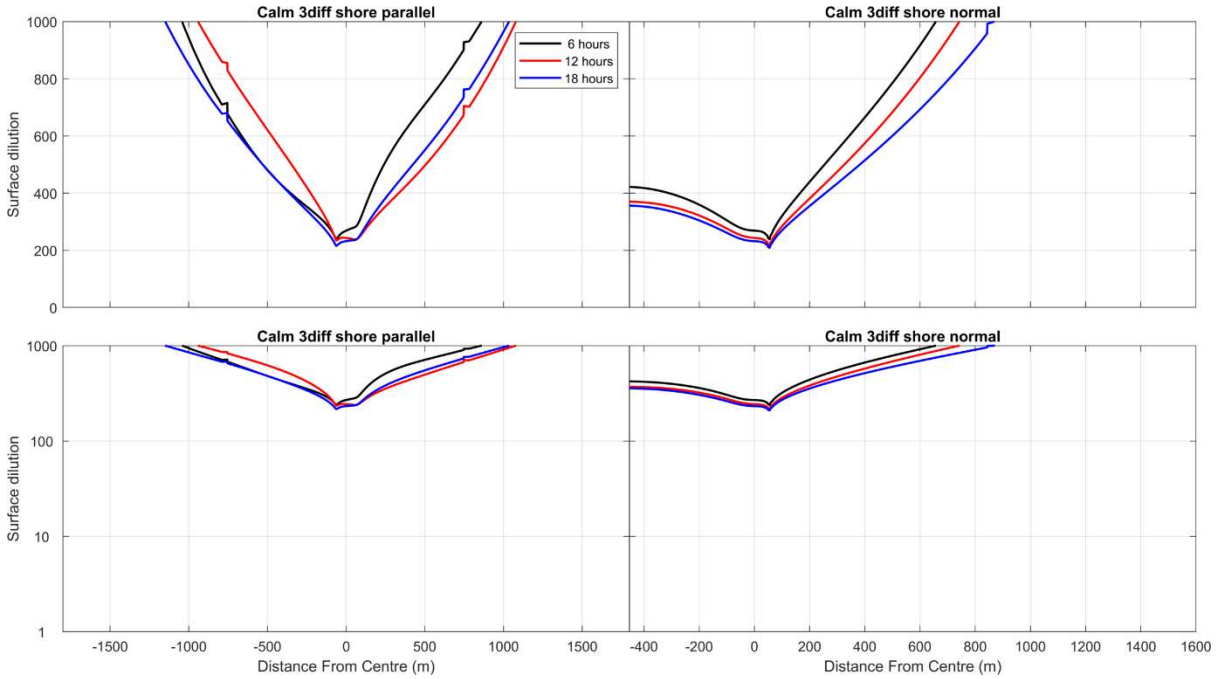

Figure 6. Mid2 Dilution.

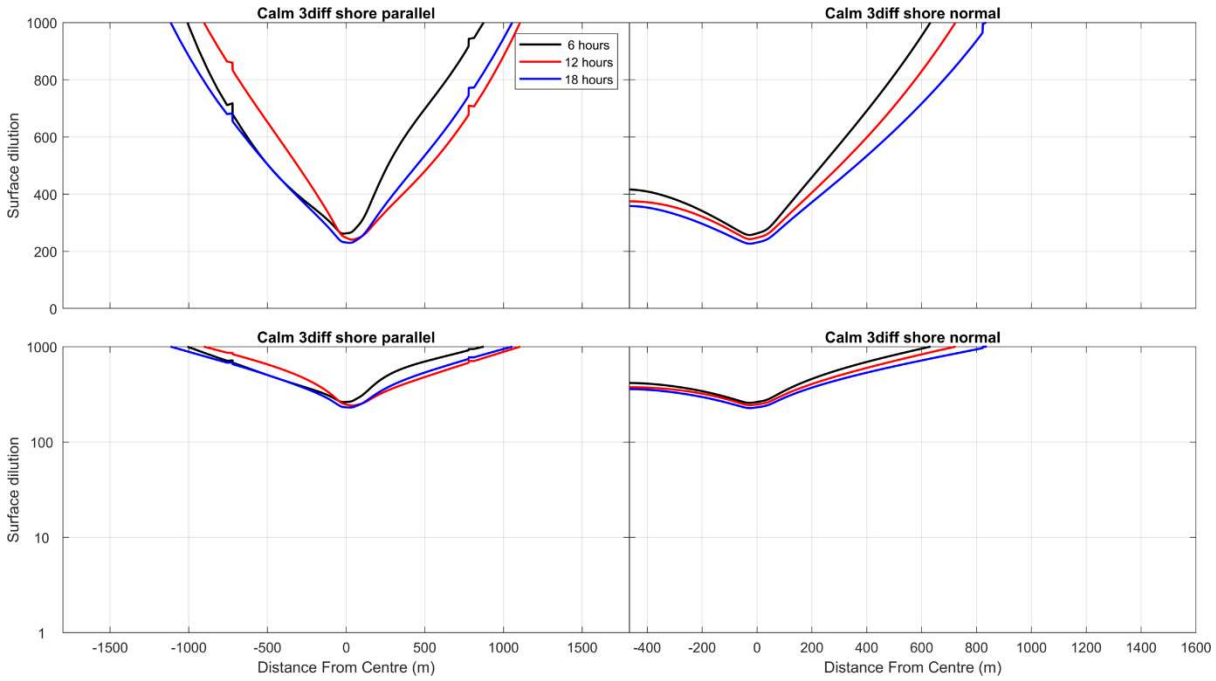

Figure 7. Worst case dilution.

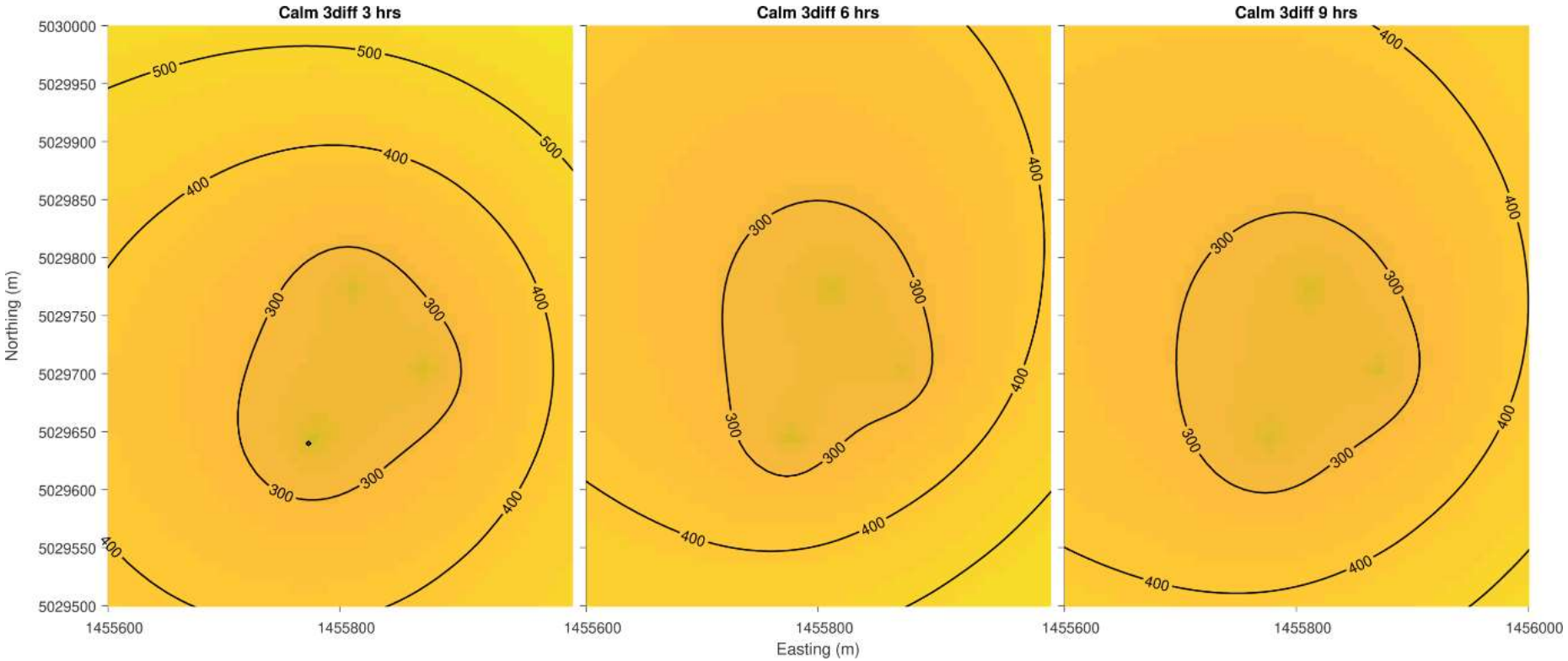

Figure 8. Dilution plots for 3, 6 and 9 hours of calm conditions with very small swell; the diameter of the 300x dilution contour can be seen to be increasing in size with